

4-3-2003

"Intelligent" Design of Molecular Materials: Understanding the Concepts of Design in Supramolecular Synthesis of Network Solids

Brian D. Moulton
University of South Florida

Follow this and additional works at: <https://scholarcommons.usf.edu/etd>

 Part of the [American Studies Commons](#)

Scholar Commons Citation

Moulton, Brian D., "'Intelligent" Design of Molecular Materials: Understanding the Concepts of Design in Supramolecular Synthesis of Network Solids" (2003). *Graduate Theses and Dissertations*.
<https://scholarcommons.usf.edu/etd/1435>

This Dissertation is brought to you for free and open access by the Graduate School at Scholar Commons. It has been accepted for inclusion in Graduate Theses and Dissertations by an authorized administrator of Scholar Commons. For more information, please contact scholarcommons@usf.edu.

"INTELLIGENT" DESIGN OF MOLECULAR MATERIALS: UNDERSTANDING
THE CONCEPTS OF DESIGN IN SUPRAMOLECULAR SYNTHESIS OF
NETWORK SOLIDS

by

BRIAN D. MOULTON

A dissertation submitted in partial fulfillment
of the requirements for the degree of
Doctor of Philosophy
Department of Chemistry
College of Arts and Sciences
University of South Florida

Major Professor: Michael J. Zaworotko, Ph.D.
Prof. Brian Space, Ph.D.
Prof. Julie P. Harmon, Ph.D.
Prof. Jerry L. Atwood, Ph.D.

Date of Approval:
April 3, 2003

Keywords: Crystal engineering, coordination polymers, supramolecular chemistry,
topology, structure-function

© Copyright 2003 , Brian Moulton

Dedication

I would like to dedicate this work to all those who paved the road before me, and to those who will travel the road after me. I hope that this contribution is successful in providing a snapshot of where the field is today. I thank those whose contributions helped define the discipline, and wish those who choose to pursue it in the future great success.

I specifically would like to dedicate this to all of my teachers and mentors, without whom this would not be possible.

Acknowledgements

First and foremost I would like to acknowledge and extend my most heartfelt thanks to Prof. Michael Zaworotko, who has given me the advice and guidance needed to grow and develop scientifically, but most of all, has extended his friendship, which has helped me grow and develop personally.

I would like to acknowledge all of the members of the Zaworotko research group. Specifically, I would like to thank Heba Abourahma, Jianjiang Lu, and Dr. Arunendu Mondal, all of who have made significant contributions to the research described herein. In addition, I would like to acknowledge Prof. Srikanth Hariharan (USF Department of Physics) who has had a notable influence on this research.

Lastly, I would like to acknowledge the Staff and Faculty of the Department of Chemistry at the University of South Florida for their support and encouragement.

Table of Contents

List of Tables	vi
List of Figures	vii
Abstract	xii
Chapter 1 – Introduction	1
1.1. Preamble	1
1.1.1. From Molecules to Crystal Engineering	1
1.1.2. Crystal Engineering vs. Crystal Structure Prediction	5
1.1.3. Supramolecular Isomerism	6
1.2. Coordination Polymer Examples	10
1.2.1. 0D (Discrete) Architectures	14
1.2.2. 1D Coordination Polymers	16
1.2.3. 2D Coordination Polymers	20
1.2.4. 3D Coordination Polymers	28
1.2.5. Hybrid structures	36
1.3. Summary	41
Chapter 2 – Three-Dimensional Structures	45
2.1. Preamble	45
2.2. Compound 1: $\{[XL_2Zn_2(\text{btc})]_8[L_2Zn_2(\text{btc})_{4/3}]_3\}_n$	45
2.2.1. Experimental	45
2.2.2. Technical description	46

2.2.3.	Space-filling models	49
2.2.4.	Illustrative Description	49
2.3.	Compound 2: $\{[L_2Zn_2(btc)_{4/3}]\}_n$	52
2.3.1.	Experimental	52
2.3.2.	Technical description	52
2.3.3.	Space-filling models	54
2.3.4.	Illustrative Description	54
2.4.	Discussion	55
2.5.	Conclusions	60
Chapter 3 – Two-Dimensional Structures		65
3.1.	Preamble	65
3.2.	Compound 3: $\{[L_2Cu_2(bdc)_2]_4\}_n$	66
3.2.1.	Experimental	66
3.2.2.	Technical description	66
3.2.3.	Space-filling models	68
3.2.4.	Illustrative description	68
3.3.	Compound 4: $\{[L_2Cu_2(bdc)_2]_3\}_n$	72
3.3.1.	Experimental	72
3.3.2.	Technical description	73
3.3.3.	Space-filling models	74
3.3.4.	Illustrative description	75
3.4.	Discussion	77
3.5.	Conclusions	84

Chapter 4 – Zero-Dimensional Structures	86
4.1. Preamble	86
4.2. Compound 5: $[L_2Cu_2(bdc)_2]_{12}$	87
4.2.1. Experimental	87
4.2.2. Technical description	88
4.2.3. Space-filling models	90
4.2.4. Illustrative description	90
4.3. Compound 6: $[L_2Cu_2(bdc)_2]_{12}$	92
4.3.1. Experimental	92
4.3.2. Technical description	93
4.3.3. Space-filling models	95
4.3.4. Illustrative description	95
4.4. Discussion	97
4.5. Conclusions	101
Chapter 5 – Additional Structures	104
5.1. Preamble	104
5.2. Compound 7: $\{L_2Cu_2(btc)_2\}_n$	106
5.2.1. Experimental	106
5.2.2. Technical description	106
5.2.3. Space-filling models	107
5.2.4. Illustrative description	108
5.3. Compound 8: $\{L_2Cu_2(btc)_2\}_n$	109
5.3.1. Experimental	109

5.3.2. Technical description	110
5.3.3. Space-filling models	111
5.3.4. Illustrative description	112
5.4. Discussion	113
5.5. Conclusions	117
Chapter 6 – Structure-Function: Magnetism	123
6.1. Preamble	123
6.2. Magnetic susceptibility	122
6.2.1. Three-dimensional structure	122
6.2.2. Two-dimensional structures	124
6.2.3. Zero-dimensional (discrete) structures	128
6.3. Conclusions	129
Chapter 7 – Conclusion & Future Directions	131
7.1. Summary	131
7.2. “Intelligent” Design	132
7.3. Predicted structures	134
7.3.1. Faceted polyhedra	134
7.3.2. Three-dimensional structure	137
7.3.3. Derivatives of compound 1	137
7.3.4. Other chromophores	138
7.3.5. Geometrically frustrated molecular magnetic materials	139
7.3.6. Enumeration of networks	139
7.4. The last word	140

References	142
Appendices	159
Appendix A-1. Crystal data and structure refinement for compound 1.	160
Appendix A-2. Crystal data and structure refinement for compound 2.	161
Appendix A-3. Crystal data and structure refinement for compound 3.	162
Appendix A-4. Crystal data and structure refinement for compound 4.	163
Appendix A-5. Crystal data and structure refinement for compound 5.	164
Appendix A-6. Crystal data and structure refinement for compound 6.	165
Appendix A-7. Crystal data and structure refinement for compound 7.	166
Appendix A-8. Crystal data and structure refinement for compound 8.	167
Appendix B-1: Geometric values for the Platonic and Archimedean Solids	168
Appendix B-2: The 80 uniform polyhedra	170
Appendix C: The 92 Johnson Solids	173
About the Author	End Page

List of Tables

Table 2.1: Selected crystallographic parameters for $\{[XL_2Zn_2(btc)]_8[L_2Zn_2(btc)_{4/3}]_3\}_n$	46
Table 2.2: Selected crystallographic parameters for $\{[L_2Zn_2(btc)_{4/3}]\}_n$	52
Table 3.1: Selected crystallographic parameters for $\{[L_2Zn_2(btc)_2]_4\}_n$	66
Table 3.2: Selected crystallographic parameters for $\{[L_2Cu_2(bdc)_2]_3\}_n$	73
Table 4.1: Selected crystallographic parameters for $[L_2Cu_2(btc)_2]_{12}$	88
Table 4.2: Selected crystallographic parameters for $[L_2Cu_2(btc)_2]_{12}$	93
Table 5.1: Selected crystallographic parameters for $\{[L_2Cu_2(btc)_2]\}_n$	106
Table 5.2: Selected crystallographic parameters for $\{[L_2Cu_2(btc)_2]\}_n$	110
Table 5.3: Number of vertices in nearest neighbor shells for $6^5.8$ networks	116

List of Figures

Figure 1.1: Common/simple metal-organic network architectures	11
Figure 1.2: Platonic (regular) and Archimedean (semi-regular) solids	15
Figure 1.3: Supramolecular isomers from the assembly of 90° ditopic nodes	16
Figure 1.4: Crystal structure of $\{[\text{Ni}(\text{bipy})(\text{benzoate})_2(\text{MeOH})_2]\cdot\text{PhNO}_2\}_n$	19
Figure 1.5: Molecular ladders	20
Figure 1.6: 2-D architectures observed in coordination polymer networks	21
Figure 1.7: Spatial supramolecular isomers of $[\text{M}(\text{bipy})_2(\text{NO}_3)_2]$ square grids	23
Figure 1.8: $[\text{Ni}(1,2\text{-bis}(4\text{-pyridyl})\text{ethane})_2(\text{NO}_3)_2]_n \cdot 2 \text{ veratrole}$	24
Figure 1.9: $[\text{Co}(\text{pyca})(\text{bipy})(\text{H}_2\text{O})_2]_n \cdot (\text{NO}_3) \cdot (\text{bipy})(\text{H}_2\text{O})_{1.5}$	25
Figure 1.10: 2-D topologies predicted for coordination polymer networks based on T-shaped nodes	26
Figure 1.11: Bilayer architecture for T-shaped nodes	27
Figure 1.12: Basic structural units of diamondoid architectures	31
Figure 1.13: Octahedral networks	32
Figure 1.14: Minimal accessible surface of $\text{Zn}_4\text{O}(\text{bdc})_3$ (calculated by Cerius2)	33
Figure 1.15: Schematic illustration of $[\text{Co}(\text{bipy})_{1.5}(\text{NO}_3)_2]_n \cdot (\text{C}_6\text{H}_6)_{1.5}$	34
Figure 1.16: Space-filling model of $[\text{Co}(\text{bipy})_{1.5}(\text{NO}_3)_2]_n \cdot (\text{C}_6\text{H}_6)_{1.5}$	34
Figure 1.17: Schematic illustration of $\{[\text{Ag}(\text{bipy})(\text{NO}_3)]\}_n$	35
Figure 1.18: Schematic of interpenetrating grids that afford a 3-D superstructure	36

Figure 1.19: $\{[\text{Ni}(\text{bipy})_2(\text{NO}_3)_2] \cdot 2\text{pyrene}\}_n$	37
Figure 1.20: modes of interpenetration	39
Figure 2.1: Space filling models of compound 1, $\{[\text{XL}_2\text{Zn}_2(\text{btc})]_8[\text{L}_2\text{Zn}_2(\text{btc})_{4/3}]_3\}_n^*$	49
Figure 2.2: Schematic representation of trimesate*	49
Figure 2.3: Schematic representation of dizinc SBU*	50
Figure 2.4: Schematic illustration of compound 1, $\{[\text{XL}_2\text{Zn}_2(\text{btc})]_8[\text{L}_2\text{Zn}_2(\text{btc})_{4/3}]_3\}_n$	51
Figure 2.5: Space filling models of compound 2, $\{[\text{L}_2\text{Zn}_2(\text{btc})_{4/3}]\}_n^*$	54
Figure 2.6: Schematic illustration of compound 2, $\{[\text{L}_2\text{Zn}_2(\text{btc})_{4/3}]\}_n$	54
Figure 2.7: Polyhedral models based on the rhombicuboctahedron	57
Figure 2.8: Space-filling polyhedral arrangements	59
Figure 2.9: Projections of polyhedral space-filling models and corresponding crystal structure projections* for compound 1	62
Figure 2.10: Projections of polyhedral space-filling models and corresponding crystal structure projections* for compound 2	63
Figure 3.1: Space filling models of compound 3, $\{[\text{L}_2\text{Cu}_2(\text{bdc})_2]_4\}_n^*$	68
Figure 3.2: Schematic illustration of the network observed in compound 3, $\{[\text{L}_2\text{Cu}_2(\text{bdc})_2]_4\}_n^*$	69
Figure 3.3: Schematic illustration of compound 3, $\{[\text{L}_2\text{Cu}_2(\text{bdc})_2]_4\}_n^*$	70
Figure 3.4: Schematic illustration of compound 3, $\{[\text{L}_2\text{Cu}_2(\text{bdc})_2]_4\}_n^*$	71
Figure 3.5: Space filling models of compound 4, $\{[\text{L}_2\text{Cu}_2(\text{bdc})_2]_3\}_n^*$	74
Figure 3.6: Schematic illustration of the network observed in compound 4, $\{[\text{L}_2\text{Cu}_2(\text{bdc})_2]_3\}_n^*$	75

Figure 3.7: Schematic illustration of compound 4, $\{[L_2Cu_2(bdc)_2]_3\}_n^*$	76
Figure 3.8: Schematic illustration of compound 4, $\{[L_2Cu_2(bdc)_2]_3\}_n^*$	76
Figure 3.9: Comparison of [001] projections of compounds 2 & 3	78
Figure 3.10: Illustration of the extraction of compound 3 from compound 2	79
Figure 3.11: Illustration of the extraction of compound 4 from compound 2.	81
Figure 3.12: Illustration of the two stacking modes observed for the 3.6.3.6 topology.	83
Figure 4.1: Illustration the predicted structure of a molecular Small rhombihexadron	87
Figure 4.2: Space filling models of compound 5, $[L_2Cu_2(bdc)_2]_{12}^*$	90
Figure 4.3: Schematic illustration of compound 5, $[L_2Cu_2(bdc)_2]_{12}$	91
Figure 4.4: Space filling models of compound 6, $[L_2Cu_2(bdc)_2]_{12}^*$	95
Figure 4.5: Schematic illustration of compound 6, $[L_2Cu_2(bdc)_2]_{12}^*$	96
Figure 4.6: Cartoon illustrations of the nSBU components of compounds 5 and 6	97
Figure 4.7: Connectivity of the molecular squares (SBUs) in 5 and 6	98
Figure 4.8: Orthographic projections of the schematic model of compound 5	99
Figure 4.9: Orthographic projections of the schematic model of compound 6	99
Figure 4.10: The nine faceted polyhedra	102
Figure 5.1: Space filling models of compound 7, $\{[L_2Cu_2(bdc)_2]_3\}_n^*$	107
Figure 5.2: Schematic illustration of the network observed in compound 7, $\{[L_2Cu_2(bdc)_2]_3\}_n^*$	108
Figure 5.3: Schematic illustration of the connectivity of molecular squares observed in compound 7	108
Figure 5.4: Space filling models of compound 8, $\{[L_2Cu_2(bdc)_2]_3\}_n^*$	111

Figure 5.5: Schematic illustration of the network observed in compound 8, $\{[L_2Cu_2(bdc)_2]\}_n^*$	112
Figure 5.6: Schematic illustration of the connectivity of molecular squares observed in compound 8	112
Figure 5.7: Perspective illustrations of the networks observed in compounds 7 and 8	115
Figure 5.8: Schematic illustration of the network observed in compound 2	118
Figure 5.9: Schematic illustration of the nodes of the network observed in compound 2	119
Figure 5.10: Schematic illustration of cubic close packing (ccp)	119
Figure 5.11: Schematic illustration of the nodes of the network observed in compound 7	120
Figure 5.12: Schematic illustration of clusters of 13 spheres	121
Figure 5.13: Networks derived from simple cubic lattice	122
Figure 6.1: Temperature-dependant magnetic susceptibility of $\{[L_2Cu_2(btc)_{4/3}]\}_n$	123
Figure 6.2: Field-dependant magnetic susceptibility of $\{[L_2Cu_2(btc)_{4/3}]\}_n$	123
Figure 6.3: Temperature-dependant magnetic susceptibility of $\{[L_2Cu_2(bdc)_2]\}_n$ 2-D supramolecular isomers	124
Figure 6.4: Spin frustrated triangular lattices	126
Figure 6.5: Geometric arrangement of spins	127
Figure 6.6: Examples of x-y spin ground states for the Kagomé lattice	127
Figure 6.7: Field-dependant magnetic susceptibility for compounds 3 and 4	127
Figure 6.8: Temperature-dependant magnetic susceptibility of $\{[L_2Cu_2(bdc)_2]\}_{12}$	128

Figure 7.1: Predicted structures of some molecular faceted polyhedra	136
Figure 7.2: Predicted structure of the Small cubicuboctahedron	136
Figure 7.3: Predicted structure of a two-dimensional coordination polymer	138
Figure 7.4: Predicted structure of a monometal Kagomé lattice	138

“Intelligent” Design of Molecular Materials: Understanding the Concepts of Design in
Supramolecular Synthesis of Network Solids

Brian Moulton

ABSTRACT

This work endeavors to delineate modern paradigms for crystal engineering, i.e. the design and supramolecular synthesis of functional molecular materials. Paradigms predicated on an understanding of the geometry of polygons and polyhedra are developed. The primary focus is on structural determination by single crystal X-ray crystallography, structural interpretation using a suite of graphical visualization and molecular modeling software, and on the importance of proper graphical representation in the presentation and explanation of crystal structures.

A detailed analysis of a selected series of crystal structures is presented. The reduction of these molecular networks to schematic representations that illustrate their fundamental connectivity facilitates the understanding of otherwise complex supramolecular solids. Circuit symbols and Schläfli notation are used to describe the network topologies, which enables networks of different composition and metrics to be easily compared. This reveals that molecular orientations in the crystals and networks are commensurate with networks that can be derived from spherical close packed lattices. The development of a logical design strategy for a new class of materials based on our understanding of the chemical composition and topology of these networks is described.

The synthesis and crystal structure of a series of new materials generated by exploitation of this design strategy is presented, in addition to a detailed analysis of the topology of these materials and their relationship to a ‘parent’ structure.

In summary, this dissertation demonstrates that molecular polygons can self-assemble at their vertexes to produce molecular architectures and crystal structures that are consistent with long established geometric dogma. The design strategy represents a potentially broad ranging approach to the design of nanoporous structures from a wide range of chemical components that are based on molecular shape rather than chemical formula. In effect, this work represents another example of the ‘molecular meccano’ approach to self-assembled structures. Most importantly, given that these materials are designed from first principles, they offer materials scientists the ability to control the chemical nature of the constituent components and therefore influence the bulk physical properties of materials.

Chapter 1

Introduction

1.1. Preamble

Whereas single crystal X-ray crystallography has represented an active area of research since shortly after the discovery of X-rays, the subject of crystal engineering has developed rapidly only in recent years. This is presumably an artifact of a number of factors. For example, the development of relatively low cost, high-speed computers has not only enhanced crystal structure determination, but also crystal structure visualization, database development and analysis, and reflection analysis and processing. Simply put, X-ray crystallographic analysis has become less time consuming, relatively inexpensive and more readily available, even for larger and/or difficult structures. The growth of crystal engineering has also coincided with advances in our understanding of intermolecular interactions, supramolecular chemistry, and the realization that several aspects of solid-state chemistry are of increasing relevance and can only be resolved with a better understanding of structure-function relationships.

1.1.1. *From Molecules to Crystal Engineering*

What is crystal engineering? The key to understanding the purpose of the discipline is to understand what is meant by the word “engineer”. The Oxford English Dictionary defines the term as: “1. *intr.* To act as an engineer. 2. a) *trans.* To employ the art of the engineer upon; to construct or manage as an engineer. b) *fig.* To arrange,

contrive, plan, superintend. Also (U.S.), to guide or carry through a measure or enterprise; to maneuver, (occas.) to 'shepherd'. 3. *fig. nonce-use*. To assail laboriously (*humorous*). Hence engi'neered ppl. a.; engi'neering ppl. a., that engineers, contriving, scheming." Key words such as *construct* or *manage*, and *arrange*, *contrive*, *plan*, or *superintend* underscore that crystal engineering involves the planned construction of a crystal, i.e. designing a crystal. Despite the apparent obviousness of the meaning based on the definitions of the component words, it is necessary to understand the motivation behind the discipline in order to truly understand how and why the field has flourished over the last decade.

In 1959, Richard Feynman provided what many practitioners have adopted as the crystal engineering "creed":

"What could we do with layered structures with just the right layers? What would the properties of materials be if we could really arrange the atoms the way we want them? They would be very interesting to investigate theoretically. I can't see exactly what would happen, but I can hardly doubt that when we have some *control* of the arrangement of things on a small scale we will get an enormously greater range of possible properties that substances can have, and of different things that we can do."¹

Such a dream generally remains to come to fruition, at least in terms of molecular self-assembly in the crystalline state. However, it has spawned and fuelled a seemingly exponential growth in research activity devoted to the subjects of crystal design and crystal engineering. Furthermore, the implications go beyond materials science since structure/function relationships in the solid state are of relevance to opportunities in the context of areas of interest that are as diverse as solvent free synthesis and drug design and development. Although it is commonly held that the term crystal engineering was first coined in a contribution by G.M.J. Schmidt concerning the subject of organic solid-

state photochemistry,² R. Pepinski was actually the first to introduce the term in 1955 in the context of designing ionic salts.³ Despite this earlier reference to the term, Schmidt's article remains as one of the seminal reports on crystal engineering and it marks an evolution in the way scientists thought about crystals and crystalline materials.

As implicit by use of the term crystal engineering, it became clear that, in appropriate circumstances, crystals could be thought of as the sum of a series of molecular recognition events, self-assembly, rather than the result of the need to avoid a vacuum, or achieve close packing. It has subsequently become clear that crystal engineering, especially in the context of organic solids, is intimately linked to concepts that have been developed in supramolecular chemistry, another field that has undergone explosive growth in recent years. Supramolecular chemistry, defined by Lehn as chemistry beyond the molecule,^{4,5} and "supramolecular assemblies" are inherently linked to the concepts of crystal engineering. In this context, crystals might be regarded as being single chemical entities, and as such are perhaps the ultimate examples of supramolecular assemblies or supermolecules. Dunitz has referred to organic crystals as "supermolecule(s) *par excellence*".^{6,7} As revealed herein, this interpretation is fully consistent with the approaches to crystal engineering practiced by ourselves and others who are presently active in the field.

Additionally, Schmidt's work emphasized that the physical and chemical properties of crystalline solids are as critically dependent on the distribution of molecular components within the crystal lattice as the properties of its individual molecular components. Therefore, crystal engineering has implications that extend well beyond materials science and into areas as diverse as pharmaceutical development and synthetic

chemistry. In the context of the former, there are important processes and intellectual property implications related to polymorphism.⁸⁻¹³ In the context of the latter, solid-phase organic synthesis can be solvent free and offer significant yield and regioselectivity advantages over solution phase reactions. In other words, crystals should not be regarded as chemical graveyards. To the contrary, it is becoming increasingly clear that binary or inclusion compounds can be used to effect a diverse range of thermal and photochemical reactions in the solid state,¹⁴⁻¹⁷ including some that cannot be effected in solution.¹⁸⁻²¹

Further advances were spawned by a series of papers and monographs in the 1980's by Desiraju²²⁻²⁴ and Etter²⁵⁻²⁷ that concentrated on using the Cambridge Structural Database²⁸ (CSD) for analysis and interpretation of noncovalent bonding patterns in organic solids. It should be noted that a considerable body of work devoted to the subjects of crystal nucleation, growth and morphology was developed concurrently. This research should be perhaps termed "engineering crystals". For more information on this area of research, the field is exemplified by the work of research groups such as Cohen,²⁹ Green,³⁰ Addadi,³¹⁻³⁵ Mann and Heywood,^{36,37} Thomas^{38,39} and Davey.^{40,41}

The seminal works by Desiraju and Etter in solid-state organic chemistry afforded the concept of *supramolecular synthons*²⁴ and led to hydrogen bonds being perhaps the most widely exploited of the noncovalent interactions in the context of crystal engineering. Their research programs addressed the use of hydrogen bonding as a design element in crystal design, and delineated the nature (strength and directionality) of the interaction. It is now readily accepted that these forces include weak hydrogen bonding interactions such as C-H...X and CH... π . Although Professor Desiraju continues his valuable contributions to the discipline, Professor Etter passed away prematurely in 1992.

1.1.2. Crystal Engineering vs. Crystal Structure Prediction

“One of the continuing scandals in the physical sciences is that it remains in general impossible to predict the structure of even the simplest crystalline solids from a knowledge of their chemical composition.”

This provocative comment by Maddox⁴² in 1988 illuminates an issue that continues to represent a challenge of the highest level of scientific and technological importance. However, it is important to stress the significant conceptual difference between crystal engineering and crystal structure prediction. In short, crystal structure prediction is precise (i.e. space group and exact details of packing are defined) and deals primarily with known molecules or compositions of molecules. Crystal engineering is less precise (e.g. network prediction) and most typically deals with entirely new phases, sometimes, but not necessarily, involving well-known molecules. Technological advances in experimental and computational methodology have accelerated the evolution of crystal engineering. In particular, the advent of CCD diffractometers facilitated the solution of crystal structures within hours or minutes rather than weeks or days and computational advances have made use of databases and visualization software inexpensive and straightforward. Therefore, although *ab initio* crystal structure prediction remains at best a significant challenge,⁴³⁻⁴⁸ even for small molecules, crystal engineering has been able to develop rapidly because its objectives are distinctly different from crystal structure prediction. The strategies of crystal engineering are fundamentally different from those of crystal structure prediction since the former is primarily concerned with design and, although more restrictive in terms of molecular components that might be employed, it is becoming increasingly synonymous with the concept of supramolecular synthesis of new solid-state structures. In other words, crystal

engineering represents a paradigm for synthesis of new solid phases with predictable stoichiometry and architecture. In contrast, predicting a crystal structure requires analysis of the recognition features of a molecular component in the context of how they will generate crystallographic symmetry operations that optimize lattice energies, i.e. it requires space group determination.

Engineering and design are far less restrictive from a conceptual perspective since they focus more broadly on the design of new and existing architectures. In effect, the principles of design are based on a blueprint, in many cases a blueprint that is first recognized *via* a serendipitous discovery, and they allow the designer to select components in a judicious manner. Therefore, a desired network structure or blueprint can be limited to chemical moieties, in many cases commercially available moieties that are predisposed to a successful outcome.

1.1.3. *Supramolecular Isomerism*

Closely related to the well-documented (but not necessarily well understood) subject of polymorphism in crystalline solids is the existence of supramolecular isomerism⁴⁹⁻⁵² in polymeric network structures. Supramolecular isomerism in this context is the existence of more than one type of network superstructure for the same molecular building blocks and is therefore related to structural isomerism at the molecular level. In other words, the relationship between supramolecular isomerism and molecules is similar to that between molecules and atoms. In some instances, supramolecular isomerism can be a consequence of the effect of the same molecular components generating different supramolecular synthons and could be synonymous with polymorphism. However, in other situations, supramolecular isomerism is the existence

of different architectures (i.e. architectural isomerism⁵³) or superstructures. In this context, the presence of guest or solvent molecules that do not directly participate in the network itself, especially in open framework structures, is important to note as it means that polymorphism represents an inappropriate term to describe the superstructural differences between network structures. Indeed, it is reasonable to assert that polymorphism can be regarded as being a type of supramolecular isomerism but not necessarily *vice-versa*. Pseudopolymorphism is a related term that has been coined to categorize solvates,^{54,55} especially in the context of pharmaceutical solids. Since solvent molecules are often integral parts of the resulting network structures, a pseudopolymorph is, at least from a supramolecular perspective, a binary phase and an entirely different class of compound.

Investigation of the relationship between supramolecular isomerism and polymorphism represents a fundamental scientific challenge. However, when one considers that bulk properties of solids are critically dependent on architecture and that crystal structure confirms composition of matter from a legal perspective, the applied relevance also becomes immediately apparent. Polymorphism in molecular crystals represents a phenomenon that is particularly important and ubiquitous in the context of pharmaceuticals and is receiving increasing attention from a scientific perspective.⁵⁶⁻⁶¹ It should also be noted that McCrone was prompted to suggest that the “*number of forms known for a given compound is proportional to the time and money spent in research on that compound*”.⁶² However, the generality of McCrone’s statement remains ambiguous despite indications that polymorphism is more general than expected from the CSD.⁶³ For example, Desiraju⁵⁵ has demonstrated that the frequency of occurrence of

polymorphic modifications is not necessarily uniform in all categories of substance. His analysis revealed that the phenomenon is probably more common with molecules that have conformational flexibility and/or multiple groups capable of hydrogen bonding or coordination. Coincidentally and importantly this is inherently the situation for many pharmaceuticals and conformational polymorphism is a subject in its own right.^{64,65} Desiraju also suggested that polymorphism can be strongly solvent-dependent. In summary, the relevance of polymorphism is clear but it remains a subject that is not fully or widely understood at a fundamental level.

Control over supramolecular isomers and polymorphs lies at the very heart of the concept of crystal engineering (i.e. design of solids). However, there is presently very little understanding concerning even the existence of supramolecular isomers, never mind how to control them. Supramolecular isomerism also lies at the heart of gaining a better understanding of supramolecular synthons and, by inference, how they develop and occur in other solid phases and even solution. The Cambridge Structural Database remains a very powerful tool in this context but it must be remembered that even such a large database will not necessarily be reflective of the full range of compounds that will be isolated and characterized in future years.

The conceptual link between polymorphism and supramolecular isomerism in organic and metal-organic networks is not immediately apparent. However, since polymorphs can be rationalized on the basis of supramolecular interactions, polymorphism can be regarded as a type of supramolecular isomerism. Implicitly, all sets of polymorphs can therefore be regarded as being supramolecular isomers, but the reverse is not necessarily the case. It should also be noted that solvates are almost always

different compounds from a crystal engineering perspective. The only exception would be in the case of inclusion compounds where the host framework remains intact in the presence of different solvent molecules, i.e. the solvent serves the function of being a guest molecule. Supramolecular isomerism as seen in metal-organic and organic networks has been classified based on analogies drawn with isomerism at the molecular level. The following classes of supramolecular isomerism have been proposed:⁵²

Structural: the components of the network (i.e. the metal moiety and the ligands the or exofunctional organic molecule) remain the same but a different superstructure exists.⁴⁹ In such a situation, the networks are effectively different compounds even though their empirical formula and chemical components are identical;

Conformational: conformational changes in flexible ligands such as bis(4-pyridyl)ethane generate a different but often related network architecture.⁴⁹

Conformational polymorphism is a closely related subject.^{64,65}

Catenane: The different manner and degrees in which networks interpenetrate or interweave can afford significant variations in overall structure and properties depending on the molecular building blocks that are utilized.⁶⁶ Interpenetrated and non-interpenetrated structures are effectively different compounds because their bulk properties will be so different.

Optical: Networks can be inherently chiral and can therefore crystallize in chiral (enantiomorphic) space groups. Therefore, an analogy can be drawn with homochiral compounds. This type of supramolecular isomerism lies at the heart of an important issue: spontaneous resolution of chiral solids.⁶⁷⁻⁷³

In the context of this body of work, it is necessary to define another type of supramolecular isomerism:

Spatial: Where the same supramolecular network (either discrete, 1-D or 2-D; note that this type of isomerism is not possible for 3-D networks) has alternate arrangements in space (i.e. they pack/stack differently). This is closely related to catenane supramolecular isomerism, where networks pack such that they are intercalated (3-D networks are capable of catenane isomerism). Spatial supramolecular isomerism specifically describes different packing arrangements where there is no catenation (i.e. intercalation).

The results that are discussed in later chapters have been limited to metal-organic coordination polymers, and no effort has been made to discuss organic solids. However, it should be noted that the subject matter is divided along these lines for convenience only since the basic concepts apply equally well to both classes of compound, and the design of organic solids remains a major goal of the Zaworotko research group.

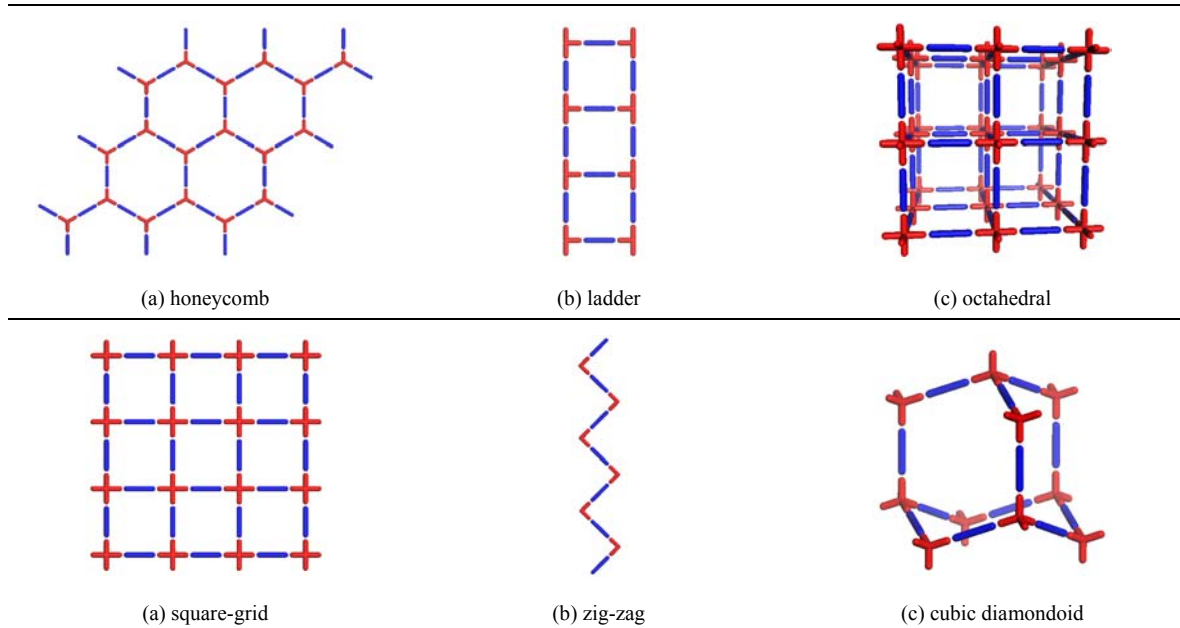
1.2. Coordination Polymer Examples

Coordination polymers exemplify how crystal engineering has become a paradigm for the design of new supramolecular structures. In this context, the work of Wells is exhaustive and seminal and can serve as a reference point. Wells was primarily concerned with the overall structure of solids, particularly inorganic compounds.^{74,75} He defined crystal structures in terms of their topology by reducing them to a series of points (nodes) of a certain geometry (tetrahedral, trigonal planar, etc.) that are connected to a fixed number of other points. The resulting structures, which can also be calculated

mathematically, can be either discrete (zero-dimensional) polyhedra or infinite (one-, two-, and three-dimensional) periodic nets.

It is perhaps surprising that it took until the 1990's for the approach of Wells to bear fruit in the laboratory. Robson⁷⁶⁻⁸³ was primarily responsible for the initial studies that facilitated rapid development of the field of coordination polymers alongside that of crystal engineering of organic solids. Robson extrapolated Wells work on inorganic network structures into the realm of metal-organic compounds and coordination polymers. In this context, the resulting “node and spacer” approach has been remarkably successful at producing predictable network architectures. Figure 1.1 illustrates some of the simplest architectures that can be generated by using commonly available metal moieties and linking them with linear “spacer” ligands. Whereas diamondoid networks represent a class of structure that could be described as mineralomimetic because there are many naturally occurring analogues, that is not the case for any of the other architectures illustrated in Figure 1.1.

Figure 1.1: Common/simple metal-organic network architectures



It should be noted that additional structures could result from the combination of components identical to those illustrated in Figure 1.1, and would thus represent examples of supramolecular isomers. Such structures are of interest for both conceptual reasons and because of their interesting properties. They are ideally suited to illustrate the concepts of crystal engineering for the following reasons:

The diversity of structures that can be obtained from the simplest of components is quite remarkable, not only in the context of coordination polymers but also organic solids and even, for that matter, discrete architectures.

Coordination polymers can be relevant in the context of inclusion chemistry. As should be clear from Figure 1.1, a recurring feature of even the simplest network structures is the presence of voids or cavities that are inherently present because of the architecture itself and the dimensions of the spacer ligands. This feature is attracting considerable interest and there are a number of recent reports concerning open framework coordination polymers that exhibit hitherto unprecedented levels of porosity and high levels of thermal stability. Indeed, there already exists a diverse range of coordination polymers with higher effective surface areas than zeolites and stability to loss of guest.⁸⁴⁻

94

From a design perspective, it should be clear from Figure 1.1 that each of the networks illustrated is based on at least two components (i.e. the node and the spacer) and, as will become clear herein, such components can be preselected for their ability to self-assemble. The network structures can therefore be regarded as examples of blueprints for the construction of networks that, in principle, can be generated from a diverse range of chemical components, i.e. they are prototypal examples of modular

frameworks. It should be noted that the construction of networks from single component systems also represents an important area of activity. Self-assembly of a single molecular component, or “molecular tectonics”, represents a different approach to crystal design and it must be remembered that most existing crystal structures are based on a single component. However, in order for single component self-assembly to be directly relevant in the context of crystal engineering, all the molecular recognition features that lead to supramolecular synthons must be present in a single molecule. 1,3,5,7-adamantanetetracarboxylic acid^{95,96} and methanetetracarboxylic acid⁹⁷ can be regarded as being prototypical for self-assembled diamondoid architectures. Both structures are sustained by one of the most well recognized supramolecular synthons – the carboxylic acid dimer.⁹⁸ Pyridone dimers have been used in a similar fashion to build diamondoid networks, in this case from tetrahedral tetrakispyridones.⁹⁹ A number of well-known inorganic structures can also be regarded as examples of self-assembly (e.g. ice, potassium dihydrogenphosphate) and one might even consider covalent bonds as conceptually related: diamond, Si, Ge, ZnS, BP, GaAs, ZnSe, CdS, CuInSe₂, CuFeS₂ (chalcopyrite). However, this section primarily focuses on the modular or multi-component approach to crystal design. Coordination polymers with multiple complementary components can be regarded as being the consequence of modular self-assembly.¹⁰⁰

The remainder of this section will be organized according to the dimensionality of the observed structures. However, it should be stressed that the modular self-assembly approach applies equally well to all levels of dimensionality since the dimensionality is often determined directly by the node. Therefore it is appropriate to include discrete 0-D structures in the discussion.

1.2.1. 0D (Discrete) Architectures

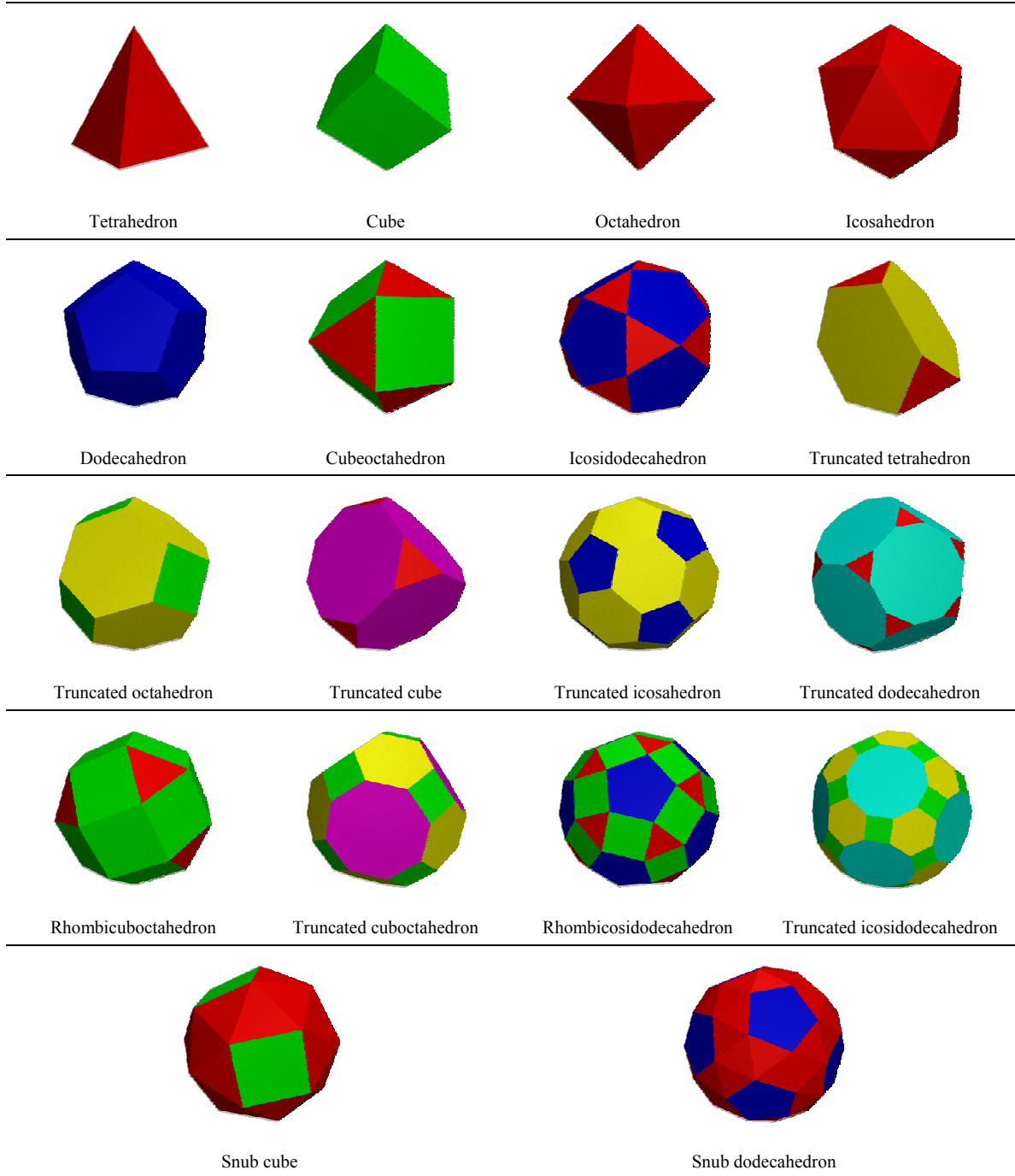
In addition to research that has focused on infinite structures, the principles of self-assembly have also been applied towards the design and isolation of discrete molecular structures. Such structures are exemplified by molecular squares^{11,101-118} and, more recently, by striking examples of new high molecular weight compounds that can be described as spheroid architectures.¹¹⁹⁻¹³⁹ The design principles behind the isolation and development of these new classes of compound are based on the concept of self-assembly in the context of geometric considerations found in regular (Platonic) and semi-regular (Archimedean) solids. Such structures are also known in zeolites (e.g. Linde A, which is based on an edge-skeleton generated by fused truncated octahedra¹⁴⁰) and in biological self-assembled systems such as mammalian picornaoviruses¹⁴¹⁻¹⁴³ and proteins.¹⁴⁴ The 5 Platonic and 13 Archimedean solids¹⁴⁵ are illustrated in Figure 1.2.

They can be constructed at the molecular level by sharing of the edges of molecular moieties that have the shape of regular polygons,¹²⁸ i.e. triangles, squares, pentagons, hexagons and octagons, or by connecting molecular vertices with linear bifunctional rod-like ligands.^{110,122} In the case of the former, closed convex surfaces are generated whereas for the latter all the faces are open windows. This subject is highly topical and several recent review articles have appeared.^{110,122,124,127,146}

The primary purpose of highlighting such structures is that they have been developed using the same principles as those used for generating the infinite structures described herein. Structures such as molecular squares are in effect supramolecular isomers of some of the infinite 1D structures described herein. In this context, it is

perhaps appropriate to consider such materials as being monodisperse coordination polymers in the same way that dendrimers are considered monodisperse polymers.

Figure 1.2: Platonic (regular) and Archimedean (semi-regular) solids



1.2.2. 1D Coordination Polymers

The range of structures that has thus far been observed in coordination polymers, in particular network structures that have been observed for some of the simplest building blocks and stoichiometries exemplifies structural supramolecular isomerism.

Figure 1.3: Supramolecular isomers from the assembly of 90° ditopic nodes

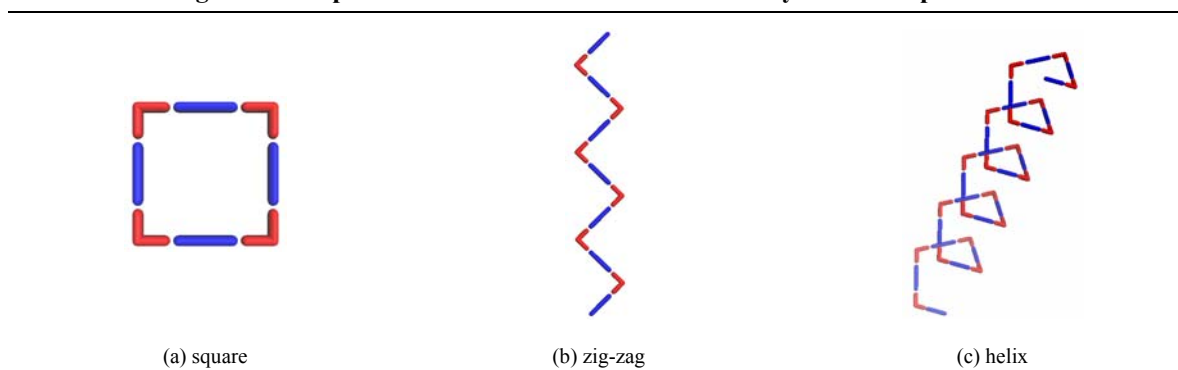


Figure 1.3 illustrates the possible structures that can result from self-assembly of either a *cis*-octahedral or a *cis*-square planar metal and a linear “spacer” ligand. There are three obvious architectures that might result and they are dramatically different from one another. The “square box” or “molecular square” architecture represents a discrete species that has been developed extensively in recent years by the groups of Fujita,¹¹⁶ Stang^{11,110,112-114,117,122,130} and Hupp.^{102,104-106,108,111,147} The other two architectures are both examples of 1D coordination polymers but they are quite different from one another. The zigzag polymer¹⁴⁸⁻¹⁵⁸ has been fairly widely encountered and such structures tend to pack efficiently and eschew open frameworks or cavities. The helix¹⁵⁹⁻¹⁷⁰ remains quite rare in the context of coordination polymers but there is added interest because it is inherently chiral, regardless of what its components might be. The inherent chirality of this architecture comes from spatial disposition rather than the presence of chiral atoms, thereby illustrating an important aspect of the solid state: it is possible for achiral

molecules to generate chiral crystals. In order to illustrate the potential for generation of chiral architectures from simple achiral building blocks, let us consider how one might design a homochiral crystal from simple molecular components.

There would appear to be at least four strategies for the design of polar crystals that are independent of the need for homochiral molecular components:

1. Achiral building blocks that crystallize in a chiral space group.
2. Achiral molecular building blocks to build a chiral framework.
3. Achiral host framework built from achiral molecular components with chiral guest(s).
4. Achiral host framework built from achiral molecular components with achiral guest(s).

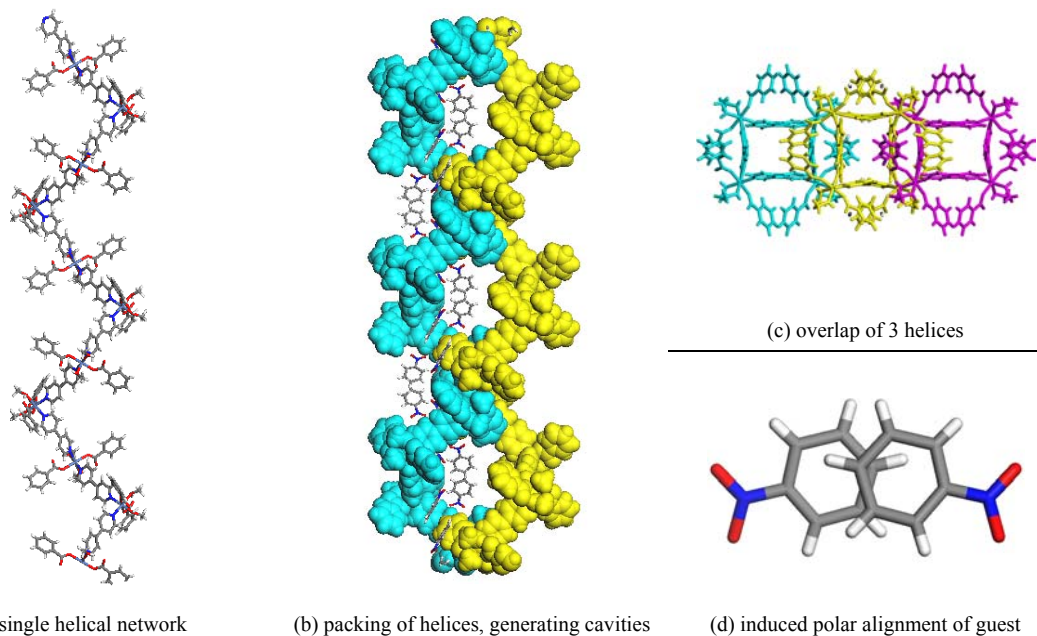
Whereas exploitation of homochiral components represents the most obvious approach because the absence of a crystallographic center of inversion is guaranteed, it in no way implies or affords any control over molecular orientation and, therefore, bulk polarity. Furthermore, reliance on the use of pure enantiomers raises the substantial problem of requiring control over stereochemistry at the molecular level without yet solving the problem of controlling stereochemistry at the supramolecular level. Indeed, strategy 1, which basically relies on serendipity, offers just as much chance of optimal control of crystal packing as the use of homochiral components. However, there are three types of polar architecture that do not need to be sustained by homochiral molecular components: helical networks^{161,165,166,171-178}; 1D acentric networks sustained by head-to-tail stacking of complementary molecules¹⁷⁹⁻¹⁸⁷; host-guest networks which are polar because of the presence of acentric guest molecules or guest aggregates.^{73,188,189}

Although the crystallization process for strategies 1-4 can inherently afford homochiral single crystals, only the use of homochiral components guarantees that all crystals in a batch will be of the same enantiomorph. Batches of crystals will often be heterochiral as both enantiomers tend to be formed equally during crystallization. Fortunately, it has been demonstrated that formation of homochiral bulk materials can be afforded by seeding with the desired enantiomer.¹⁶⁵

$[\text{Ni}(\text{bipy})(\text{benzoate})_2(\text{MeOH})_2]^{166}$ (bipy = 4,4-bipyridine), Example 1, illustrates the issues raised above. Example 1 self-assembles as a helical architecture that is sustained by linking of octahedral metal moieties with linear spacer ligands. Furthermore, it persists in the presence of several guests, even if 4-hydroxybenzoate ligands (i.e. ligands that are capable of forming strong hydrogen bonds) are employed. The crystal structure of the nitrobenzene clathrate is presented in Figure 1.4 and reveals the presence of large chiral cavities that induce the guest molecules to form chiral dimers. The guest molecules are trapped in a closed environment since helices from adjacent planes close off the 500 \AA^3 cavities. The helical chains generated by Example 1 pack such that they are staggered but they align in a parallel fashion. Therefore the bulk crystal is polar as every helix in an individual crystal is of the same handedness. Example 1 illustrates the attractiveness of self-assembly and crystal engineering for generation of polar architectures. In particular, there is no prerequisite for homochiral molecular components and host guest compounds have the potential to be modular and fine-tunable since the guest molecule might be used to impart functional properties. It should also be stressed that, at least in principle, all existing achiral moieties can be incorporated into polar structures. The problem that has yet to be solved is how reliably

and predictably to avoid crystallographic centers of inversion and how to control alignment of molecular dipoles.

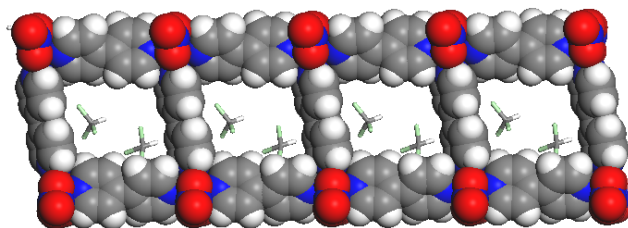
Figure 1.4: Crystal structure of $\{[\text{Ni}(\text{bipy})(\text{benzoate})_2(\text{MeOH})_2] \cdot \text{PhNO}_2\}_n$



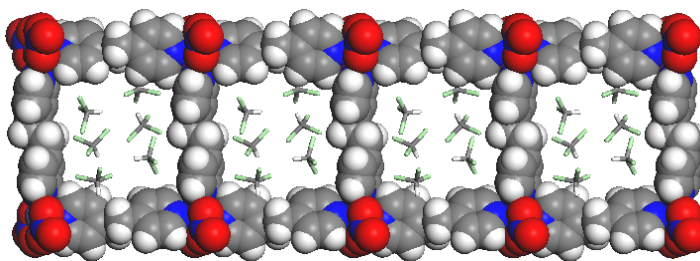
Another example of a coordination polymer that self-assembles into a helical architecture is represented by the result of complexation of a 2,2'-bipyridine based exo-ditopic macrocyclic ligand with Ag^+ cations. The single strand helical assembly is one of four possible arrangements and contains channels that run through the center of the assembly. These channels contain acetonitrile solvent molecules. The helices align anti-parallel with respect to each other and, therefore, a racemic mixture of the right- and left-handed helices is obtained.¹⁶⁷

Molecular ladders represent another type of 1D coordination polymer.^{67,101,190-197} They differ in two important ways from molecular chains and helices. Most obviously, their stoichiometry is different since they are the result of self-assembly of 1.5 spacer ligands per metal. Therefore, the molecular building unit is effectively a “T-shape”

Figure 1.5: Molecular ladders



(a) Crystal structure of $\{[\text{Co}(\text{bipy})_{1.5}(\text{NO}_3)_2] \cdot 2\text{CH}_3\text{Cl}\}_n$



(b) Crystal structure of $\{[\text{Co}(\text{bipyeta})_{1.5}(\text{NO}_3)_2] \cdot 3\text{CH}_3\text{Cl}\}_n$

moiety. Second, they necessarily contain cavities within the individual molecular ladders. These cavities are determined by the length, shape and orientation of the spacer ligand. Simple examples of molecular ladders are represented by the coordination polymers $[\text{M}(\mu\text{-L})_{1.5}(\text{NO}_3)_2]_n$ ($\text{L} = \text{bipy}$,¹⁹⁸ 2a, or bis(4-pyridyl)ethane),⁴⁹ 2b). Examples of these structures (examples 2 and 3) are illustrated in Figure 1.5, which reveals how they contain cavities that are large enough to sustain individual or pairs of molecules. The cavities are hydrophobic in nature and their diagonal dimensions are defined by M-M separations of ca. 16 and 19 Å, respectively. This means that the effective dimensions of the cavities are ca. 13 and 16 Å, respectively.

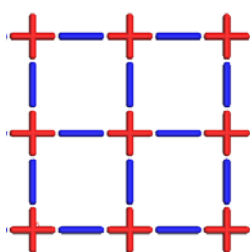
1.2.3. 2D Coordination Polymers

The strategy of exploiting known coordination geometries of metals to propagate 2D structures via coordination with linear bifunctional spacer ligands has yielded many examples of coordination polymers with various metal moieties and architectures. The

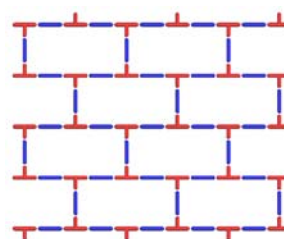
ratio of metal and ligand, and the nature of the coordination of terminal ligands (i.e. degree of chelation) are the primary factors that determine the topology of the network. Figure 1.6 illustrates some of the 2D network structures that have thus far been observed in coordination polymers.

Square grid networks exemplify a particularly simple and commonly reported example of a predictable 2D metal-organic network. Square grid coordination polymers are based on 1:2 metal:ligand complexes with linear bifunctional spacer ligands. They were first reported using cyano ligands¹⁹⁹⁻²⁰² and have recently been expanded in terms of chemical type and cavity size to include pyrazines,²⁰³⁻²⁰⁵ bipy^{86,206-211} and longer analogues of bipy.^{209,212} These compounds can be regarded as being analogues of clays since they would be expected to have the ability to intercalate guest molecules. However, they have added features that are not likely to be present in clays. For example, cavities lie within the plane of the structure. These cavities are suitable for either interpenetration or enclathration of a possibly wide range of organic guest molecules. There also exists

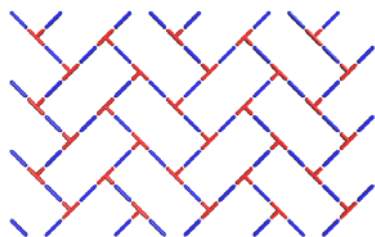
Figure 1.6: 2-D architectures observed in coordination polymer networks



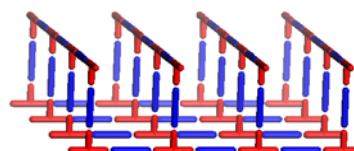
(a) 4^4 square grid



(a) 6^3 brick-wall



(a) 6^3 herringbone



(a) $\frac{1}{2}$ of the bilayer architecture

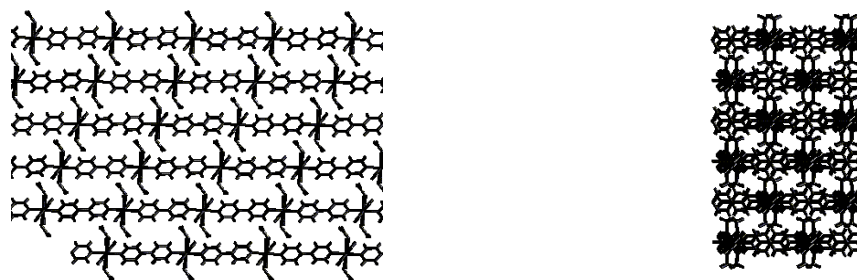
potential for incorporating catalytically active sites into such structures.⁷⁸ Furthermore the cavities are tunable as the length and width of the spacer ligand controls the size of the cavities that occur within the polymeric structure, although interpenetration can mitigate against the existence of frameworks with very large cavities.⁶⁶

Open framework square grid networks generated with bipy spacer ligands were first reported by Fujita *et al.*⁷⁸ Fujita's structures are based on Cd(II) and other examples have subsequently been reported based on a number of other transition metals, including Co(II) and Ni(II) and Zn(II). Although these 2D coordination networks are isostructural within the coordination grid (effective dimensions of the diagonals are ca. 13 x 13 Å), the crystal structures of compounds can differ in the manner in which the networks stack with respect to each other (interlayer separations range from 6-8 Å).

The compounds $[M(\text{bipy})_2(\text{NO}_3)_2] \cdot \text{guest}$ (M = Co, Ni) have been studied extensively²¹³ by Zaworotko, *et al.*, and they report three basic spatial supramolecular isomers (Figure 1.7).

Type A compounds crystallize with similar cell parameters (monoclinic C2/c; a=21.5, b=11.5, c=13; $\beta=102^\circ$), have 2:1 guest:host stoichiometry and interplanar separations of ca. 6 Å. The crystal packing appears to be influenced by C-H...O hydrogen bond interactions between the bipy ligands of one square grid and the nitrate anions of adjacent square grids. The square grids do not align with a unit cell face and adjacent grids are slipped in one direction by ca. 20%, i.e. every sixth layer repeats. The crystal packing of Type B compounds is also controlled by weak interactions between adjacent layers. They generally crystallize with 2.5 guest molecules per metal center and cell parameters are fairly consistent (monoclinic P2₁/c; a=16, b=14.75, c=16; $\beta=100^\circ$).

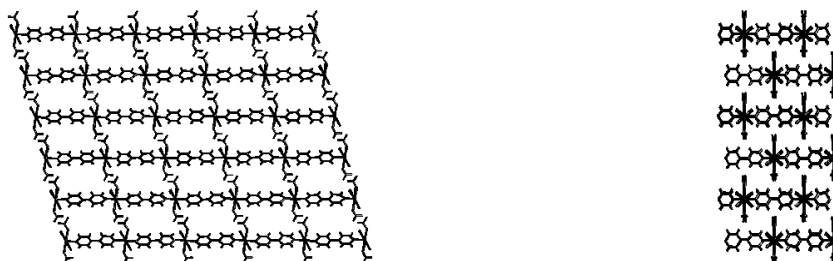
Figure 1.7: Spatial supramolecular isomers of $[M(\text{bipy})_2(\text{NO}_3)_2]$ square grids



(a) Type A grids viewed along [100] and [001] (reorienting the structure so that [001] is the stacking axis)



(b) Type B grids viewed along [100] and [001] (reorienting the structure so that [001] is the stacking axis)



(c) Type C grids viewed along [100] and [001] (reorienting the structure so that [001] is the stacking axis)

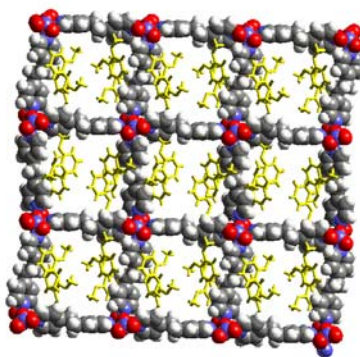
The interlayer separation is ca. 8 Å. Type C compounds have interlayer separations that are similar to those seen for Type B compounds. Four examples of type C compounds have 3:1 stoichiometry: three crystallize in space group $C2/c$ (monoclinic; $a=16$, $b=11.5$, $c=23$; $\beta=100^\circ$), the other crystallizes in space group Cc . The latter compound exhibits similar cell parameters except that there is a tripling of the a -axis and the cell volume. Another example of a type C grid crystallizes in space group Pn (monoclinic; $a=11.4$, $b=22.8$, $c=15.9$; $\beta=93.3^\circ$). Although these cell parameters are inconsistent with the previous four structures, the packing of the grids is appropriate for type C grids. The

positioning of the grids facilitates inclusion of one guest molecule in the center of each grid. The other guest molecules lie between the grids and engage in stacking interactions between the bipy ligands and themselves.

In all of these compounds the proportion of the crystal that is occupied by guest molecule is ca. 50% by volume. In such a situation it becomes reasonable to question whether interactions between the guest molecules determine the cavity shape and crystal packing of the square grid polymers rather than *vice-versa*. This issue is addressed later.

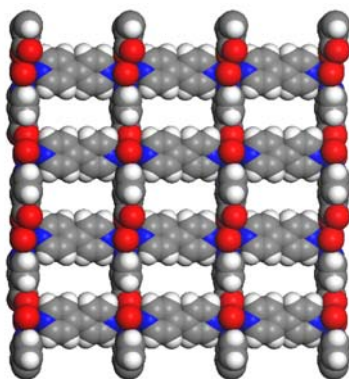
As these square grid architectures are inherently modular, it should be possible to extend their dimensions by simply using longer spacer ligands. An example of such a structure, $[\text{Ni}(\text{1,2-bis(4-pyridyl)ethane})_2(\text{NO}_3)_2]_n \cdot 2 \text{ veratrole}$, is illustrated in Figure 1.8. This structure has grid dimensions ca. 20% larger than the smaller grids (diagonal dimensions are ca. 16 x 16 Å) large enough to enclathrate more than one aromatic guest. Larger grids (ca. 20 x 20 Å) have also been reported using tetra(4-pyridyl)porphyrin.²¹⁴

Figure 1.8: $[\text{Ni}(\text{1,2-bis(4-pyridyl)ethane})_2(\text{NO}_3)_2]_n \cdot 2 \text{ veratrole}$



Grids in which there are two types of spacer ligand have also been reported.^{211,215} Figure 1.9 reveals the structure of such a compound, which is appropriately termed a rectangular grid.

Figure 1.9: $[\text{Co}(\text{pyca})(\text{bipy})(\text{H}_2\text{O})_2]_n \cdot (\text{NO}_3)_n \cdot (\text{bipy})(\text{H}_2\text{O})_{1.5}$

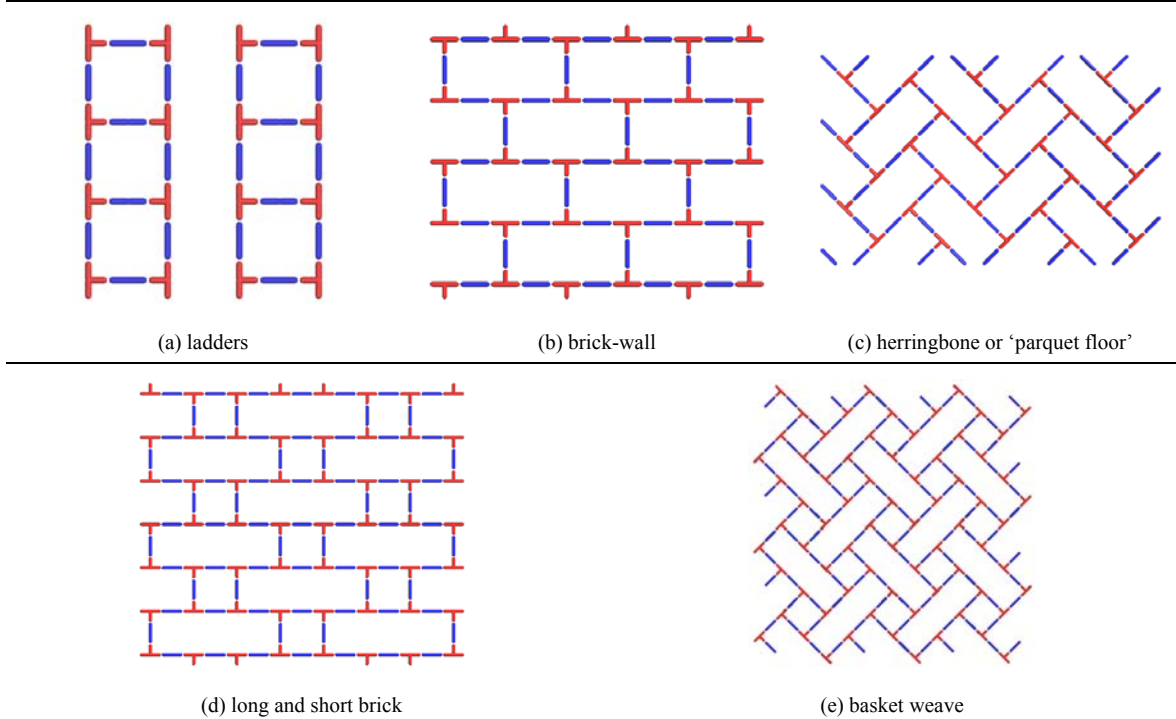


Another metal geometry or node that is of particular interest because of its potential range of supramolecular isomers is the T-shaped geometry, i.e. a *mer*-substituted octahedral metal moiety or a trisubstituted square planar metal moiety with 1:1.5 metal : spacer ligand ratio. This node has thus far produced examples of 1D, 2D and 3D networks. Three distinct 2D supramolecular isomers have already been reported: brick wall,^{86,190,192,216-221} herringbone^{86,222-224} and bilayer.²²⁵⁻²²⁸ It is interesting to note that, if one calculates the possible tiling patterns (i.e. all points lie in the same plane) that are possible for T-shaped nodes (Figure 1.10), only 3 of the 5 possibilities have already been realized.

The brick architecture (1.10b) is observed as the product of the reaction between heptacoordinate Cd(II) and 1,4-bis((4-pyridyl)methyl)-2,3,5,6-tetrafluorophenylene.⁷⁸ The T-shape geometry is the result of two terminal nitrate ligands chelating in a bidentate manner, thereby occupying 4 of the 7 coordination sites. The structure is triply interpenetrated and, as such, does not possess channels or cavities. In a similar system using the non-fluorinated pyridyl based ligand, a 1D ladder structure (1.10a) was observed. The brick architecture was also seen in $[\text{Ni}(4,4'\text{-azopyridine})_{1.5}(\text{NO}_3)_2]_n$,

which interpenetrates with two perpendicular $[\text{Ni}(4,4'\text{-azopyridine})_2(\text{NO}_3)_2]_n$ square grid networks.²²⁰

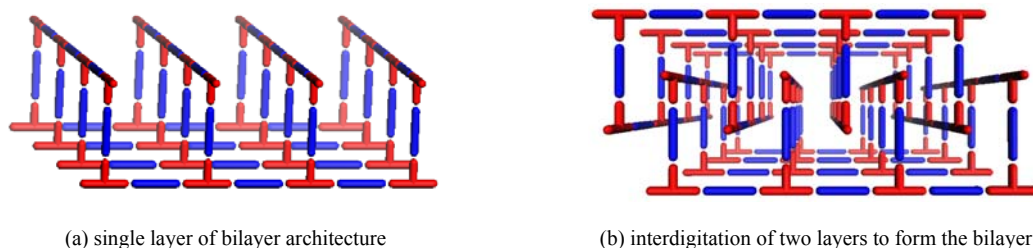
Figure 1.10: 2-D topologies predicted for coordination polymer networks based on T-shaped nodes



The herringbone or 'parquet floor' architecture (1.10c) has recently been observed by several groups.^{216,222,223} In these structures, the coordination sphere is similar to that of the brick architectures: heptacoordinate Cd(II) or Co(II), with two terminal bidentate nitrate ligands and coordination to one end of three 4,4'-azopyridine bridging ligands; an isostructural example has also been reported with 1,2-bis(4-pyridyl)ethyne as the bridging ligand.²²⁶

Another two-dimensional structure that can result from the assembly of T-shaped nodes is the bilayer architecture (Figure 1.11), which has a finite third-dimension and was therefore not predicted when the points were constrained to lie in a plane. The bilayer architecture has been observed in at least three compounds.²²⁵⁻²²⁷ It has been observed as

Figure 1.11: Bilayer architecture for T-shaped nodes



the product from the reaction of $\text{Co}(\text{NO}_3)_2$ and bipy, which also generates ladder, square grid and herringbone architectures. The bilayer form of $[\text{Co}(\text{bipy})_{1.5}(\text{NO}_3)_2]$ is observed if crystallization occurs in the presence of CS_2 or H_2O . The bilayers pack by partial interdigitation, which allows 1D channels to run through the structure (Figure 1.11b). This structure is particularly relevant since it represents one of the first reported examples of a compound that might be termed a “metal-organic zeolite”, i.e. the structure is porous and stable to loss of guest.²²⁷ The bilayer architecture has also been reported for systems using 1,2-bis(4,-pyridyl)ethane.²²⁹

The number of supramolecular isomers already observed in the $\text{Co}(\text{NO}_3)_2/\text{bipy}$ system indicates how important selection of template and crystallization conditions are. It seems reasonable to assert that it is only a matter of time and effort before the long-and-short brick (1.10d) and weave (1.10e) motifs illustrated in Figure 1.10 will also be realized.

In terms of topology, it should be noted that brick and herringbone motifs are both examples of 6^3 -nets and can therefore be regarded as being closely related to honeycomb 6^3 -nets.⁷⁵ Honeycomb networks are quite common in organic structures because of the availability of trigonal nodes (i.e. 1,3,5-trisubstituted benzenes such as trimesic acid and species such as the guanidinium cation) but they seldom occur in the context of metal-organic polymers because trigonal and trigonal bipyramidal coordination geometries are

rare. However, $[\text{Cu}(\text{pyrazine})_{1.5}]\text{BF}_4^{230}$ is based on trigonal Cu(I) and it should therefore be unsurprising that it crystallizes as a honeycomb 6^3 -net. That there now exist a number of ligands with trigonal geometry^{110,122,124,128,133,135,231-237} means that it is likely that a wider range of honeycomb structures will be generated in the near future.

1.2.4. 3D Coordination Polymers

It might be anticipated that the challenge of designing 3D network architectures represents an added level of complexity in comparison with 2D architectures and it in many ways represents the ultimate challenge to crystal engineers since it leads most directly to crystal structure control and prediction. For example, in most situations, a finite number of structural isomers can be calculated if all nodes must lie in the same plane. However, a larger number of possibilities might exist when that limitation is relaxed. It is therefore perhaps ironic that 3D networks generated via self-assembly of tetrahedral or octahedral nodes exemplify two of the simplest examples of predictable networks.

Tetrahedral nodes are predisposed to generate diamond-like (diamondoid) architectures, whereas octahedral nodes are expected to afford octahedral networks. These architectures can be obtained for both organic (typically hydrogen bonded) and metal-organic (i.e. coordination polymer) systems. Interpenetration can occur in these compounds, thereby mitigating against enclathration and porosity. However, interpenetration can also be exploited as a potentially important design paradigm for rational transformation of some of the 2D networks described earlier into 3D frameworks. This principle is discussed in a later section with respect to interpenetration

of identical networks (homocatenation), and interpenetration of different networks (heterocatenation).

The diversity of components that is available for crystal engineering of diamondoid networks and the means by which they self-assemble spans the full range of chemistry. The breadth of chemical moieties that might be used for crystal engineering is particularly well illustrated by the range of diamondoid networks that have been reported in recent years. Diamondoid architectures using a tetrahedral metal (Zn or Cd) as the node and cyanide ligands (CN⁻) as the spacer represent prototypical examples of diamondoid coordination polymers. Zn(CN)₂ and Cd(CN)₂ form diamondoid networks with 2-fold interpenetration.^{79,81-83} However, Cd(CN)₂ can also be obtained as a single network with CCl₄ filling the cavity.⁷⁹ This result illustrates two principles that have broad implications for crystal engineering: interpenetration can be avoided in the presence of an appropriate template or guest molecule; such compounds might be regarded as catenated and non-catenated supramolecular isomers of each other.

A diamondoid architecture also results when Zn(CN)₄²⁻ is reacted with Cu(I). The resulting anionic network might be viewed as consisting of tetrahedral zinc nodes that are linked to tetrahedral copper nodes by cyanide spacers. However the nature of coordination at the copper and zinc ions remains ambiguous. Analysis of the structural data indicated that it is most appropriate to consider the coordination of the copper as 100% organometallic (Cu-C) and the coordination of the zinc 100% metal-organic (Zn-N). The ionic nature of this particular framework means that the presence of a counter ion in the resulting cavities is required. N(CH₃)₄⁺ fits comfortably inside the adamantoid cavity and precludes interpenetration.

A report²³⁸ on the crystal structure and properties of [Cu(2,5-dimethylpyrazine)₂(PF₆)] represents one of the first examples of a metal-organic diamondoid structure and the related compound [Cu(4,4'-bipy)₂(PF₆)] was reported shortly thereafter.²³⁰ Both structures exemplify the modular assembly design strategy and contain anions in the cavities generated by the diamondoid structure. In the case of the latter, the intermetallic separations are 11.16 Å and result in cavities that are sufficiently large to facilitate 4-fold interpenetration as well as inclusion of the counter ions. A diamondoid architecture propagated by silver(I) and bipy, ([Ag(4,4'-bipy)₂](CF₃SO₃)), was reported²³⁹ shortly thereafter and it also exhibits 4-fold interpenetration with anions in cavities. The Ag-Ag separations are 11.6 Å. The 4-cyanopyridine analogue was reported in the same article and exhibits metal-metal separations of 9.93 Å. Despite the variations observed in the dimensions of these networks, both exhibit 4-fold levels of interpenetration.

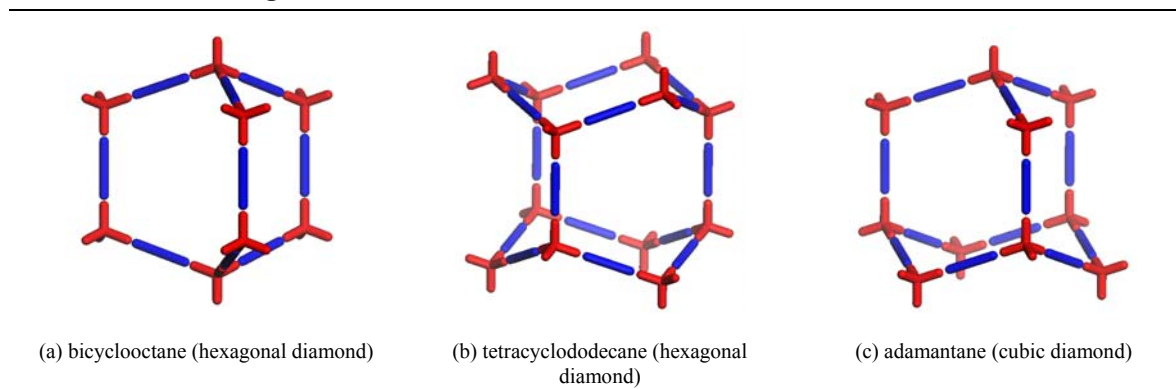
Subsequent studies resulted in a plethora of diamondoid metal-organic structures and 2-, 3-, 4-, 5-, 7-, and 9-fold levels of interpenetration.²⁴⁰⁻²⁴² It should be noted that, although interpenetration reduces or eliminates porosity, there are at least two important properties that can be addressed with such structures: they are predisposed to form acentric networks since there is no inherent center of inversion at a tetrahedral node (i.e. an odd level of interpenetration and an unsymmetrical ligand will necessarily generate a structure that exhibits polarity¹⁰⁰); these structures could be useful for selective anion exchange.

In the context of the former, a series of neutral diamondoid architectures have been prepared with bridging ligands of varying size.^{82,230,242-244} These compounds are of

general formula ML_2 ($M=T_d$ metal; L = bridging anionic ligand) and it follows that a neutral network will be generated if a +2 metal is coordinated to two -1 anionic ligands. $Zn(\text{isonicotinate})_2$ and $Cd(\text{trans-4-pyridylacrylate})_2$ exhibit 3- and 5-fold degrees of interpenetration respectively and possess interesting properties in the context of polarity.²⁴⁵ In the former compound, the Zn-Zn distance is ca. 8.8 Å. This is consistent with the previous structures that exhibit 4-fold interpenetration. The Cd-Cd distance is ca. 11.5 Å, similar to the intermetallic distances observed in the 4-fold interpenetrated structures that also contain counterions.

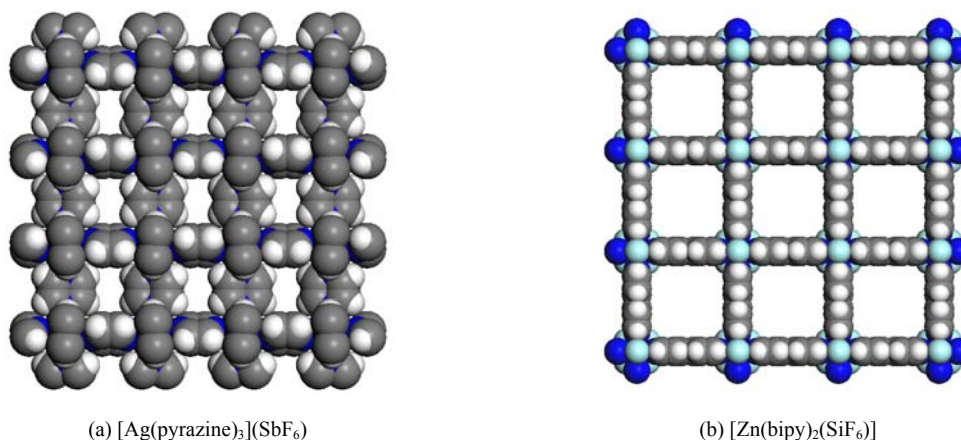
It is interesting to note that all diamondoid coordination polymers observed to date have possessed the cubic diamondoid structure. It is, perhaps, surprising that there have been no reports of the hexagonal diamond architecture. The two networks have identical predicted densities, geometric strain and lattice energies. One notable difference is that hexagonal diamond has two types of cavity (illustrated in Figure 1.12a-b), and as such this system is closely related to the two-dimensional networks based on T-shaped nodes where the long-and-short brick and basket weave topologies have not yet been reported.

Figure 1.12: Basic structural units of diamondoid architectures



Octahedral networks are also a common and obvious synthetic target. Prototypical examples of octahedral networks are exemplified by iron cyano compounds. Such compounds are very well documented and they have been used for centuries as pigments. An early X-ray study²⁴⁶ of Berlin Green, $[\text{Fe}^{\text{III}}\text{Fe}^{\text{III}}(\text{CN})_6]$, Prussian Blue, $[\text{KFe}^{\text{II}}\text{Fe}^{\text{III}}(\text{CN})_6]$, and Turnbull's Blue, $[\text{K}_2\text{Fe}^{\text{II}}\text{Fe}^{\text{II}}(\text{CN})_6]$, demonstrated that the iron cations act as the node in octahedral arrays in which they are linked by linear cyano ligands. These compounds form isostructural networks that vary only in the degree of potassium inclusion and the oxidation states of the iron atoms. Berlin Green can therefore be regarded as being the prototypical example of an open framework octahedral network, however, the limited length and lack of chemical versatility of the cyano ligand means that it has little relevance in the context of porosity.

Figure 1.13: Octahedral networks

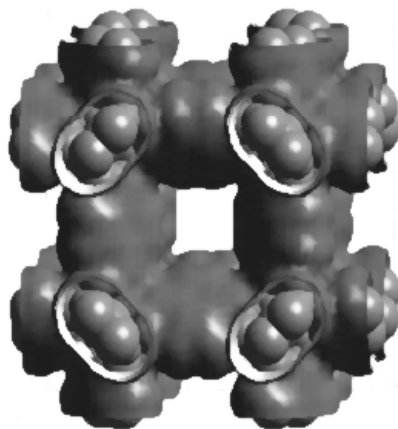


Synthetic metal-organic octahedral networks were first reported in 1995. $[\text{Ag}(\text{pyrazine})_3](\text{SbF}_6)$ ²⁴⁷ is sustained by octahedral Ag(I) cations and relatively short pyrazine ligands. The framework is necessarily cationic and is illustrated in Figure 1.13a. A neutral analogue is exemplified by $[\text{Zn}(\text{bipy})_2](\text{SiF}_6)$.²⁰⁷ In this structure (Figure 1.13b), the SiF_6^{2-} counterions cross-link the square grids that are formed by Zn and bipy

to form a rigid octahedral polymer. The structure cannot interpenetrate because the walls of the channels are blocked by bipy ligands. The resulting channels have an effective cross-section $8 \times 8 \text{ \AA}$ and represent ca. 50% of the volume of the crystal. Solvent molecules are readily eliminated but the framework collapses irreversibly on loss of solvent. Perhaps the most salient feature of this structure is that the structure is entirely predictable in terms of both shape and dimensions. $[\text{Zn}(\text{bipy})_2(\text{SiF}_6)]$ crystallizes in space group $P4/mmm$ with $Z = 1$. In other words, the point group at Zn, D_{4h} , is propagated into space group symmetry. Furthermore, the cell parameters are determined by the intermetallic separations. The Cu analogue of $[\text{Zn}(\text{bipy})_2(\text{SiF}_6)]$ is isostructural and is of particular relevance since it has a higher capacity for methane adsorption than any previously studied porous material and it is stable to loss of guest.⁸⁴

Octahedral coordination polymers remain much less common than their diamondoid counterparts but a recent report revealed a novel metal-organic coordination polymer, $\text{Zn}_4\text{O}(\text{bdc})_3$ (bdc = 1,3-benzenedicarboxylate), that suggests an exciting future for such compounds.⁸⁹ $\text{Zn}_4\text{O}(\text{bdc})_3$ is a relatively simple and inexpensive material to prepare and is remarkably stable after loss or exchange of guest, remaining crystalline at temperatures

Figure 1.14: Minimal accessible surface of $\text{Zn}_4\text{O}(\text{bdc})_3$ (calculated by Cerius2)



above 300°C. The key feature that makes $Zn_4O(bdc)_3$ special is that it exhibits a relative degree of porosity that is hitherto unprecedented in crystalline solids.

As revealed by Figure 1.14, the octahedral framework exhibits a large amount of surface area that remains accessible to guest molecules because it contains pores and cavities that are large enough to accommodate and release organic molecules such as chlorobenzene and dimethylformamide. Calculations and experimental data indicate that *ca.* 60% of the structure is available and accessible. This compares to the typical value of *ca.* 30% seen in zeolites.¹⁴⁰

In addition to the obvious networks, i.e. diamondoid and octahedral, there are numerous examples of novel 3D networks that have been observed in recent years. Many can be described as supramolecular isomers of low dimensional structures. Two such

Figure 1.15: Schematic illustration of $[Co(bipy)_{1.5}(NO_3)_2]_n \cdot (C_6H_6)_{1.5}$

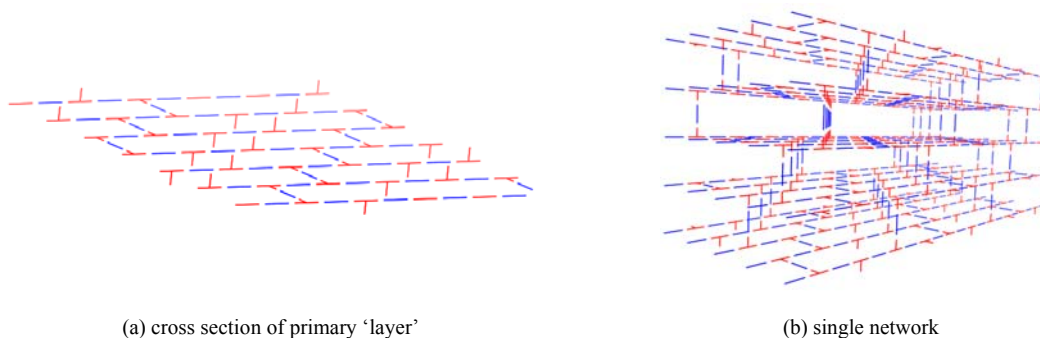
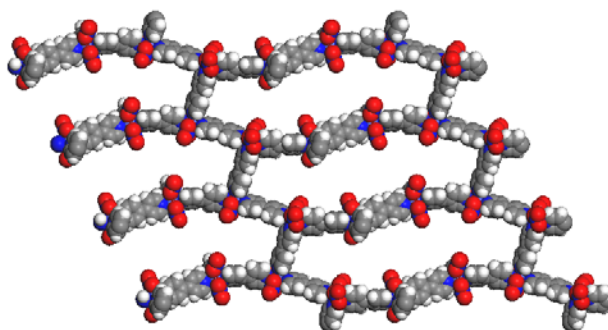
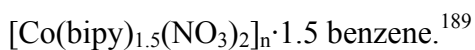


Figure 1.16: Space-filling model of $[Co(bipy)_{1.5}(NO_3)_2]_n \cdot (C_6H_6)_{1.5}$



(a) cross section of single network illustrating the connectivity within the primary layer

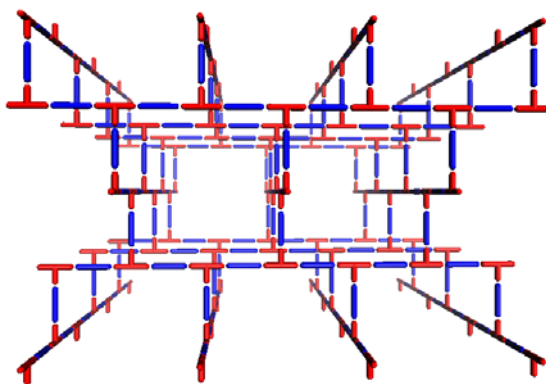
structures are supramolecular isomers formed by self-assembly of T-shape nodes. As discussed earlier, such self-assembly can afford 3D architectures that have not been seen in naturally occurring compounds. Figure 1.15 reveals one of these structures:



The cavities are revealed in Figure 1.16 and they are exceptionally large, having an effective cross-section $8 \times 40 \text{ \AA}$. These large cavities are capable of sustaining both 3-fold interpenetration and inclusion of guest molecules in channels. Although the networks are inherently centrosymmetric, the crystal is polar because the guest molecules align in such a manner that their supramolecular structure cannot contain a centre of inversion.

$[\text{Ag}(\text{bipy})(\text{NO}_3)]_n$ generates another type of supramolecular isomer for self-assembly of T-shaped components. It self-assembles into linear Ag-bipy chains that cross-link via Ag-Ag bonds. This particular 3D structure has been described as a “Lincoln Log” type structure (Figure 1.17) and exhibits a 3-fold level of interpenetration that is open enough to facilitate ion exchange of the loosely bound nitrate anions.²⁴⁸

Figure 1.17: Schematic illustration of $\{[\text{Ag}(\text{bipy})(\text{NO}_3)]\}_n$



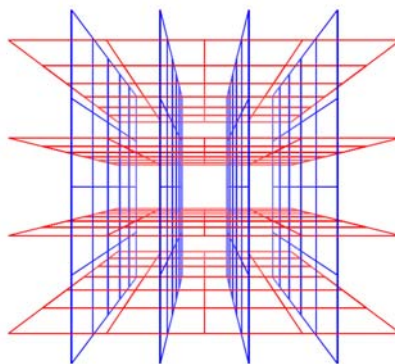
249

1.2.5. Hybrid structures

An alternate approach to building 3D structures that seems to offer considerable potential is manipulation of existing 2D structures. There are two relatively simple strategies in this context: cross-linking of 2D structures; interpenetration of identical or different 2D networks.

Cross-linking becomes feasible if one selects an appropriate 2D structure that has functionality in the axial direction. Such an approach has been widely used by clay chemists and hence the term “pillaring” might be applied to describe such a process. $[\text{Zn}(\text{bipy})_2(\text{SiF}_6)]$ could be used as a prototype in the context of coordination polymers since it can be regarded as having been generated from square grid coordination polymers that are cross-linked by $\mu\text{-SiF}_6$ anions. In the context of hydrogen-bonded structures, guanidinium sulfonates represent a class of compounds that have been cross-linked in a rational manner so as to generate infinite 3D structures.^{53,188,250-252}

Figure 1.18: Schematic of interpenetrating grids that afford a 3-D superstructure



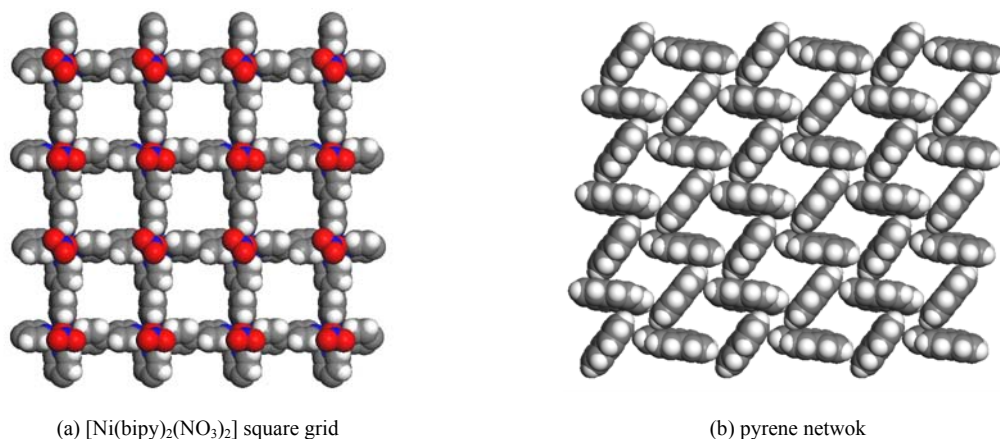
249

Interpenetration is a widely encountered phenomenon that mitigates against the existence of frameworks with very large cavities. However, Figure 1.18 reveals that there are situations in which interpenetration can occur, generate porosity and afford 3D

structures. Square grid polymers that are based on longer spacer ligands such as 1,2-bis(4-pyridyl)ethane (bipy-eta) or 1,2-bis(4-pyridyl)ethylene (bipy-ete) can interpenetrate in such a fashion.⁶⁶ However, an even more intriguing situation that could have important implications for design of new hybrid materials is exemplified by the crystal structure of the square grid coordination polymer $\{[\text{Ni}(\text{bipy})_2(\text{NO}_3)_2] \cdot 2\text{pyrene}\}_n$.²⁵³

Close examination of the crystal packing in this compound reveals that the pyrene molecules form an independent noncovalent network that is complementary from a topological perspective with the square grid. The resulting crystal represents a compound in which two very different types of 2D net interpenetrate. The square grid coordination networks (Figure 1.19a) possess inner cavities of ca. $8 \times 8 \text{ \AA}$ and stack in such a manner that they lie parallel to one another with an interlayer separation of ca. 7.9 \AA . The pyrene nets (Figure 1.19b) are sustained by edge-to-face interactions and contain cavities of ca. dimensions $6.5 \times 3.5 \text{ \AA}$. The planes of the neighboring molecules intersect at an angle of ca. 60° and there are no face-to-face stacking interactions between the molecules. The pyrene nets can be regarded as distorted 4^4 nets if the node is the point in space at which the vectors of the four pyrene planes intersect. An alternate interpretation is that nodes

Figure 1.19: $\{[\text{Ni}(\text{bipy})_2(\text{NO}_3)_2] \cdot 2\text{pyrene}\}_n$



exist at the point of the edge-to-face interactions. The pyrene net could then be regarded as a distorted brick wall form of a 6^3 net. It is important to note that either a 4^4 or a 6^3 planar net is complementary from a topological sense with the 4^4 coordination polymer net and ensures that the coordination polymer nets must pack in a staggered manner.

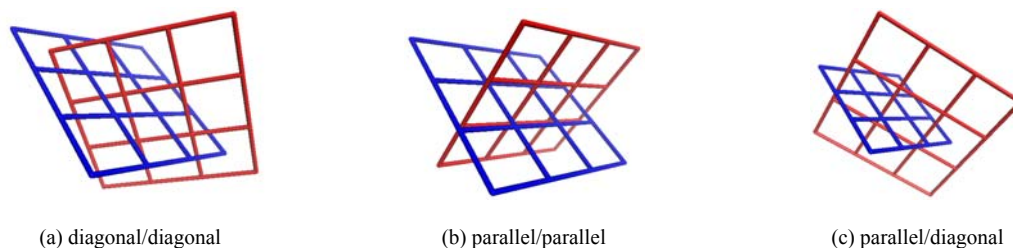
Given that cavity size within the pyrene nets is complementary with the width and height of a single aromatic ring, it should be unsurprising that the pyrene nets thread orthogonally with the bipy ligands of the coordination polymer via face-to-face and edge-to-face interactions and that the calculated volumes of the two nets are similar. This is to be expected based on the observation that bipy square grids are self-complementary as they can interpenetrate in a 2-fold fashion.²⁰⁸ The interpretation of this crystal structure as interpenetrating covalent and noncovalent nets is potentially important in the context of understanding the structure and stoichiometry of compounds that are based on interpenetrated covalent and noncovalent nets. The structure also illustrates how polarity in crystals can be generated from subtle packing of achiral components, since the pyrene molecules form chiral nets.

It should be noted that this type of packing is not found uniquely in $\{[\text{Ni}(\text{bipy})_2(\text{NO}_3)_2] \cdot 2\text{pyrene}\}_n$. Its naphthalene analogue, $\{[\text{Ni}(\text{bipy})_2(\text{NO}_3)_2] \cdot 3\text{naphthalene}\}_n$, can be interpreted as being the result of interpenetration of hexagonal and square nets²⁵⁴ and a study of a series of more than twenty related compounds has revealed the presence of noncovalent nets in every one of these compounds.²⁵⁵

That interpenetration can vary and be influenced by subtle effects are exemplified by this class of compound. It has been reported that for coordination polymers in which

44 networks that are planar and identical interpenetrate, two types of interpenetration are typically observed, both of which are examples of inclined interpenetration.⁶⁶ The most commonly encountered form might be described as diagonal/diagonal inclined interpenetration²⁵⁵ and was observed in the prototypal $[M(\text{bipy})_2\text{X}_2]_n$ compound, $[\text{Zn}(\text{bipy})_2(\text{H}_2\text{O})_2]\text{SiF}_6$.²⁰⁸ The other mode of interpenetration might be described as parallel/parallel inclined interpenetration.^{220,256} These types of interpenetration are illustrated in Schemes 1.20a and 1.20b, respectively, and differ in how the networks orient and cut through each other. Parallel refers to the structure in which a “spacer” ligand from one network threads through the cavity of the other, diagonal refers to the structure in which a “node” from one network (e.g. the metal moiety) is within the cavity of the other.

Figure 1.20: modes of interpenetration



One would anticipate that the structure that is adopted by a particular compound would be influenced by several geometric factors: the relative size of the cavity; the distance between adjacent nodes within a network; the thickness of the layers and how this limits the interlayer separation of adjacent networks; the steric bulk of the node. In this context, it is important to note that, with all other things equal, the diagonal/diagonal mode of interpenetration facilitates an interlayer separation that is 41.4% greater than that of the parallel/parallel mode. Furthermore, the diagonal/diagonal mode ensures a staggered orientation of parallel layers whereas an eclipsed orientation is necessary if the

parallel/parallel structure is present. Therefore, in terms of steric considerations, the diagonal/diagonal mode would appear to be most likely to be favored. However, circumstances where the interlayer separation would ideally be shorter, or where the metal atoms in adjacent layers would be eclipsed (e.g. to maximize interlayer interactions) could favor the parallel/parallel mode.

The examples illustrated above that are based on complementary covalent and noncovalent networks exhibit a new mode of inclined interpenetration that is a hybrid of the modes described above: *parallel/diagonal inclined interpenetration*.²⁵⁵ The noncovalent 4⁴ arene networks exhibit parallel inclined interpenetration with respect to the 4⁴ metal-organic coordination networks, whereas the covalent coordination networks demonstrate diagonal inclined interpenetration with respect to the arene networks (Figure 1.20c). This salient structural feature means that the nitrate groups of adjacent parallel coordination polymer grids are staggered and that the interlayer separation is a consequence of the size of the arene network. It should therefore be unsurprising that Type A grids result when templated by the smallest arenes (benzene and derivatives) as they exhibit smaller interlayer separations than type B and C packing. Grid types B and C occur in the presence of larger or more arenes.

Given that cavity size within the aromatic networks is complementary with the width and height of a single aromatic ring, the self-assembly of aromatic molecules in the compounds reported herein is readily sustained by edge-to-face and face-to-face interactions with the hydrocarbon portion of the bipy moieties. These interactions are presumably a primary driving force for the clathration of the guests and a mitigating factor against interpenetration. Interpenetration was not encountered in the square grid

coordination polymer networks described above and stacking interactions are seen in all compounds. It is also interesting to note that only three packing modes are observed in 13 compounds of similar composition. However, a question that cannot yet be answered with certainty concerns whether or not the noncovalent networks of aromatic molecules can exist in the absence of the coordination polymers. In this context, the existence of a 1:1 binary compound between ferrocene and pyrene²⁵⁷ represents an important prototype since pairs of ferrocene molecules are stacked inside a pyrene 2D network that is sustained by noncovalent C-H... π interactions.

1.3. Summary

It is clear that there are a number of applications in which crystal engineering of coordination polymers may make an immediate contribution. Several of these are summarized below. Of course, there are other applications dependant on organic components for which crystal engineering has the opportunity to make an equal contribution; this subject matter should form the basis of future dissertations from the Zaworotko research group.

New classes of adsorbent, “organic and metal-organic clays and zeolites”, represent an area in which considerable progress has already been made. Such compounds offer clear potential for the following: efficient, cost-effective alternatives to current methods of enantiomeric separations; new materials for separation of gases, liquids and solutes; new industrial heterogeneous catalysts; new drug delivery matrices (e.g. matrix for oral delivery of otherwise unstable drugs); a new generation of chemical sensors; new storage matrices for gases such as methane. Recent results indicate that

synthetic metal-organic polymers can offer high levels of thermal stability and can supercede zeolites in terms of surface area and capacity for small guest molecules.^{84,89}

The rational design of polar materials for use in materials science also represents an aspect of crystal engineering that has already provided promising developments. Unfortunately, in most organic crystals, anti-parallel architectures predominate, thereby canceling dipoles of highly polarizable molecules and mitigating against optimization of bulk polarity. Fortunately, there now exists an extended range of modular, open framework organic and metal-organic solids. Many of these compounds contain architectures (e.g. square grid, honeycomb, octahedral) that favor incorporation of polar strands into channels, thereby reducing the driving force for anti-parallel alignment. Results obtained by the groups of Hollingsworth²⁵⁸⁻²⁶² and Hulliger et al.²⁶³⁻²⁷⁰ suggest that such compounds, in particular channel type inclusion compounds, hold considerable promise in the context of the design of solids that possess fine tunable bulk polarity. Diamondoid networks also offer considerable potential in this context since tetrahedral nodes do not contain a center of inversion.¹⁰⁰ The recent results of Lin's group indicate that diamondoid networks can couple high thermal stability with high SHG activity.²⁴⁰

Metal-organic polymers offer considerable potential in the context of molecular magnetism, semi-conductors and conductors.²⁷¹⁻²⁷⁷ Once again, the possibility of design and fine-tuning becomes apparent when one develops structures with predictable architectures that are based on paramagnetic metal ions. The presence of guest molecules can be a desirable feature as it would be expected to offer a degree of fine-tuning that is not inherently present in single component compounds.

The fundamental precept of crystal engineering is that all information necessary for design of extended 1D, 2D and 3D structures is already present at the molecular level in existing chemical species. Recent advances in our understanding of supramolecular chemistry and supramolecular synthons have been aided by the advent of CCD diffractometers coupled with ever more powerful visualization and analysis tools. It should therefore be unsurprising that control over supramolecular architectures has advanced rapidly in recent years. That these tools are now routinely available means that an even more concerted and systematic approach to gaining an understanding of the subtle factors that control architectures in the solid state is feasible. The rational design of supramolecular structure necessarily relies on invoking the concepts of self-assembly, in effect supramolecular synthesis, and exploits noncovalent forces as varied as the following:

- Hydrogen bonding, including both strong hydrogen bonding (e.g. O-H---O) and weak hydrogen bonding (e.g. C-H---O and even C-H--- π);
- Coordinate covalent bonds (e.g. metal-organic polymers);
- Electrostatic and charge transfer attractions;
- Aromatic π -stacking interactions.

The principles of crystal engineering and supramolecular synthesis have been used to design, isolate and characterize a number of novel network structures that are prototypal because they are based on modular components. However, these networks are typically based on relatively small molecular components and the number and chemical type of components is typically restricted. It is in these two areas that there appears to be almost unlimited potential for supramolecular synthesis. In the context of coordination

polymer networks, several recent reviews indicates how wide the range of chemical components and accessible network motifs has become.²²⁷ However, the scale of these structures is such that cavities and channels are on the order of 10 Å and, to date, each cavity is identical. Careful selection of appropriate substrates or components and ever more control over crystal packing will offer the potential for rational design of an even more extensive array of modular (i.e. binary, ternary or even higher order) structures than those that are currently available. In particular, judicious choice of secondary building units,⁹² supermolecules or biomolecules as templates and nodes should afford composite materials with nanoscale dimensions and cavities.

The same is likely to be true concerning the rational development of structures that are based on components that are at first glance incompatible. A number of examples of pure crystalline compounds that are based on metal-organic polymers and metal oxide clusters have been reported in recent years.^{209,278-280} Such composite materials would represent “uncharted territory” but they are a natural outgrowth of modular approaches to chemistry and now appear to be at hand. In essence, suprasupermolecular²⁸¹ synthesis in the solid state represents an area that should experience considerable advancements and, whereas prediction of crystal structures remains an elusive goal that will continue to be addressed, it does not preclude short-term applications of crystal engineering in a number of important areas. H.G. von Schnering’s 1981 anecdote therefore seems particularly appropriate to summarize the current opportunities for crystal engineering and design.²⁸²

“The peasant who wants to harvest in his lifetime cannot wait for the *ab initio* theory of weather”

Chapter 2

Three-Dimensional Structures

2.1. Preamble

For reasons that should become clear in later chapters, the first structures that shall be discussed are two three-dimensional coordination polymers that result from the self-assembly of trimesate and zinc(II) ions.²⁸³ Although an isostructural copper(II) analogue of compound 2 has been previously reported,²⁸⁴ the synthesis and structural characterization of compound 1 prompted a reinterpretation of this structure, which has led to a better understanding of some of the structural features and physical properties. These structures serve as the source of inspiration for the design principles that are discussed throughout the remainder of the body of this work.

2.2. Compound 1: $\{[XL_2Zn_2(\text{btc})]_8[L_2Zn_2(\text{btc})_{4/3}]_3\}_n$

2.2.1. Experimental

In a typical reaction, a 10 mL solution of $Zn(NO_3)_2 \cdot 6H_2O$ (220 mg; 0.741 mmol) and 1,3,5-benzenetricarboxylic acid (220 mg; 1.05 mmol) in methanol are layered onto a 10 mL solution of nitrobenzene containing pyridine (0.23 mL; 2.8 mmol). Large single crystals (0.30 x 0.30 x 0.15 mm) form within hours under ambient conditions.

Single crystals suitable for X-ray crystallographic analysis were selected following examination under a microscope. Selected crystallographic parameters are presented in Table 2.1. Complete crystallographic data for compound 1 can be found in Appendix A-1.

Table 2.1: Selected crystallographic parameters for $\{[XL_2Zn_2(btc)]_8[L_2Zn_2(btc)_{4/3}]_3\}_n$	
Crystal class	Cubic
Space group (#)	$Pm\bar{3}m$ (221)
a = b = c =	20.4582(13) Å
V =	8562.5(9) Å ³

Single-crystal X-ray diffraction data for compound 1, and all subsequent compounds described throughout this dissertation, were collected on a Bruker-AXS SMART APEX/CCD diffractometer using $Mo_{K\alpha}$ radiation ($\lambda = 0.7107$ Å) at 100 K. Diffracted data have been corrected for Lorentz and polarization effects, and for absorption using the SADABS v2.02 area-detector absorption correction program (Siemens Industrial Automation, Inc., © 1996). The structures were solved by direct methods and the structure solution and refinement was based on $|F|^2$. All non-hydrogen atoms were refined with anisotropic displacement parameters whereas hydrogen atoms were placed in calculated positions when possible and given isotropic U values 1.2 times that of the atom to which they are bonded. All crystallographic calculations were conducted with the SHELXTL v.6.1 program package (Bruker AXS Inc., © 2001).

2.2.2. Technical description

The structure results from μ_2 -coordination of each of three trimesate carboxylates to two zinc(II) ions. Two of the carboxylates are involved in the formation of a dizinc tricarboxylate chromophore, whereas the other is involved in the formation of a dizinc tetracarboxylate chromophore. Although it is anticipated that coordinating solvent and/or base (i.e. pyridine) will be coordinated to the apical positions of the metal chromophores, none were located from the diffraction data. Only a single coordinated atom, arbitrarily assigned as nitrogen, was refined. This is most likely due to the fact that these positions

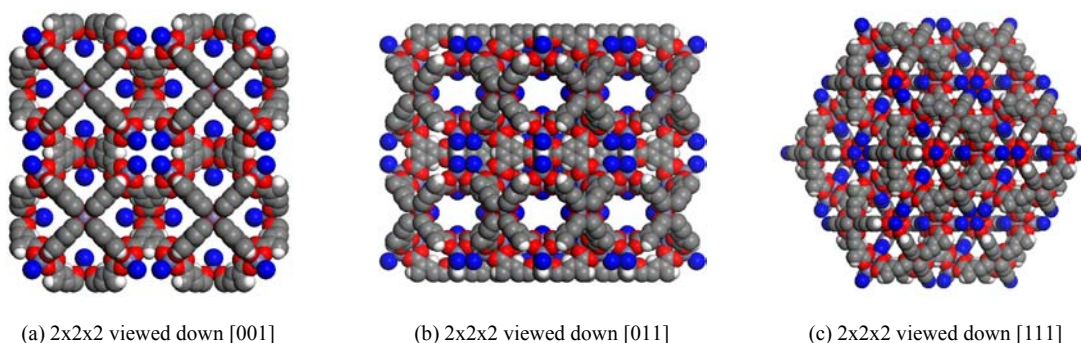
are highly disordered. Not only can the positions be water, methanol or pyridine, each of these can also be disordered by rotation about the coordination axis. It should also be noted that each dizinc tricarboxylate chromophore is ionic: $2 \times \text{Zn}^{2+}$ and $3 \times \text{CO}_2^-$ results in a net 1+ charge, therefore requiring a 1- counter anion to maintain charge balance. No anions were located from the diffraction data. Although the anion is most likely nitrate, based on the synthesis from zinc(II)nitrate hexahydrate, it may also be hydroxide or methoxide. The anion may be coordinated to one of the zinc ions, or it may be located in the void space in the crystal lattice. Additional electron density, attributed to disordered solvent or guest molecules, was modeled as variable occupancy isotropic carbon atoms.

The crystal structure is in a high symmetry cubic crystal class having $\text{Pm}\bar{3}\text{m}$ cell symmetry. There are 3 crystallographically independent zinc ions. Two zinc ions are involved in the dizinc tricarboxylate chromophore ($d_{\text{Zn}\dots\text{Zn}} = 3.5121(69)$) and sit on a 3-fold rotation axis and axial glide plane. The former zinc is involved in the dizinc tetracarboxylate chromophore ($d_{\text{Zn}\dots\text{Zn}} = 2.970(12)$), and sits on a 4-fold rotation axis and an axial glide plane. It also sits close to an inversion center, which generates the other zinc in the chromophore. There are three crystallographically independent oxygen atoms, each coordinated to one of the zinc atoms at distances of 2.017(22), 1.920(24), and 1.954(24) Å. The rotation axes generate the remaining oxygen atoms in each of the chromophores. There are six crystallographically independent carbon atoms, which when bonded to the oxygen atoms, and taking into account the cell symmetry, complete the trimesate ions. Two hydrogen atoms were placed in calculated positions, based on the geometry defined by the trimesate ring (i.e. sp^2 hybridized, aromatic carbon). Atom coordinates and occupancies can be found in the electronic supplementary data.

If you consider the asymmetric unit the basic formula unit, $Z = 48$ and the cell contents are, excluding coordinated ligands, $Zn_{22}C_{108}H_{36}O_{72}X_{16}$, where X represents a monoanion (most likely nitrate). The empirical formula is $Zn_{11}C_{54}H_{18}O_{36}X_8$, which gives $Z = 2$. To better describe the structure, it is necessary to differentiate the zinc ions that are involved in the tricarboxylate chromophore and the tetracarboxylate chromophore. Examination of the site occupancies of the zinc ions reveals that they are present in an 8:3 ratio. Furthermore, for each tricarboxylate chromophore there are three coordinated trimesates, each one shared with two other chromophores, which corresponds to one full trimesate per chromophore ($3 \times \frac{1}{3}$). For each tetra-carboxylate chromophore there are four coordinated trimesates, each one shared with two other chromophores, which corresponds to four-thirds of a trimesate per chromophore. Therefore, the basic formula unit can be written as $[X_4Zn_8(\text{trimesate})_4][Zn_3(\text{trimesate})_2]$. In order to better illustrate that the structure is based on dizinc carboxylate chromophores, this can be rewritten in terms of Zn_2 units: $[XL_2Zn_2(\text{btc})]_8[L_2Zn_2(\text{btc})_{4/3}]_3$, where btc = 1,3,5-benzenetricarboxylate (i.e. trimesate), and L represents a coordinated ligand (most likely water, methanol or pyridine). The molecular formula is therefore represented by $\{[XL_2Zn_2(\text{btc})]_8[L_2Zn_2(\text{btc})_{4/3}]_3\}_n$ to illustrate that the compound is a coordination polymer. The $[XL_2Zn_2(\text{btc})]$ portion can also be represented as $[XLZn_2(\text{btc})]$, if the anion is considered to be coordinated to the zinc.

2.2.3. Space-filling models

Figure 2.1: Space filling models of compound 1, $\{[XL_2Zn_2(btc)]_8[L_2Zn_2(btc)_{4/3}]_3\}_n^*$

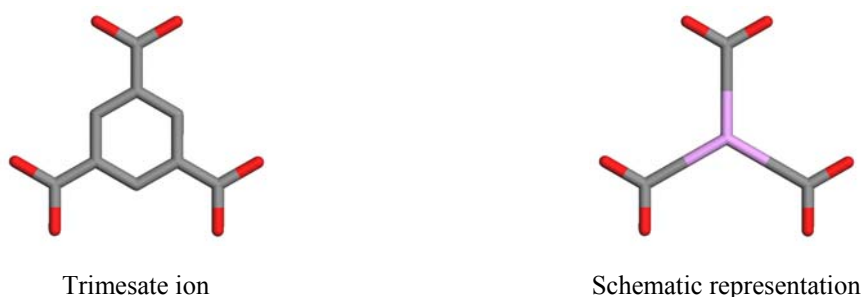


* Carbon (grey), oxygen (red), nitrogen (blue), hydrogen (white); apically coordinated molecules represented as nitrogen with remaining atoms absent; non-coordinated solvent/guest removed for clarity

2.2.4. Illustrative Description

The primary interaction in compound 1 is the carboxylate coordination to the metal ions. The carboxylates are predisposed to be in a trigonal planar geometric arrangement (i.e. at 120° with respect to one another). The trimesate is therefore replaced by an S_4 star graph with terminal carboxylates (Figure 2.3). It should be noted that the S_4 used in this context is not a crystallographic symmetry element but rather the notation used for star graphs (i.e. S for ‘star’, and 4 for the number of nodes).

Figure 2.2: Schematic representation of trimesate*



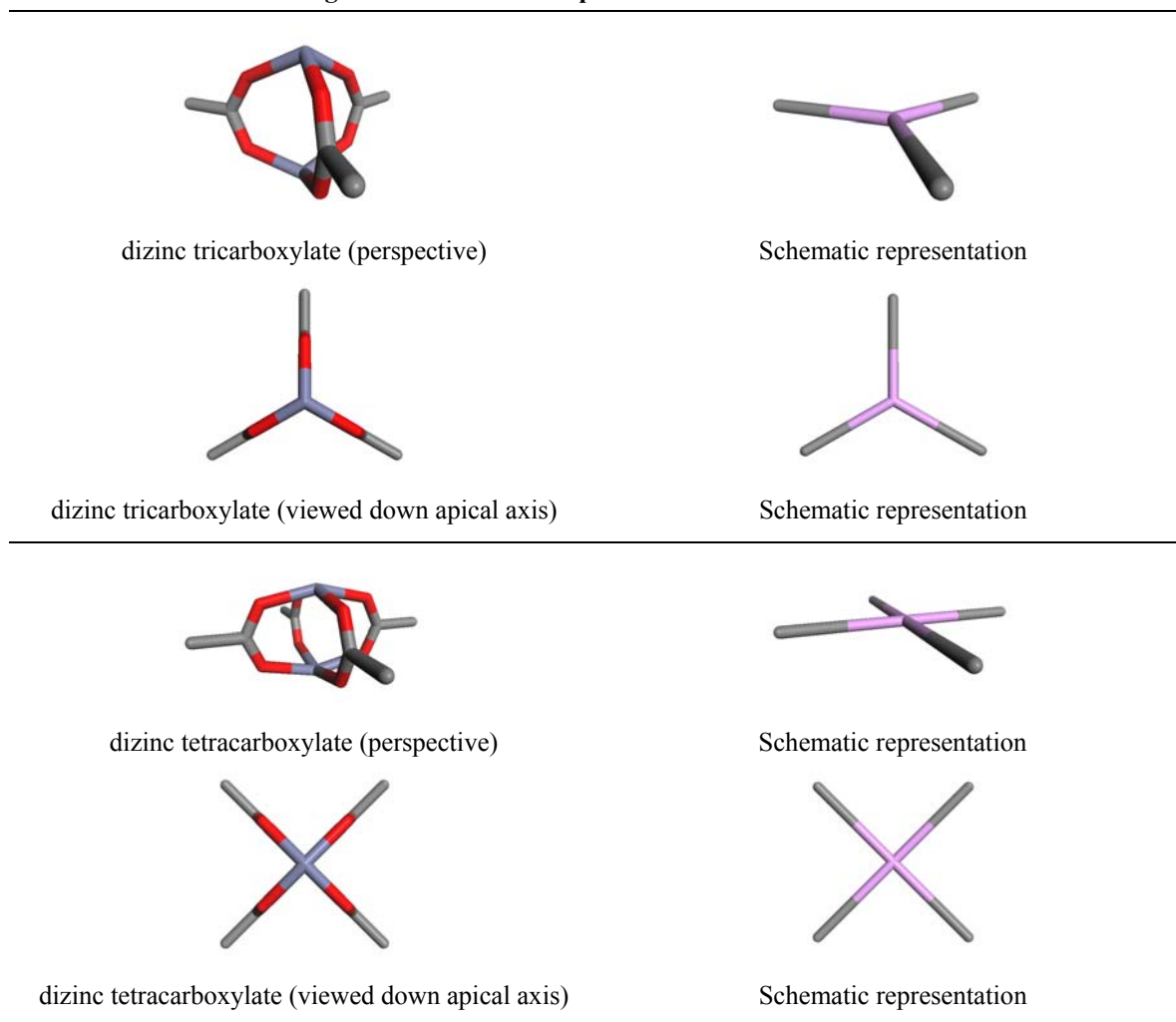
* Protons have been deleted

Furthermore, there are two dizinc chromophores (SBUs²⁸⁵) that have to be considered: tricarboxylate and tetracarboxylate. The tricarboxylate SBU is similar to the

trimesate in that it orients the carboxylates in a trigonal geometry; however, an important distinction is that, in the SBU, the planes of the carboxylates are orthogonal to the graph plane. This is not an important structural feature with respect to the overall topology, and is therefore removed by treating the two zincs as a single node located at the midpoint of the vector between them (Figure 2.4).

The tetracarboxylate SBU is similarly represented by an S_5 star graph, by treating the two zincs as a single node that orients the carboxylates at 90° with respect to one another (Figure 2.4).

Figure 2.3: Schematic representation of dizinc SBU*

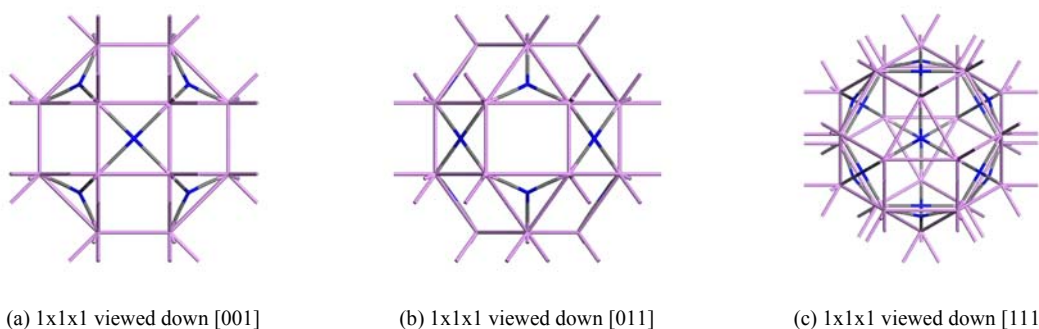


* Apically coordinated ligands have been deleted

The reduction of the SBUs to a single node results in the removal of the carboxylate oxygen atoms. Therefore, with the oxygen atoms removed, the schematic representation of the trimesate ion looks, at first glance, identical to the schematic representation of the trigonal SBU. An important difference in terms of the overall structure is that the SBU representation is larger (4.11 vs. 3.83 Å), and the SBU representation has out-of-plane atomic components that have been removed. Based on these differences, the SBU component is considered to be the ‘bulk’ of the structure, and the trimesate component to be the ‘geometric director’.

In order to illustrate this in the schematic, the central nodes of the trimesate S_4 star graphs are connected to form triangles around the trigonal SBU and squares around the square SBU (Figure 2.5).

Figure 2.4: Schematic illustration of compound 1, $\{[XL_2Zn_2(btc)]_8[L_2Zn_2(btc)_{4/3}]_3\}_n$



* SBU nodes are blue, trimesate nodes are orchid; grey connections illustrate chemical connectivity, orchid connections the boundaries of the triangular and square SBUs

Several structural features become immediately evident on inspection of the schematic representation of compound 1: there are ‘open’ squares (i.e. squares with no SBU at the center) and ‘filled’ squares (i.e. squares with an SBU at the center); the ‘open’ squares lead to porosity (i.e. channels running through the crystal parallel to [001] and [011]); there are large spherical cavities with octahedral symmetry, and if a schematic of

several unit cells is viewed, cubic cavities and smaller spherical cavities with octahedral symmetry become evident.

2.3. Compound 2: $\{[L_2Zn_2(btc)_{4/3}]\}_n$

2.3.1. Experimental

In a typical reaction, a 10 mL methanolic solution of $Zn(NO_3)_2 \cdot 6H_2O$ (202 mg; 0.679 mmol) and 1,3,5-benzenetricarboxylic acid (126 mg; 0.600 mmol) is layered onto a 10 mL methanolic solution of benzene containing pyridine (0.10 mL; 1.24 mmol). Large single crystals (0.30 x 0.25 x 0.20 mm) form within hours under ambient conditions.

Selected crystallographic parameters are presented in Table 2.2. Complete crystallographic data for compound 2 can be found in Appendix A-2.

Table 2.2: Selected crystallographic parameters for $\{[L_2Zn_2(btc)_{4/3}]\}_n$	
Crystal class	Cubic
Space group (#)	$Fm\bar{3}m$ (225)
a = b = c =	26.5200(13) Å
V =	18651.8(16) Å ³

2.3.2. Technical description

The structure results from μ_2 -coordination of each of three trimesate carboxylates to two zinc(II) ions. Each carboxylate is involved in the formation of a dizinc tetracarboxylate chromophore. Although it is anticipated that coordinating solvent and/or base (i.e. pyridine) will be coordinated to the apical positions of the metal chromophores, none were located from the diffraction data. Only a single coordinated atom, arbitrarily assigned as oxygen, was refined. As in compound 1, this is due to the ligand being one of water, methanol or pyridine, with the additional problem of rotational disorder around

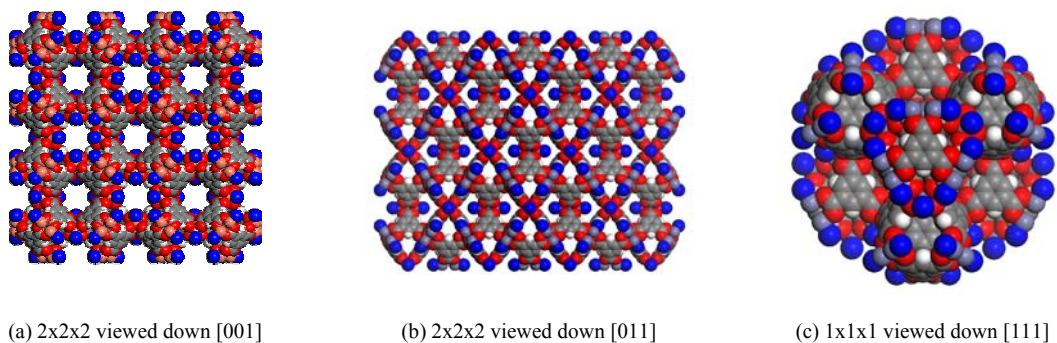
the coordination vector. Additional electron density, attributed to disordered solvent or guest molecules, was modeled as variable occupancy isotropic carbon atoms.

The crystal structure is in a high symmetry cubic crystal class having $Fm\bar{3}m$ cell symmetry. There is only one crystallographically independent zinc ion, one independent oxygen atom and three independent carbon atoms (excluding coordinated and non-coordinated solvent/base). The zinc ion sits on a 4-fold rotation axis and near an inversion center. The oxygen is coordinated to the zinc at a distance of 1.9997(79) Å, and sits on a general position. The 4-fold rotation axis generates one-half of the tetracarboxylate chromophore, and the other half is generated by the center of inversion ($d_{Zn...Zn} = 2.9488(18)$). Treatment of the carbon atoms with the appropriate symmetry operations completes the trimesate ions and, thus, the basic molecular framework of the crystal. A hydrogen atom was placed in a calculated position, based on the geometry defined by the trimesate ring (i.e. sp^2 hybridized, aromatic carbon). Atom coordinates and occupancies can be found in electronic supplementary data.

This asymmetric unit gives $Z = 192$, and the cell contents are, not including coordinated ligands, $Zn_{48}C_{288}H_{96}O_{192}$. The empirical formula is $ZnC_6H_2O_4$, giving $Z = 48$. Again, this is not very illustrative of the overall structure. In this instance, all zinc ions are involved in a tetracarboxylate chromophore and the basic formula unit is $[L_2Zn_2(btc)_{4/3}]$, where $btc = 1,3,5$ -benzenetricarboxylate (i.e. trimesate), and L represents a coordinated ligand (most likely water, methanol or pyridine). The molecular formula is therefore represented by $\{[L_2Zn_2(btc)_{4/3}]\}_n$ to illustrate that the compound is a coordination polymer.

2.3.3. Space-filling models

Figure 2.5: Space filling models of compound 2, $\{[L_2Zn_2(btc)_{4/3}]\}_n^*$

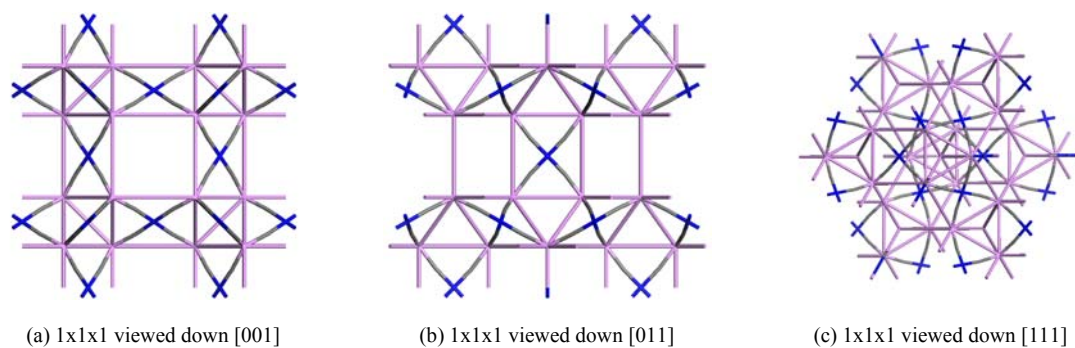


* Carbon (grey), oxygen (red), nitrogen (blue), hydrogen (white); apically coordinated molecules represented as nitrogen with remaining atoms absent; non-coordinated solvent/guest removed for clarity

2.3.4. Illustrative Description

The crystal structure of compound 2 can be reduced in a similar fashion as compound 1. In this instance, however, the material is sustained by square SBUs only. Therefore, the schematic is generated by connecting SBU S_5 star graphs only (Figure 2.4), and by again connecting the centers of the trimesate S_4 star graphs such that they surround the SBU nodes (Figure 2.6).

Figure 2.6: Schematic illustration of compound 2, $\{[L_2Zn_2(btc)_{4/3}]\}_n$



* SBU nodes are blue, trimesate nodes are orchid; grey connections illustrate chemical connectivity, orchid connections the boundaries of the triangular and square SBUs

Several structural features become immediately evident on inspection of the schematic representation of compound 2: there are ‘open’ squares and ‘filled’ squares;

the 'open' squares lead to porosity (i.e. channels running through the crystal parallel to [001] and [011]); there are large spherical cavities with octahedral symmetry, and if a schematic of several unit cells is viewed, cubic and tetrahedral cavities become evident.

2.4. Discussion

The purpose of generating schematics is to simplify the technical descriptions by creating graphical representations that aid in understanding the structural features of the materials. To begin, it is important to summarize the technical descriptions to establish which structural features are to be represented. In each of the structures, the primary building units are trimesates and zinc(II) ions, the secondary building units (SBUs) are dizinc carboxylates: tri- and tetracarboxylates in compound 1, and tetracarboxylates in compound 2. From a structural perspective, it is essential that these SBUs, and the connectivity thereof, be illustrated by a schematic representing either structure.

Compounds 1 and 2 have very similar compositions, that being trimesate and zinc(II). There are, however, several important differences: compound 1 is ionic; compound 1 has trigonal and square SBUs; compound 2 has only square SBUs. Still, there are many similarities: both compounds crystallize in a high symmetry cubic crystal class; both compounds have large spherical cavities of approximately the same dimensions with octahedral symmetry; both compounds have large pores (ca. 8 Å) that run through the crystal; both compounds can be reduced to schematics that have open faces and closed faces. The important question that must now be addressed is what can be learned from these structures?

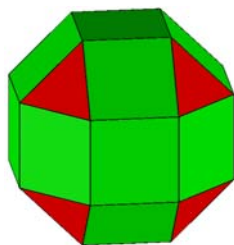
Perhaps one of the most striking similarities between the two compounds is the presence of large spherical cavities having approximately the same dimensions. In

compound 1, the distance measured between the interior zinc centers of the trigonal SBUs is 17.0 Å, and the distance measured between the interior zinc centers of the square SBUs is 17.5 Å. This difference can be attributed to the longer $d_{Zn...Zn}$ distance observed for the trigonal SBU. The distance measured between the interior zinc centers of the square SBUs in compound 2 is 15.8 Å. Taking into account an ionic radius for Zn^{2+} of 0.74 Å, the effective interior diameter of the spherical cavities are 15.5 Å and 14.3 Å for compounds 1 and 2, respectively. The effective volumes of the cavities are, therefore, 1950 Å³ (1.95 nm³) and 1530 Å³ (1.53 nm³), respectively. It should be noted that although these cavities are anticipated to be filled with solvent or guest molecules coordinated to the zinc, Williams has demonstrated that a copper(II) material isostructural to compound 2 maintains its structure on loss of coordinated water and pyridine, which can easily escape through the open channels.²⁸⁴

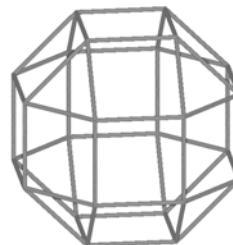
A close examination of the schematics for both compounds reveals that the shape of the cavity is congruent with the edge skeleton of the rhombicuboctahedron,²⁸⁶ an Archimedean solid (Figure 2.7). However, as has been previously indicated, not all of the faces of the rhombicuboctahedron are present. Indeed, in compound 1 there exists a set of polygonal faces (squares and triangle), linked at their vertices, which define the spherical cavity. Furthermore, there is a set of complementary polygonal faces (squares) linked at their vertices, which define the absent faces. The latter set defines the set of faces that are present for the cavity in compound 2. These two polyhedra are referred to as ‘faceted’ polyhedra²⁸⁷ and are included in the group of 80 uniform polyhedra. Specifically the sphere representing the cavity in compound 1 is named the Small

cubicuboctahedra, and in compound 2 it is named the Small rhombihexahedra (Figure 2.7).

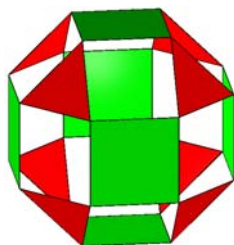
Figure 2.7: Polyhedral models based on the rhombicuboctahedron



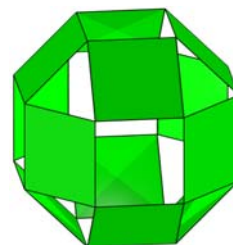
Rhombicuboctahedron



Rhombicuboctahedron edge-skeleton



Small cubicuboctahedron (compound 1)



Small rhombihexahedron (compound 2)

The Platonic and Archimedean solids are a subset of the uniform polyhedra²⁸⁸ that have a complete, concave exterior shell comprised of regular polyhedra (all edges equal length). Their geometries are well defined and have been known for centuries. A table illustrating the five platonic solids and the thirteen Archimedean solids and some key geometric values is given in Appendix B-1. It is interesting to note, that there are very few, if any, accounts reporting the dihedral angle between faces linked at their vertices for any of the uniform polyhedra. Of course, this is very easy to calculate given any 3 vertices from both faces. This value is particularly relevant for the Small cubicuboctahedron and Small rhombihexahedron as it defines the angle at which the SBUs are linked. It should, therefore, be unsurprising that the dihedral angle between the triangle and square in the Small cubicuboctahedron is $125^{\circ} 16'$ and the dihedral angle

between the squares in the Small rhombihexahedron is $117^{\circ} 12'$, which is very close to the 120° that is expected based on the trimesate geometry. Another value that is of interest with respect to connecting SBUs by trimesate, is the angle between the centers of linked polygons, measured across the vertex linking them. In most cases, this value is the same as the dihedral angle, however, for the Small rhombihexahedron this value is exactly 120° (in comparison to a dihedral angle of 117.2°).

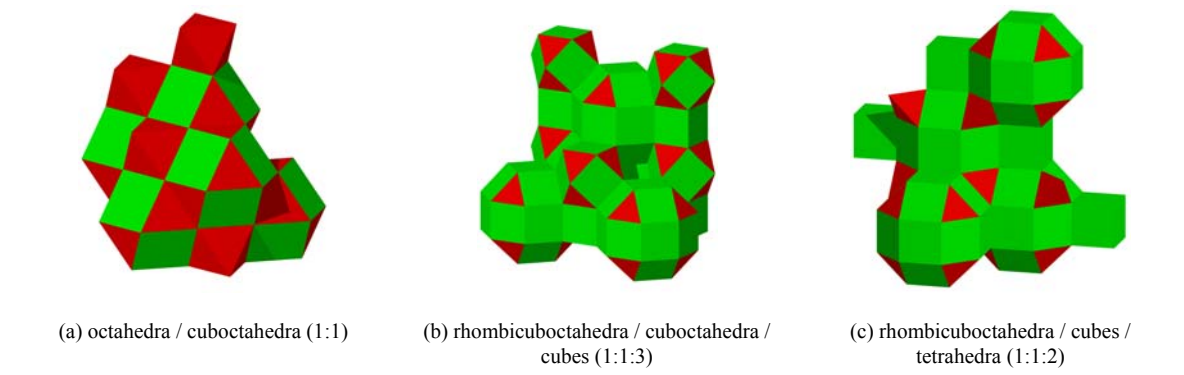
Of course, compounds 1 and 2 are not discrete spheres, rather three-dimensional solids. Therefore, the next thing that must be considered is the possible arrangements of Platonic and Archimedean solids that tile space (i.e. space-filling polyhedra). There are only eleven ways that Platonic and Archimedean polyhedra, and combinations thereof, can pack to fill space²⁸⁹ (note that there are additional arrangements involving the other uniform polyhedra, such as prisms):

1. cubes (uniary)
2. truncated octahedral (uniary)
3. tetrahedra / octahedra (binary; 2:1)
4. tetrahedra / truncated tetrahedra (binary; 1:1)
5. octahedra / truncated cubes (binary; 1:1)
6. octahedra / cuboctahedra (binary; 1:1)
7. truncated cuboctahedra, truncated octahedra, cubes (tertiary; 1:1:3)
8. rhombicuboctahedra / cuboctahedra / cubes (tertiary; 1:1:3)
9. rhombicuboctahedra / cubes / tetrahedra (tertiary; 1:1:2)
10. truncated cuboctahedra / truncated cubes / truncated tetrahedra (tertiary; 1:1:2)
11. truncated octahedra / cuboctahedra / truncated tetrahedra (tertiary; 1:1:2)

The uniform polyhedra that are of interest in the context of this discussion are a subclass of the Platonic and Archimedean solids, the faceted polyhedra. Only polyhedra

with vertices that have $2n+2$ edges ($n = \text{integer} \geq 1$) meeting at each vertex have derivative faceted polyhedra (i.e. they have the same edge-skeleton as the parent Platonic or Archimedean solid, however, they have polygons that are joined only at their vertex). Only five of the eighteen Platonic or Archimedean solids meet this criterion, which lead to nine faceted polyhedra: four have complementary pairs of faceted polyhedra

Figure 2.8: Space-filling polyhedral arrangements



(cuboctahedron, icosidodecahedron, rhombicuboctahedron, rhombicosidodecahedron), the other has a congruent pair (octahedron). In order to achieve space-filling for faceted polyhedra, the edge framework of the packing mode must also satisfy the requirement that $2n+2$ edges meet at each vertex. This reduces the number of possible space-filling polyhedral arrangements to three that are possible for faceted polyhedra (Figure 2.8):

1. octahedra / cuboctahedra (binary; 1:1)
2. rhombicuboctahedra / cuboctahedra / cubes (tertiary; 1:1:3)
3. rhombicuboctahedra / cubes / tetrahedra (tertiary; 1:1:2)

As has been previously indicated, compounds 1 and 2 have structures that can be described in terms of the packing of rhombicuboctahedra. This limits the possible packing modes to two. In compound 1, there are triangular faces that are linked only at their vertices, which precludes the packing mode of rhombicuboctahedra, cubes and

tetrahedra (Figure 2.8(c)), because tetrahedra have edge-fused triangles. Therefore there is only one possible structure for Small cuboctahedra (i.e. compound 1) that can result: rhombicuboctahedra, cuboctahedra and cubes. Similarly, the only possible structure for Small rhombihexahedra (i.e. compound 2) is rhombicuboctahedra, cubes and tetrahedra, because the set of square faces of the Small rhombihexahedra are edge-fused in the alternate packing mode (Figure 2.8(b)).

2.5. Conclusions

In summary, carboxylate SBUs can be viewed as molecular polygons (i.e. triangle and squares), which self-assemble at their vertices via polycarboxylate linkers to produce molecular architectures and crystal structures that are consistent with long established geometric constraints. These structures inherently contain open windows because they are based on linking of vertices rather than edges. They therefore differ in terms of design and function from structures that are generated from Platonic and/or Archimedean building blocks. Only three three-dimensional space-filling frameworks are possible for these structures, two contain only squares and the other triangles and squares. Therefore, these frameworks are likely to be prototypal for a wider range of porous networks since there are many molecular species that can be described as molecular triangles and squares. The crucial aspect in the design of these structures is the geometry of the vertices, which for the structures described herein approximates trigonal planar symmetry (120°). The remaining structure (Figure 2.8(a)) will result from the self-assembly of molecular squares at their vertices by a square planar ‘geometric director’ (90°).

The synthesis of variants of compound 1 is most easily achieved by metal substitution. Zinc(II) is particularly well suited for such a synthesis because it can adopt

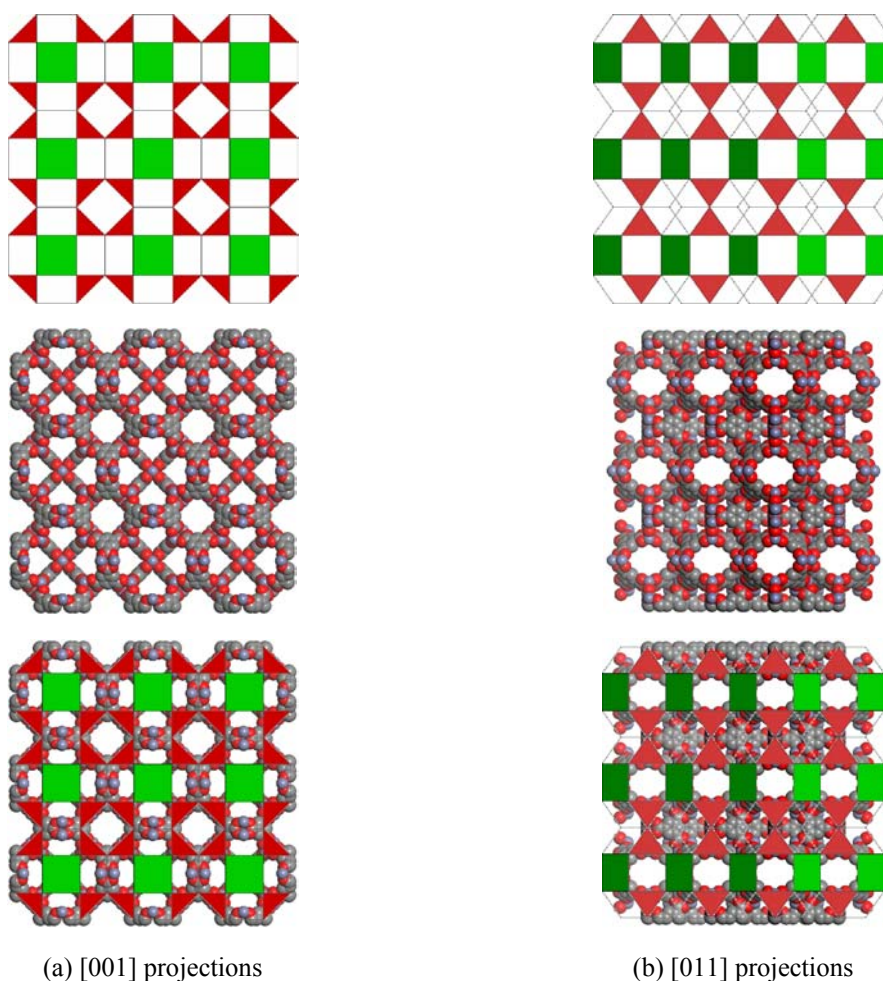
both a tetrahedral coordination geometry (necessary for synthesis of trigonal SBU) and octahedral coordination geometry (necessary for synthesis of square SBU). There are, however, examples of other transition metals that can adopt both coordination environments with carboxylates (e.g. Mn, Co, La), although none have been observed to occur in the same structure. It is, in principle, also possible to synthesize a mixed transition metal material that has a tetrahedral metal and octahedral metal in the appropriate stoichiometry (8:3). Indeed, it may also be possible to have mixed oxidation state metals in the same material, whereby there is a tetrahedral +1 transition metal together with a +2 octahedral transition metal. In this instance the framework would be anionic, and would require one counter cation per trigonal SBU. Additionally, variants could be synthesized by using alternate tricarboxylates that orient the SBUs at 120° with respect to one another.

Variants of compound 2, on the other hand, are expected to be far more common. Indeed, it has already been pointed out that a copper(II) analogue has already been reported. The attractive feature of compound 2 is that it is electronically neutral for +2 transition metals, and is sustained by dimetal tetracarboxylate SBUs, which are ubiquitous amongst the transition metals. Of course, variants could also be synthesized by using alternate tricarboxylates that orient the SBUs at 120° with respect to one another.

In consideration of the increasing number of reports of supramolecular isomerism by coordination compounds, the most remarkable aspect of these structures is that they are the only structures that can possibly occur for the observed coordination environments. Regrettably, the information learned from the structural analysis of these

structures was not known in advance, as they are also entirely predictable, including the space group. This is due to the fact that the space groups for polyhedral packings were reported nearly a century ago:²⁹⁰ the space group of the rhombicuboctahedra, cuboctahedra and cubes packing is $Pm\bar{3}m$, the same as that observed for compound 1; the space group of the rhombicuboctahedra, cubes and tetrahedra packing is $Fm\bar{3}m$, the same as that observed for compound 2. Cell dimensions could have been determined, within an acceptable chemical tolerance, based on the known covalent bond lengths in trimesate and coordination bond lengths in carboxylate SBUs. This information would have

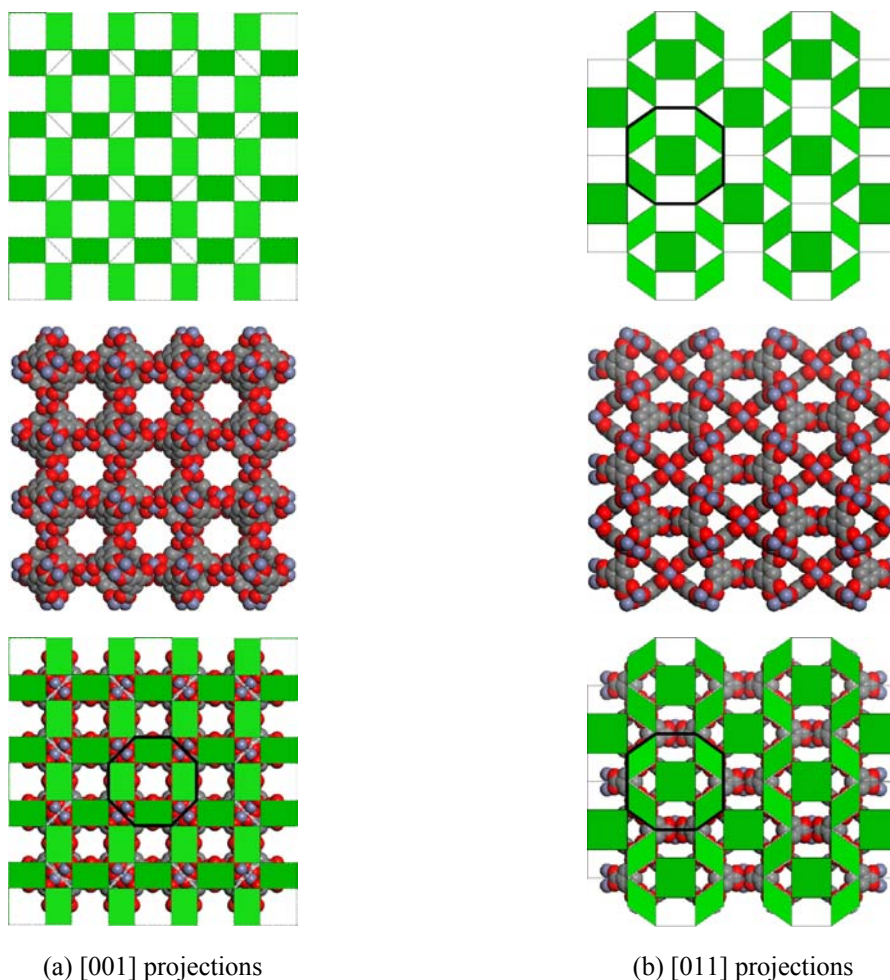
Figure 2.9: Projections of polyhedral space-filling models and corresponding crystal structure projections* for compound 1



* Hydrogens and apically coordinated ligands have been deleted

permitted the calculation the exact coordinates of all framework atoms prior to synthesis. As an example of the predictability of the structures and an illustration of how well the polyhedral packings approximate the crystal structure, Figure 2.9 illustrates the projections of the Small cubicuboctahedra faceted polyhedral packing viewed down [001] and [011], the same projections for the crystal structure for compound 1, and an overlay of the two projections.

Figure 2.10: Projections of polyhedral space-filling models and corresponding crystal structure projections* for compound 2



* Hydrogens and apically coordinated ligands have been deleted

Figure 2.10 illustrates the projections of the Small rhombihexahedron faceted polyhedral packing viewed down $[001]$ and $[011]$, the same projections for the crystal structure for compound 2, and an overlay of the two projections.

The remainder of the body of this work will address design principles for lower order structures that can be learned from this analysis, and should underscore the rarity of the degree of predictability observed for compounds 1 and 2.

Chapter 3

Two-Dimensional Structures

3.1. Preamble

It should be clear that structures related to compounds 1 and 2 will be possible if the synthesis is done in the presence of isophthalic acid (1,3-benzenedicarboxylic acid; H₂bdc) instead of trimesic acid (1,3,5-benzenetricarboxylic acid; H₃btc). In essence, this can be viewed as “trimming” one of the carboxylates of the trimesate ion in compounds 1 and 2. However, it is not immediately obvious what structures will result or what the number of structures is that is possible. In chapter 2, it was demonstrated that there is only one architecture that can possibly result from the assembly of trimesate ions with zinc(II), if the carboxylates form only dimetal tetracarboxylates. Although it is possible to control this by synthetic means, it is perhaps easier to use a transition metal that only forms the dimetal tetracarboxylate cluster. Not only is copper(II) a prototypical example of such a metal, but the dicopper tetracarboxylates are also the most ubiquitous carboxylate metal clusters present in the CSD.²⁸ Furthermore, syntheses of structures based on the dicopper tetracarboxylates will necessarily afford neutral networks. Therefore, reactions between isophthalate ions and copper(II) have been investigated, both theoretically and synthetically, to study the range of structures possible for such a system and to determine if there is any degree of predictability to these structures.

3.2. Compound 3: $\{[L_2Cu_2(bdc)_2]_4\}_n$ ²⁹¹

3.2.1. Experimental

In a typical reaction, a 10 mL ethanolic solution of $Cu(NO_3)_2 \cdot 2.5H_2O$ (231 mg; 0.993 mmol) is layered onto a 10 mL ethanolic solution containing 1,3-benzenedicarboxylic acid (166 mg; 0.999 mmol), benzene (2.0 mL; 22 mmol) and pyridine (0.23 mL; 2.8 mmol). Large, blue-green, crystalline tetragonal plates (0.20 x 0.20 x 0.05 mm) form within hours under ambient conditions.

Selected crystallographic parameters are presented in Table 3.1. Complete crystallographic data for compound 3 can be found in Appendix A-3.

Crystal class	Tetragonal
Space group (#)	P4/ncc (126)
a = b =	18.7912(8) Å
c =	16.8886(10) Å
V =	5963.5(8) Å ³

3.2.2. Technical description

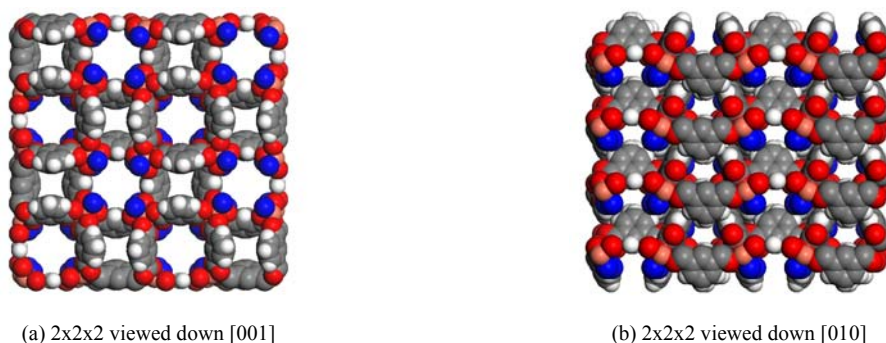
The structure results from μ_2 -coordination of each of the isophthalate carboxylates to two copper(II) ions. Each carboxylate is involved in the formation of a dicopper tetracarboxylate chromophore. Unlike compounds 1 and 2, the apically coordinated ligand, pyridine, was located and refined from the diffraction data. Additional electron density, attributed to disordered solvent or guest molecules present in the crystal lattice void space, was modeled as variable occupancy isotropic carbon atoms.

The crystal structure adopts a tetragonal crystal class with P4/ncc cell symmetry. No atoms sit on special positions, with the exception of an atom attributed to disordered guest or solvent. There is only one crystallographically independent copper ion, with another copper ion being generated by the n-glide plane ($d_{\text{Cu}\dots\text{Cu}} = 2.6676(7) \text{ \AA}$) to form the observed chromophore. There are four crystallographically independent oxygen atoms coordinated to the copper ion ($d_{\text{Cu}\dots\text{O}} = 1.9959(20), 1.9500(20), 1.9417(19), 2.0063(20) \text{ \AA}$), with four others also being generated by the n-glide plane to complete the chromophore. Each isophthalate ion contains four crystallographically independent carbon atoms, and there is one crystallographically independent nitrogen ($d_{\text{Cu}\dots\text{N}} = 2.1582(23)$) and five carbon atoms attributed to the pyridine ligand.

The asymmetric unit, excluding disordered solvent/guest, is therefore $\text{CuC}_{13}\text{H}_9\text{NO}_4$ (there are an additional 4.5 disordered isotropic carbon atoms), which gives $Z = 16$ to account for the entire unit cell composition. In keeping with the standard of using a more descriptive formula that better illustrates the structure of the material, this can be rewritten as $\{[\text{Cu}_2(\text{bdc})_2(\text{py})_2]\}_n$. This illustrates that the structure is based on dicopper SBUs formed via bdc ions, where each of four bdc moieties are shared with another SBU corresponding to four-halves per SBU (i.e. 2). This also indicates that the structure is polymeric; however, it does not indicate the dimensionality of the structure.

3.2.3. Space-filling models

Figure 3.1: Space filling models of compound 3, $\{[L_2Cu_2(bdc)_2]_4\}_n^*$



* Carbon (grey), oxygen (red), nitrogen (blue), hydrogen (white); L = pyridine is represented as a single nitrogen with remaining atoms deleted for clarity; non-coordinated solvent/guest removed for clarity

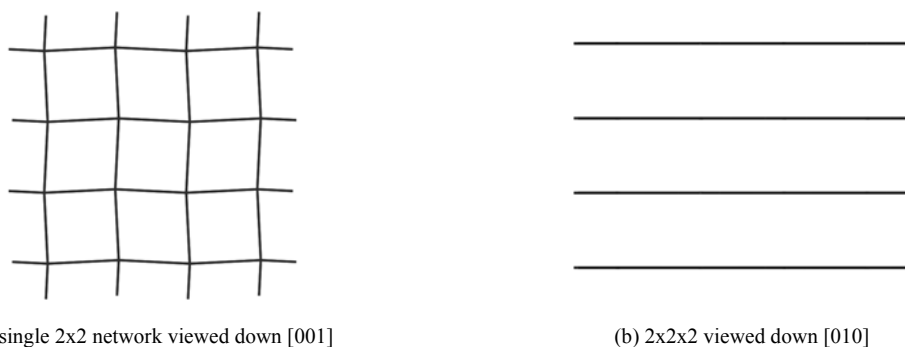
3.2.4. Illustrative description

The first consideration in looking at coordination polymers is the dimensionality of the network; the next is, perhaps, the topology; followed by the degree of interpenetration. It is anticipated that there is more than one supramolecular isomer possible for $\{L_2Cu_2(bdc)_2\}_n$ coordination polymers. Indeed, this will be demonstrated to be the case in subsequent sections and chapters. Therefore, in order to understand the differences between the supramolecular isomers, these features must be defined for each material.

Perhaps the easiest method for determining these features is to examine the basic connectivity of the dimetal tetracarboxylate SBUs. This is accomplished by linking the midpoints of the copper-copper bond in each SBU in such a manner that it reflects the connectivity defined by the bdc. The network is illustrated in Figure 3.2.

Immediately apparent on examination of the schematics is that the network is two-dimensional, non-interpenetrated and possesses the square grid (4^4)-net topology. A 4^4 -net can also be represented as a 4.4.4.4-net, which refers to the sequence of n-gons

Figure 3.2: Schematic illustration of the network observed in compound 3, $\{[L_2Cu_2(bdc)_2]_4\}_n^*$



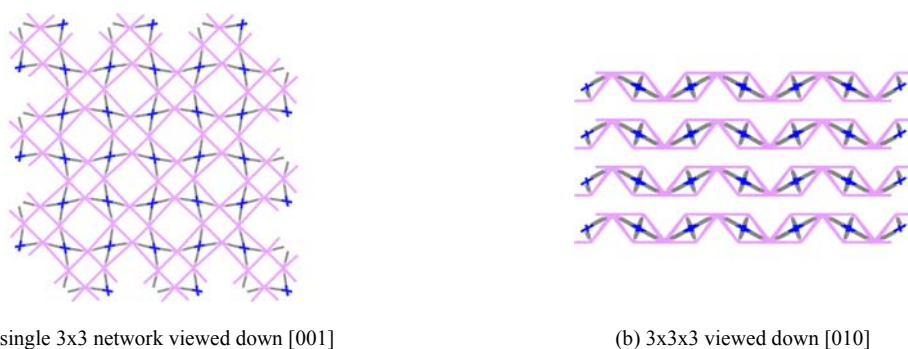
* derived from crystal structure coordinates and unit cell

around each vertex (i.e. four 4-gons, or squares). The dimensions of the grid are 9.407(8) x 9.407(8) Å and it is not an ideal square topology, with opposite interior angles of 95.63° and 84.37°. However, all of the lattice points from a single network do lie perfectly in a plane, as seen in figure 3.2b. It should be noted that the a and b unit cell dimension (18.7912 Å) is slightly less than two times the size of the individual squares due to the slight deviation from linear of the lattice vectors (174.37°).

Although this description accurately illustrates many of the key structural features of compound 3, a particular feature that is absent is the undulating nature of the networks, which is apparent in figure 3.1b. Also, the hypothesis at the beginning of this section was related to the possible relationship between the trimesate structure and isophthalate structures. The previous description fails to draw any illustrative comparison, as it does not address the molecular square representation of the SBU.

Therefore the crystal structure can be reduced in a similar fashion as compounds 1 and 2. The main difference being that the node representing the isophthalate is only ditopic (in comparison to the tritopic btc); however, the nodes are still predisposed at 120° with respect to one another. As such, it is no longer appropriate to compare the node to star graphs. The resulting schematic is illustrated in figure 3.3.

Figure 3.3: Schematic illustration of compound 3, $\{[L_2Cu_2(bdc)_2]_4\}_n$ *

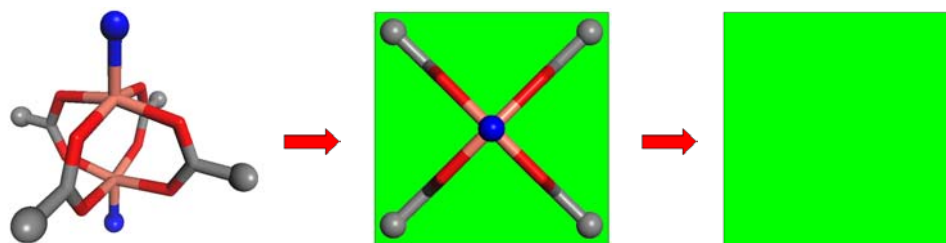


* derived from crystal structure coordinates and unit cell; SBU nodes are blue, trimesate nodes are orchid; grey connections illustrate chemical connectivity, orchid connections the boundaries of the triangular and square SBUs

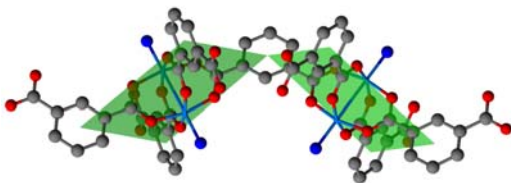
Several additional structural features become apparent on inspection of the new schematic: the undulating nature of the network, which was the desired result; and, interestingly, the presence of two channels having different dimensions (7.976 x 7.976 Å and 7.630 x 7.058 Å). This latter feature also explains why there are two squares per unit cell. These figures are made even clearer if the “filled” squares (i.e. the squares with SBUs at their center) are illustrated as such, where the squares are necessarily linked at their vertices at an angle of 120° (Figure 3.4).

This “cartoon” illustration reveals an additional structural feature that was not obvious by examining the previous schematics: the association of four SBUs to form bowl-shaped clusters of SBUs. The bowls are 18.613 Å across at the widest part of the bowl, and 7.976 Å across at the narrowest point. The clusters are therefore considered to be nanometer-scale building units, or nSBUs. In the context of zeolites (from which the acronym SBU is derived), they may also be considered tertiary building units (TBUs). The molecular formula of compound 3 is therefore represented as $\{[L_2Cu_2(bdc)_2]_4\}_n$ to illustrate this structural feature, and to differentiate it from its supramolecular isomers.

Figure 3.4: Schematic illustration of compound 3, $\{[L_2Cu_2(bdc)_2]_4\}_n^*$



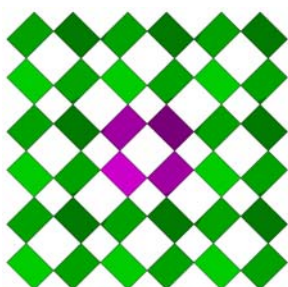
(a) reduction of dimetal tetracarboxylate to square illustration



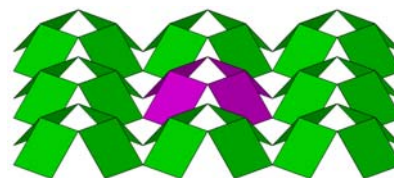
(b) molecular squares bridged by bdc



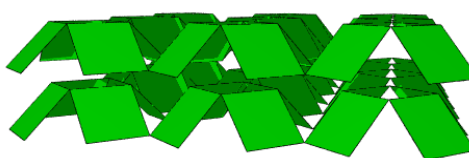
(c) bowl-shaped nSBU



(d) single network viewed down [001]



(e) perspective view of single layer



(f) perspective view of stacking of layers

* modeled from idealized coordinates

Compound 3 demonstrates that four square SBUs can indeed combine to form one bowl shaped nSBU, which in turn self-assembles with other nSBUs to form the undulating sheet structure depicted in Figure 3.4e. Taking into consideration that the bowls are composed of atoms, each bowl has an effective outer diameter of 0.94 nm; a depth (as measured by the perpendicular distance from the center of the base to mid-point of a line joining the top hydrogen atoms on opposite bdc moieties) of 0.84 nm and a

solvent-accessible volume of 0.518 nm^3 .^[16] The bowls are occupied by disordered benzene or pyridine guests and by the bottom of a bowl from the adjacent sheet. The layers therefore pack in an eclipsed fashion as illustrated in Figure 3.4f, giving rise to a channel between adjacent bowls. The channels are hour-glass shaped with a cavity of maximum dimensions of *ca.* $0.90 \times 0.90 \times 0.65 \text{ nm}$ and are occupied by benzene or pyridine guest molecules (in one unit cell the solvent-accessible volume is 0.28 nm^3 ^[16]). Between these cavities the channel narrows to an opening of *ca.* $0.15 \times 0.15 \text{ nm}$, which restricts the movement of the guest molecules through the channel. The distance between guest molecules is 0.81 nm . The total volume of both types of cavity represents *ca.* 23% of the volume of the unit cell.^[17] Single crystals maintained at room temperature under vacuum overnight gave identical Thermogravimetry-MS curves to those obtained directly from solution, indicating that **1** is stable at ambient temperatures. However, thermogravimetry also indicates that crystals of **1** are not stable to loss of guest because the pyridine ligands must be removed from the metal cluster to facilitate free release of guest molecules.

3.3. Compound 4: $\{[\text{L}_2\text{Cu}_2(\text{bdc})_2]_3\}_n$ ^{292,293}

3.3.1. Experimental

In a typical reaction, a 10 mL ethanolic solution of $\text{Cu}(\text{NO}_3)_2 \cdot 2.5\text{H}_2\text{O}$ (231 mg; 0.993 mmol) is layered onto a 10 mL ethanolic solution containing 1,3-benzenedicarboxylic acid (166 mg; 0.999 mmol), nitrobenzene (2.0 mL; 19 mmol) and pyridine (0.23 mL; 2.8 mmol). Prismatic, blue-green, crystalline hexagonal plates ($0.15 \times 0.15 \times 0.05 \text{ mm}$) form within hours under ambient conditions.

Selected crystallographic parameters are presented in Table 3.2. Complete crystallographic data for compound 4 can be found in Appendix A-4.

Table 3.2: Selected crystallographic parameters for $\{[L_2Cu_2(bdc)_2]_3\}_n$	
Crystal class	Trigonal
Space group (#)	P3c1 (158)
a = b =	18.6200(17) Å
c =	19.8040(27) Å
V =	5946.2(11) Å ³

3.3.2. Technical description

The structure results from μ_2 -coordination of each of the isophthalate carboxylates to two copper(II) ions. Each carboxylate is involved in the formation of a dicopper tetracarboxylate chromophore. The apically coordinated ligand, pyridine, was located and refined from the diffraction data. Additional electron density, attributed to disordered solvent or guest molecules present in the crystal lattice void space, was modeled as variable occupancy isotropic carbon and oxygen atoms.

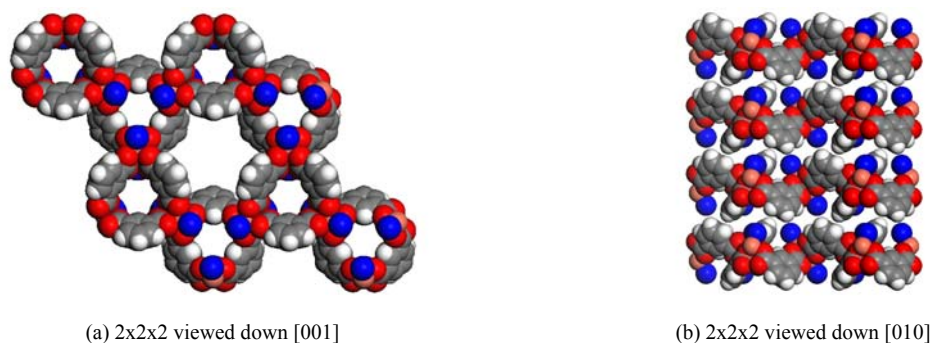
The crystal structure adopts a trigonal crystal class with P3c1 cell symmetry. No atoms sit on special positions, with the exception of atoms attributed to disordered guest or solvent. There are two crystallographically independent copper ions, which comprise a dimetal chromophore ($d_{Cu...Cu} = 2.6612(8)$ Å). There are eight crystallographically independent oxygen atoms coordinated to the copper ions ($d_{Cu1...O} = 1.9422(77)$, 1.9559(80), 1.9772(71), 1.9841(69) Å; $d_{Cu2...O} = 1.9507(72)$, 1.9677(71), 1.9749(74), 1.9884(72) Å), which complete the coordination in the chromophore. There are two crystallographically independent isophthalate ions (which include the eight oxygen

atoms), and there are two crystallographically independent pyridine ligands ($d_{Cu1...N} = 2.126(11)$; $d_{Cu2...N} = 2.184(10)$).

The asymmetric unit, excluding disordered solvent/guest, is therefore $Cu_2C_{26}H_{18}N_2O_8$, which gives $Z = 6$ to account for the entire unit cell composition. In keeping with the standard of using a more descriptive formula that better illustrates the structure of the material, this can be rewritten as $\{[Cu_2(bdc)_2(py)_2]\}_n$. This illustrates that the structure is based on dicopper SBUs formed via bdc ions, where each of four bdc moieties are shared with another SBU corresponding to four-halves per SBU (i.e. 2). This also indicates that the structure is polymeric; however, it does not indicate the dimensionality of the structure. It should be noted that this is the same basic molecular formula that was derived for compound 3, demonstrating that this structure is a supramolecular isomer, as anticipated.

3.3.3. Space-filling models

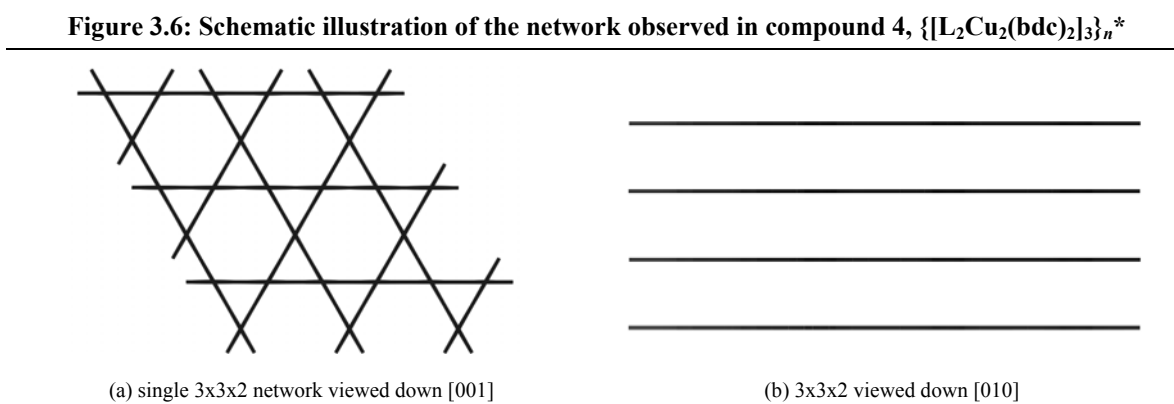
Figure 3.5: Space filling models of compound 4, $\{[L_2Cu_2(bdc)_2]_3\}_n^*$



* Carbon (grey), oxygen (red), nitrogen (blue), hydrogen (white); L = pyridine is represented as a single nitrogen with remaining atoms deleted for clarity; non-coordinated solvent/guest removed for clarity

3.3.4. Illustrative description

It is clear from examination of their respective space-filling models and crystallographic parameters, that compounds 3 and 4 are structurally different, despite having the same basic chemical composition. As such, they would appear to be prototypal structural supramolecular isomers. In order to better characterize their relationship, it is useful to reduce the crystal structure of compound 4 to a series of schematic representations in the same manner as was employed for compound 3. Figure 3.6 illustrates the basic connectivity of the SBUs (compare to figure 3.2).



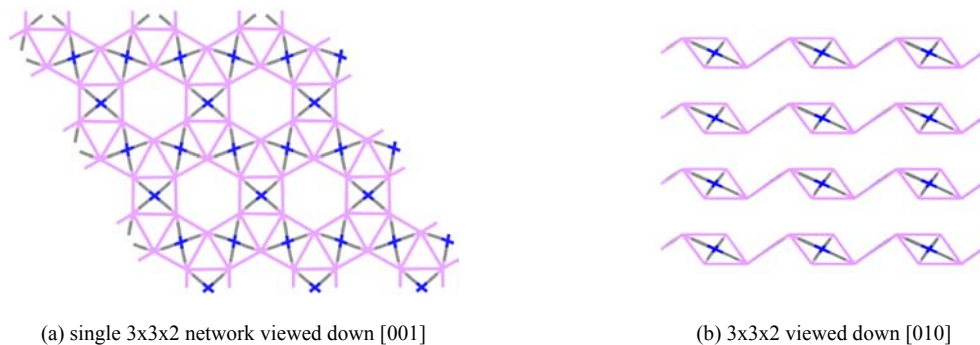
* derived from crystal structure coordinates and unit cell

As was the case for compound 3, most of the basic structural features of compound 4 are immediately revealed on examination of these schematic representations: compound 4 is a two-dimensional non-interpenetrated network possessing the 3.6.3.6 network topology (i.e. around each vertex there is a 3-gon (triangle), 6-gon (hexagon), 3-gon and a 6-gon, in that order). It is also important to note that this topology is known as a Kagomé lattice²⁹⁴, which will become relevant in later discussions. The length of the sides of the hexagons alternate between 9.307 and 9.315 Å, whereas there are two types

of equilateral triangles that have the same dimensions. Additionally, it should be noted that the networks stack with one another in an eclipsed fashion.

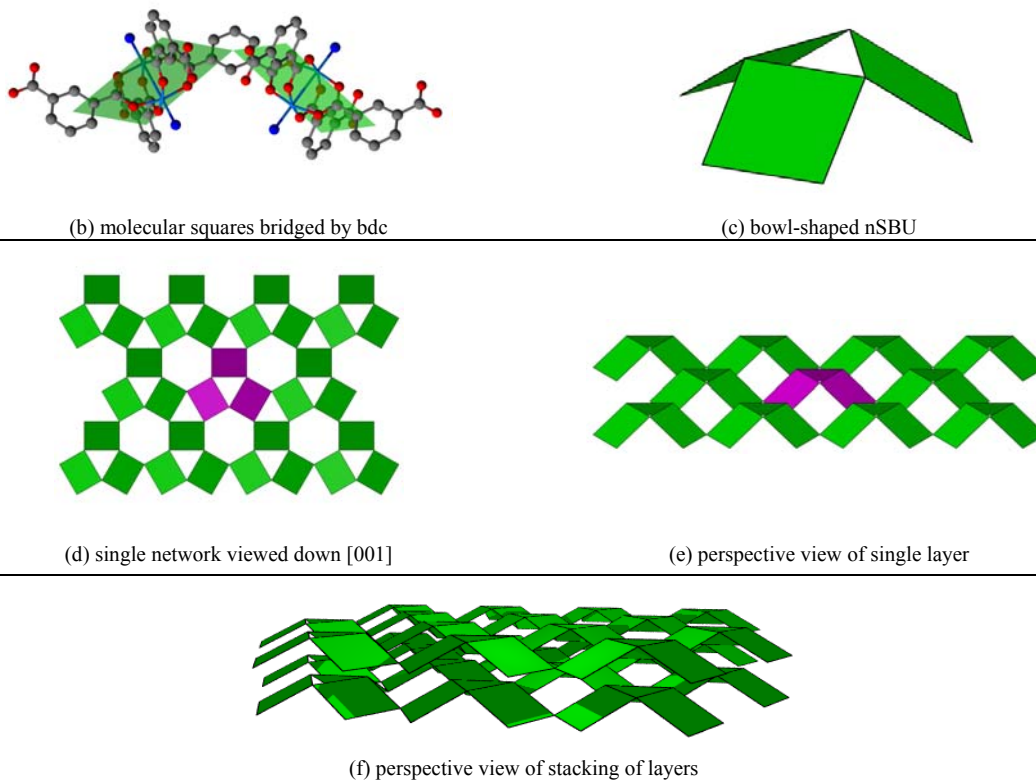
Figure 3.7 illustrates the schematic representation of compound 4 based on molecular squares. Figure 3.8 illustrates the cartoon representation of compound 4.

Figure 3.7: Schematic illustration of compound 4, $\{[L_2Cu_2(bdc)_2]_3\}_n^*$



* derived from crystal structure coordinates and unit cell; SBU nodes are blue, trimesate nodes are orchid; grey connections illustrate chemical connectivity, orchid connections the boundaries of the triangular and square SBUs

Figure 3.8: Schematic illustration of compound 4, $\{[L_2Cu_2(bdc)_2]_3\}_n^*$



* modeled from idealized coordinates

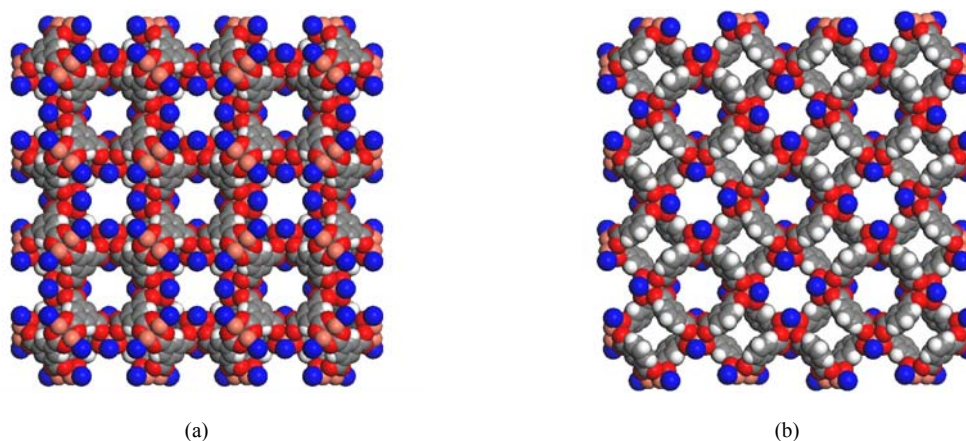
Compound 4 can therefore be described as the result of self-assembly of bowl-shaped triangular nSBUs to yield a nanoscale Kagomé lattice. Cu_2 dimers are positioned at the lattice points and are bridged via the bdc ligands, thereby generating large hexagonal cavities within the layer. The bowl-shaped nSBU facilitates efficient packing when the bowls are eclipsed, which results in eclipsing of the hexagonal cavities (1.11 nm diameter) and hexagonal channels of the same dimension. The layers are undulating due to the curvature imparted by the bdc moiety, having a 1.24 nm amplitude, and overlap adjacent layers by ca. 20 %. The apical positions of the Cu_2 dimers are occupied by coordinated pyridine ligands, and highly disordered solvent molecules occupy the hexagonal channels (ca. 28% by weight). Thermal analysis (TGA/DSC) indicates the included solvent and the pyridine ligands can be removed at ca. 200°C, and that the desolvated lattice is thermally stable to temperatures in excess of 300°C. The most intense peaks observed in the X-ray powder diffraction (XPD) patterns from the bulk sample are consistent with those calculated from single crystal diffraction data.

3.4. Discussion

The hypothesis at the beginning of this chapter was that the structures that could be made via reaction of isophthalate with copper(II) would result in a series of structures that could be rationalized based on “trimming” the trimesate ions in compound 2. In other words, any new structures should be able to be extracted from compound 2. It should be stressed that the hypothesis does not inherently predict the crystal structure of the new compounds, only that any networks based on isophthalate should be a subset of the three-dimensional network based on trimesate. It is fully anticipated that lower dimensional networks will exhibit spatial supramolecular isomerism.

The most apparent similarities are observed between compound 2 and compound 3. Figure 3.9 illustrates the [001] projections of each compound, which have been chosen so that they are the same dimensions. Also, for the sake of continuity, the projection of compound 2 has been derived from the crystal data of the isomorphous structure based on copper(II).

Figure 3.9: Comparison of [001] projections of compounds 2 & 3



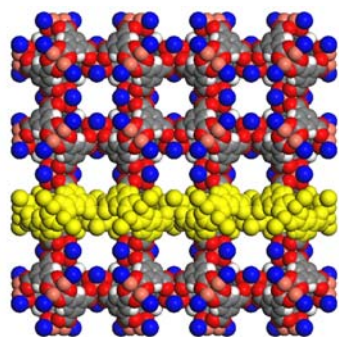
* Carbon (grey), oxygen (red), nitrogen (blue), hydrogen (white); L = pyridine is represented as a single nitrogen with remaining atoms deleted for clarity; non-coordinated solvent/guest removed for clarity

Indeed, the two projections are nearly superimposable. The only discernable difference is that the “small” channels that are open in compound 3, are occupied by the dicopper tetracarboxylate chromophore that results from the extension of the additional carboxylate. Although, at first glance, the lattice parameters of the two compounds do not appear to be coincident, the projection of compound 3 has been rotated by 45° to facilitate easy comparison. Therefore, in order to compare the metrics of the two networks the diagonal of the ab plane must be compared to the a and b lattice parameters of compound 2. For compound 3, $a = b = 18.79 \text{ \AA}$ and the diagonal is therefore $\sqrt{(2 \cdot 18.79^2)} = 26.57 \text{ \AA}$. In consideration of the similarities seen in Figure 3.9, it is

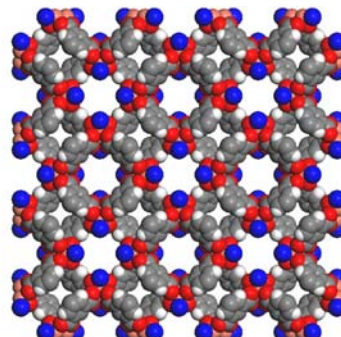
unsurprising that this value is very close to the 26.52 Å length of the a and b axes of compound 2.

It is, perhaps, simply a coincidence that the orientations of the crystals are such that these similarities are immediately apparent following a simple visual examination of the structures. A closer examination reveals that the two-dimensional tetragonal sheet can be derived from compound 2, by extracting the (004) plane. In other words, the centers of each of the SBUs associated with an individual network lie on the (004) plane. Of course, it has already been shown that the networks are undulating, and in order to extract a nearly complete layer, it is necessary to “trim” the third carboxylate of the trimesate along the C-C bonds that lay 4 Å above and below the (004) plane. The network that results is illustrated in Figure 3.10, along with a highlight of its disposition in compound 2. It should also be noted that due to the cubic symmetry of the material, the (004) plane is equivalent to the (040) and (400) planes. The network illustrated in Figure 3.10b differs from compound 3 only in the absence of a proton in the 5-position of the isophthalate (compare to Figure 3.9b).

Figure 3.10: Illustration of the extraction of compound 3 from compound 2



(a) compound 2 viewed down the [001] projection; the 4⁴-net cross section is highlighted in yellow



(b) the 4⁴-net extracted from compound 2

* Carbon (grey), oxygen (red), nitrogen (blue), hydrogen (white); L = pyridine is represented as a single nitrogen with remaining atoms deleted for clarity; non-coordinated solvent/guest removed for clarity

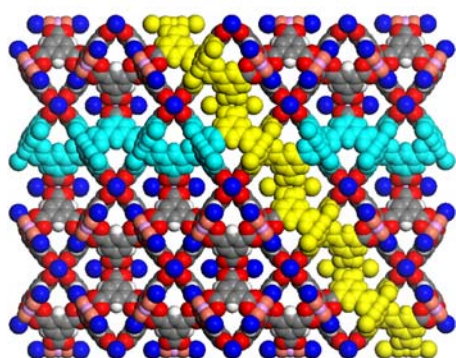
Based on this analysis, it is natural to examine other crystallographic planes of compound 2 to look for additional networks that can be extracted in such a manner. All two-dimensional networks that are related to compound 2, should, in principle, be easily derived from a systematic analysis of the many crystallographic planes. Of course, the primary motivation behind this is to determine if there exists a relationship between compound 2 and compound 4.

It should be obvious that, due to the hexagonal symmetry of the 3.6.3.6-network observed for compound 4, if there exists a plane that can be extracted from compound 2 that is commensurate with compound 4, it must be perpendicular to the [111] axis of compound 2. This is because the [111] axis for cubic unit cells is necessarily a hexagonal axis. Unfortunately, the projection down [111] of compound 2 does not have obvious similarities to compound 4 (Figure 2.2c); however, the hexagonal symmetry is clear. The relationship between cubic and hexagonal cell parameters is given by $a_{\text{cubic}} = \sqrt{2} a_{\text{hex}}$, therefore it is anticipated that the cell parameters for the 3.6.3.6-network will be $26.52 / \sqrt{2} = 18.75 \text{ \AA}$. This is close to the 18.62 \AA observed for compound 4; however, it should be noted that compound 2 is the zinc(II) structure, and if the calculation is done using the cell parameter for the copper(II) compound (26.343 \AA) the predicted value is adjusted to 18.627 \AA .

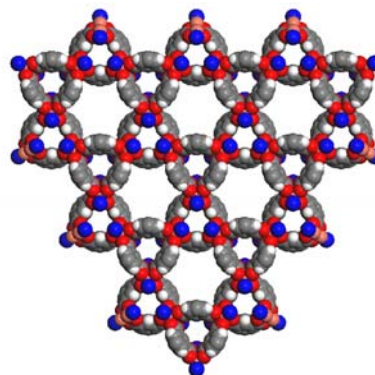
In order to examine planes perpendicular to [111], it is useful to view the crystal structure down the [011] projection, which is perpendicular to [111] (note that [101] and [110] are equivalent axes in a cubic crystal class). Indeed, extraction of successive planar cross sections that are parallel to these axes, reveals that the (222) plane corresponds to the 3.6.3.6-network observed for compound 4. Figure 3.11 illustrates the projection

down [011], and highlights the cross section corresponding to the tetragonal 4⁴-network (cyan) and the cross section corresponding to the trigonal 3.6.3.6-network (yellow).

Figure 3.11: Illustration of the extraction of compound 4 from compound 2.



(a) compound 2 viewed down the [011] projection; the 4⁴-net cross section is highlighted in cyan, the 3.6.3.6-net is highlighted in yellow



(b) the 3.6.3.6-net extracted from compound 2

* Carbon (grey), oxygen (red), nitrogen (blue), hydrogen (white); L = pyridine is represented as a single nitrogen with remaining atoms deleted for clarity; non-coordinated solvent/guest removed for clarity

Again, due to the undulating nature of the network, in order to extract a nearly complete layer it is necessary to “trim” the third carboxylate of the trimesate along the C-C bonds that lay 4 Å above and below the (222) plane. The network that results is illustrated in Figure 3.11b. This network differs from compound 4 only in the absence of a proton in the 5-position of the isophthalate (compare to Figure 3.5a).

Due to the modular nature of compounds 3 and 4, they are amenable to derivitization. There are four main strategies to facilitate the synthesis of topological analogues: metal substitution, dicarboxylate ligand modification or substitution, coordinated ligand substitution or removal, and guest incorporation. The dimetal tetracarboxylate chromophore is known for most of the transition metals and it is anticipated that the material properties will be dramatically altered by incorporation of alternate metals or mixed metals, and the effect of varying the oxidation state of the metals is also expected to have dramatic results. Chemical modification of the bdc ligand

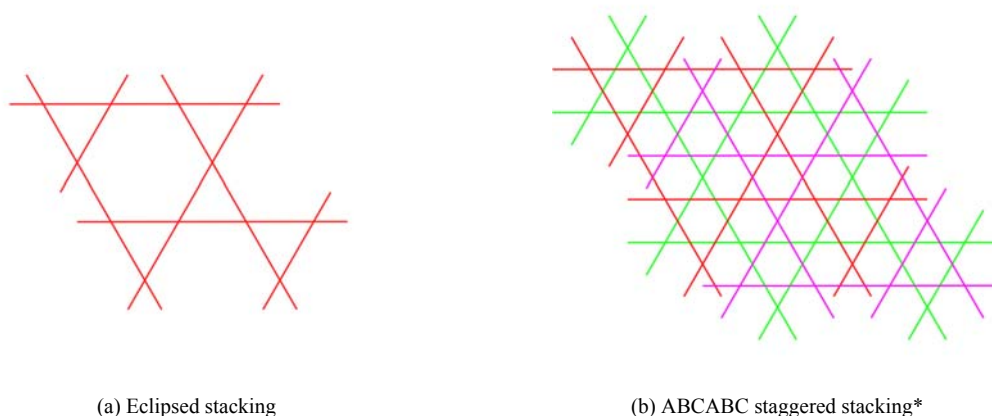
will likely have two major implications: separation of the layers and altering the intradimer electronic coupling. Incorporation of bulky substituents in the 2- or 5-position should lead to a larger spacing between the layers, and incorporation of electron donating or withdrawing substituents may enhance and reduce the intradimer coupling, respectively. It has already been demonstrated that substitution of the coordinating ligand has a marginal effect on the magnetic properties of related systems,²⁸⁴ so it is anticipated that coordination of an appropriate ligand in the apical positions of the SBUs may enhance a desired physical property. Furthermore, varying the size of the coordinated ligand may lead to the ability to control the interlayer separation. This may also be achieved by the incorporation of a guest molecule between layers, and, additionally, the incorporation of an appropriate guest between layers or in the open channels may lead to multifunctional materials. For the latter, it is anticipated that incorporation of optically active, conducting or magnetic molecules will have substantial influence on the bulk physical properties of the parent network.

As has been emphasized, lower dimensional structures, such as the two-dimensional networks observed for compounds 3 and 4, may exhibit spatial supramolecular isomerism by exhibiting different interlayer orientations. The synthesis of supramolecular isomers could be achieved by modification of synthetic methods. Additionally, chemical modifications such as those listed above, may also lead to various stacking modes for the layers.

For example, several examples of the 3.6.3.6-network have been prepared by substituting the coordinated ligand. This is achieved *in situ*, not by substitution after synthesis of compound 4 (although this method is currently being investigated). In

consideration of the fact that the coordinated pyridine ligands in compound 4 protrude above and below each layer, it should be unsurprising that the synthesis of a topologically equivalent network with 4-picoline coordinated in the apical position results in an increase in interlayer separation by 2.8 Å. Surprisingly, however, the synthesis of the same network with isoquinoline coordinated in the apical position results in the decrease of the interlayer separation by 1.2 Å. A closer look at the crystal structure of the latter compound reveals that the layers do not stack in an eclipsed fashion, but rather adopts a staggered orientation. Figure 3.12 illustrates the two modes of stacking and underscores the implications with respect to bulk porosity that the stacking modes have. This mode minimizes the steric effects of the apically coordinated ligands, while at the same time contributes additional steric effects between the layers (i.e. it deviates from the ideal “stacking bowls” orientation).

Figure 3.12: Illustration of the two stacking modes observed for the 3.6.3.6 topology.



* Three networks colored red, magenta and green, respectively.

The purpose of this discussion is devoted solely to the structural analysis and development of strategies for the design of network topologies. Therefore, specific details on the synthesis of these structures will be left to other members of the Zaworotko research team to elaborate on. Indeed, there is an entire class of conformational

supramolecular isomers of the 4⁴ tetragonal coordination polymer, and several additional examples of the 3.6.3.6 trigonal coordination polymer that have also been prepared.

3.5. Conclusions

In summary, compound 3 exhibits an infinite two-dimensional structure formed by the self assembly of nSBUs which are formed by four square carboxylate bridged dimetal(II) SBUs (this compound has been synthesized with zinc(II) in addition to the copper compound described above). It should be emphasized that compound 3 is curved as a result of the 120° angle subtended by the bdc ligands. The shape and chemical nature of the bowls in compound 3 resembles calixarenes and the ability to incorporate guest molecules that are known to form complexes with calixarenes is actively being investigated.

Compound 4 exhibits an alternate two-dimensional network formed by three square dimetal(II) tetracarboxylate SBUs (the zinc(II) analogue has also been synthesized). The network is also curved as a result of the 120° angle subtended by the bdc ligands. The basic chemical composition of both networks is $\{L_2M_2(bdc)_2\}_n$ (L = coordinated ligand/solvent; M = transition metal; bdc = isophthalate), highlighting the fact that they are architectural supramolecular isomers. In order to differentiate the two networks in the chemical formula, they are rewritten to illustrate the nature of the nSBUs that assemble to afford the overall structure: $\{[L_2M_2(bdc)_2]_4\}_n$ (compound 3) and $\{[L_2M_2(bdc)_2]_3\}_n$ (compound 4).

The topology of compound 3 is exemplified by a 4⁴-network and the topology of compound 4 is exemplified by a 3.6.3.6-network (also known as a Kagomé lattice).

These compounds dramatically underscore the potential afforded by supramolecular

chemistry for the design of molecular nanostructure assemblies with specific topologies and emphasize how the composition of a material is not the only feature one must consider when designing a phase that exhibits particular bulk physical properties. Although these compounds have identical composition, their relative porosities are clearly different, and even more dramatic differences are observed in comparing the magnetic properties of the two compounds. This will be discussed in more detail in a later chapter.

From a design perspective, perhaps the most important information that can be learned from compounds 3 and 4 is that they can both be extracted from a higher-dimensional network (compound 2) that has a closely related chemical composition. Furthermore, a detailed analysis of compound 2 suggests that compounds 3 and 4 are the *only* two-dimensional networks that are possible for the periodic assembly of molecular squares linked by their vertices. It should also be noted that these networks are not specifically dependant on the exploitation of a 120° ligand. In principle, any ditopic carboxylate ligand that subtends an angle greater than 90° can afford either network. Indeed, both networks have been observed for ligands that subtend 144° (e.g. thiophene dicarboxylate and *N*-methylpyrrole dicarboxylate).

Based on these results, a more detailed analysis of compound 2 reveals additional supramolecular isomers, that are not two-dimensional, which are possible for $\{L_2M_2(bdc)_2\}_n$. The next chapter deals with these compounds in more detail.

Chapter 4

Zero-Dimensional Structures

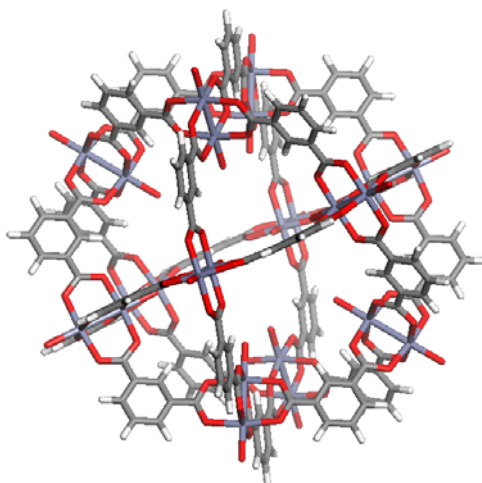
4.1. Preamble

One of the key observations regarding the structure of compounds 1 and 2 is the presence of large, spherical cavities having octahedral symmetry (chapter 2). These cavities are described as having structures that can be approximated by models of faceted polyhedra, or more specifically by Small cubicuboctahedra for compound 1 and by Small rhombihexahedra for compound 2. It occurred to us that it should, in principle, be possible to construct the discrete molecular spheres by replicating the synthetic conditions, with the use of isophthalic acid instead of trimesic acid. Of course, it has been shown in chapter 3 that these synthetic conditions afford two-dimensional networks; however, it was anticipated that the discrete spherical supramolecular isomers should also be possible.

As was the case for the two-dimensional structures, the reaction of isophthalate with copper(II) ions will preferably afford dicopper tetracarboxylate SBUs, and as such should only result in the synthesis of molecular Small rhombihexahedra. This assumes that the synthesis conditions can be modified to afford the discrete supramolecular isomer preferentially over the two-dimensional structures, and possibly over additional supramolecular isomers having other dimensionalities. It should be noted that this is one of the rare examples of a supramolecular structure that was predicted prior to synthesis.

Indeed, models of the structure were constructed and analyzed prior to its eventual synthesis. Figure 4.1 illustrates a model of the compound that was presented at the International Chemical Congress of Pacific Basin Societies on December 18, 2000.

Figure 4.1: Illustration the predicted structure of a molecular Small rhombihexadron



The molecule was successfully identified on December 31, 2001 and, interestingly, an additional discrete supramolecular isomer was also identified.¹³⁹ The latter structure would indicate that the initial hypothesis that all supramolecular isomers based on dimetal tetracarboxylate SBUs could be extracted from compound 2 is flawed.

4.2. Compound 5: $[L_2Cu_2(bdc)_2]_{12}$

4.2.1. *Experimental*

In a typical reaction, a 10 mL methanolic solution of $Cu(NO_3)_2 \cdot 2.5H_2O$ (231 mg; 0.993 mmol) and 1,3-benzenedicarboxylic acid (166 mg; 0.999 mmol) is layered onto a 10 mL methanolic solution containing nitrobenzene (2.0 mL; 19 mmol) and pyridine (0.23 mL; 2.8 mmol). Prismatic, blue-green, single crystals (0.15 x 0.15 x 0.10 mm) form within hours under ambient conditions.

Alternatively, microcrystals can be obtained quantitatively by direct mixing of the above reagents.

Selected crystallographic parameters are presented in Table 4.1. Complete crystallographic data for compound 5 can be found in Appendix A-5.

Table 4.1: Selected crystallographic parameters for $[L_2Cu_2(btc)_2]_{12}$	
Crystal class	Cubic
Space group (#)	$Im\bar{3}m$ (229)
a = b = c =	27.6895(17) Å
V =	21229.8(21) Å ³

4.2.2. Technical description

The structure results from μ_2 -coordination of each of the isophthalate carboxylates to two copper(II) ions. Each carboxylate is involved in the formation of a dicopper tetracarboxylate chromophore. Although it is anticipated that coordinating solvent and/or base (i.e. pyridine) will be coordinated to the apical positions of the metal chromophores, none were located from the diffraction data. Only a single coordinated atom, arbitrarily assigned as oxygen, was refined. This is most likely due to the fact that these positions are highly disordered. Not only can the positions be water, methanol or pyridine, each of these can be further disordered by rotation about the coordination axis. Additional electron density, attributed to disordered solvent or guest molecules present in the crystal lattice void space, was modeled as variable occupancy isotropic carbon atoms. One of these carbon atoms, which has a 40% occupancy (not taking into account a special position constraint that imposes an additional 50% occupancy), is positioned 1.436(90) Å away from one of the apically coordinated oxygen atoms. No other electron density was located near this particular carbon or coordinated oxygen. This is suggestive that this

position can be attributed to methanol, disordered over two positions; however, additional data is required in order to make more definitive conclusions. From a design perspective, knowledge of the exact nature of the coordinated ligand is not necessary, as it is not directly involved in directing the network topology. Furthermore, it has been demonstrated in related materials that these positions can be exchanged or removed while maintaining the basic architecture.

The crystal structure adopts a cubic crystal class with $Im\bar{3}m$ cell symmetry. There are two crystallographically independent copper ions that sit on a four-fold rotation axis, which comprise the core of the dimetal tetracarboxylate chromophore ($d_{Cu...Cu} = 2.6039(25)$ Å). Each copper ion has one crystallographically independent oxygen corresponding to isophthalate coordination ($d_{Cu1...O1} = 1.9592(53)$ Å; $d_{Cu2...O2} = 1.9522(53)$ Å), and one oxygen corresponding to the coordinated ligand or solvent that sits on a four-fold rotation axis ($d_{Cu1...O11} = 2.1644(105)$ Å; $d_{Cu2...O21} = 2.1646(129)$ Å). The remaining structure is generated from five crystallographically independent carbon atoms, three have hydrogens placed in calculated positions, two sit on a mirror plane, and the appropriate space group symmetry operations.

The empirical formula, excluding disordered solvent/guest, is therefore $Cu_8H_4O_5$, which gives $Z = 48$. To be consistent with previous analysis this is modified to illustrate the presence of the SBU: $Cu_2C_{16}H_8O_{10}$ or, more generally, $L_2Cu_2(bdc)_2$, where $L =$ water, methanol or pyridine. This clearly illustrates that compound 5 is a supramolecular isomer of compounds 3 and 4. Although in the previous structures the formula was a polymer, the basic structural unit in compound 5 is a discrete molecule.

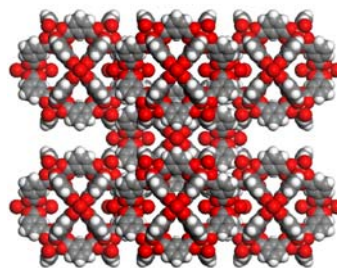
An analysis of the crystal structure indicates that there are twelve SBUs per molecule, and the final molecular formula is therefore $[\text{L}_2\text{Cu}_2(\text{bdc})_2]_{12}$, which gives $Z = 2$.

4.2.3. Space-filling models

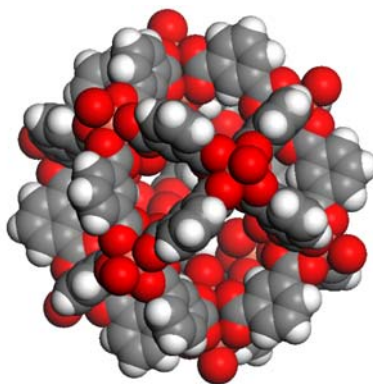
Figure 4.2: Space filling models of compound 5, $[\text{L}_2\text{Cu}_2(\text{bdc})_2]_{12}$ *



(a) 1x1x1 viewed down [001]



(b) 1x1x1 viewed down [011]



(c) discrete molecular unit (random orientation)

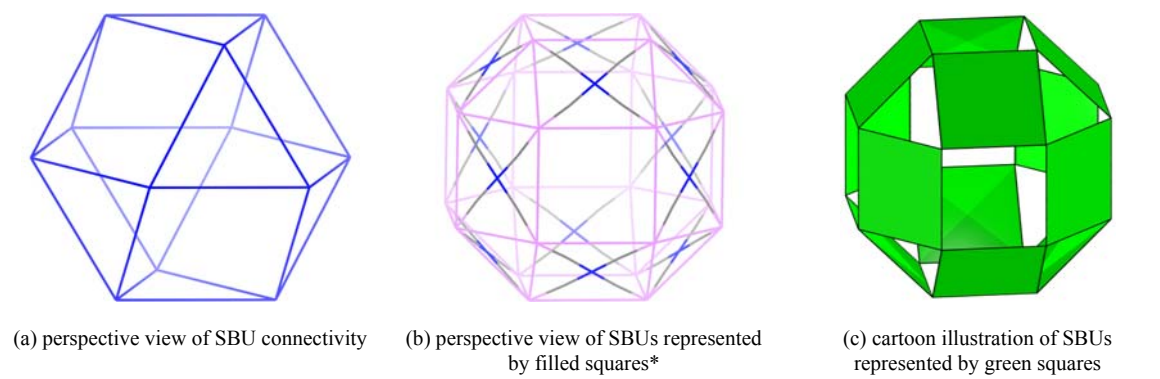
* Carbon (grey), oxygen (red), hydrogen (white); coordinated ligand is represented as a single oxygen with remaining atoms deleted for clarity; non-coordinated solvent/guest removed for clarity

4.2.4. Illustrative description

The reduction of compound 5 to a representative schematic is made easier by the prior analysis of compound 2. Indeed, from the outset, the goal of this synthesis was the directed assembly of a molecular Small rhombihexahedra. Therefore, unlike the analysis of the previous compounds, the schematic *preceded* the structural data. It is, of course, important to verify that the structure is as was predicted and previously illustrated in Figure 2.7. Therefore, schematic illustrations derived from the crystal structure data are

given in Figure 4.3. These schematics are limited to a single molecular entity and illustrate the basic connectivity of the SBUs (Figure 4.3a) and the expanded schematic based on the interpretation that SBUs can be approximated by molecular squares (Figure 4.3b). The cartoon illustration of a Small rhombihexahedra is also illustrated for comparison (Figure 4.3c).

Figure 4.3: Schematic illustration of compound 5, $[L_2Cu_2(bdc)_2]_{12}$



* SBU nodes are blue, isophthalate nodes are orchid; grey connections illustrate chemical connectivity, orchid connections the boundaries of the square SBUs

The first feature that is immediately apparent is that the net defining the connectivity of the SBUs is congruent with the edge-skeleton of a cuboctahedron, an Archimedean solid. Secondly, as anticipated, the network defining the edges of the molecular squares is congruent with the edge-skeleton of a Small rhombicuboctahedron, another Archimedean solid. Lastly, the schematic illustrating the SBUs as filled squares is identical to the cartoon depiction of a Small rhombihexahedron.

Therefore, compound 5 can be described as being composed of vertex linked molecular squares (green) that self-assemble into small rhombihexahedra. Compound 5 contains coordinated ligands that are apically bonded to the metal ions that lie at the exterior and interior surface of the molecular sphere. The internal diameter of the sphere as measured across opposite interior copper ions is 16.02 Å, which corresponds to an

effective interior diameter of 14.53 Å (based on an ionic radii for Cu²⁺ of 0.73 Å). The internal cavity therefore has a volume of 1606 Å³ (1.606 nm³). Alternatively, if the interior diameter is measured between opposite coordinated oxygen atoms, the effective diameter is 8.65 Å and the volume is 339 Å³. To put this in context, the diameter of C₆₀ is approximately 7 Å and the effective volume is approximately 326 Å³, meaning that compound 5 could in principle, encapsulate C₆₀. Compound 5 represents one of the largest spheroid structures that has been crystallographically characterized to date, with a molecular volume of ca. 10600 Å³ (i.e. >10nm³).

4.3. Compound 6: [L₂Cu₂(bdc)₂]₁₂

4.3.1. Experimental

In a typical reaction, a 10 mL methanolic solution of Cu(NO₃)₂·2.5H₂O (231 mg; 0.993 mmol) and 1,3-benzenedicarboxylic acid (166 mg; 0.999 mmol) is layered onto a 10 mL methanolic solution containing nitrobenzene (2.0 mL; 19 mmol) and lutidine, 2,6-dimethylpyridine, (0.25 mL; 2.1 mmol). Prismatic, blue-green, single crystals (0.20 x 0.20 x 0.15 mm) form within hours under ambient conditions.

Alternatively, microcrystals can be obtained quantitatively by direct mixing of the above reagents.

Selected crystallographic parameters are presented in Table 4.2. Complete crystallographic data for compound 6 can be found in Appendix A-6.

Crystal class	Hexagonal
Space group (#)	$P6_3/m$ (176)
a = b =	28.6458(19) Å
c =	28.1649(26)
V =	20015.2(28) Å ³

4.3.2. Technical description

The structure results from μ_2 -coordination of each of the isophthalate carboxylates to two copper(II) ions. Each carboxylate is involved in the formation of a dicopper tetracarboxylate chromophore. Although it is anticipated that coordinating solvent and/or base (i.e. pyridine) will be coordinated to the apical positions of the metal chromophores, none were located from the diffraction data. Only a single coordinated atom, arbitrarily assigned as oxygen, was refined. This is most likely due to the fact that these positions are highly disordered. Not only can the positions be water or methanol (note that the synthesis is done in the presence of a non-coordinating base, lutidine), each of these can be further disordered by rotation about the coordination axis. Additional electron density, attributed to disordered solvent or guest molecules present in the crystal lattice void space, was modeled as variable occupancy isotropic carbon atoms. Some of these carbon atoms are positioned in close proximity of the apically coordinated oxygen atoms, indicative that these positions can be attributed to disordered methanol; however, additional data is required in order to make definitive conclusions.

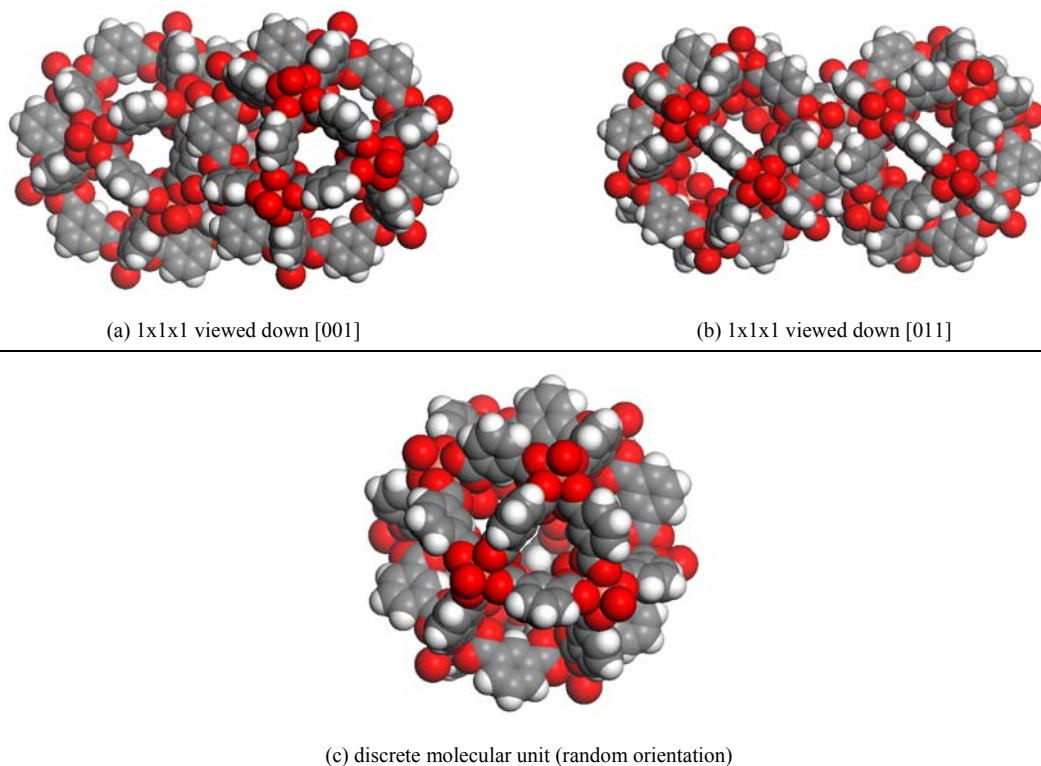
The crystal structure adopts a hexagonal crystal class with $P6_3/m$ cell symmetry. There are six crystallographically independent copper ions, which comprise the core of three dimetal tetracarboxylate chromophores ($d_{Cu1...Cu2} = 2.6085(48)$ Å; $d_{Cu3...Cu4} = 2.6132(47)$ Å; $d_{Cu5...Cu6} = 2.6084(36)$ Å;). There are twenty-six crystallographically

independent oxygens: three equatorially coordinated to each of Cu1-Cu4, four equatorially coordinated to each of Cu5 and Cu6 ($\bar{d}_{\text{Cu}\dots\text{O}} = 1.959 \text{ \AA}$, $\sigma = 0.019 \text{ \AA}$), and one apically coordinated to each copper ($\bar{d}_{\text{Cu}\dots\text{O}} = 2.182 \text{ \AA}$, $\sigma = 0.013 \text{ \AA}$). There are forty crystallographically independent carbon atoms with twenty hydrogens placed in calculated positions. Cu1 – Cu4 sit on a mirror plane, as do twelve of the oxygen atoms and sixteen carbon atoms.

The empirical formula, excluding disordered solvent/guest, is therefore $\text{Cu}_8\text{H}_4\text{O}_5$ ($\text{Cu}_4\text{C}_{32}\text{H}_{16}\text{O}_{20}$ from the atom listing), giving $Z = 48$. Following the format established for the previous compounds, this can be rewritten as $\text{Cu}_2\text{C}_{16}\text{H}_8\text{O}_{10}$ or $\text{L}_2\text{Cu}_2(\text{bdc})_2$ to illustrate that the structure is sustained by dicopper tetracarboxylate chromophores. This confirms that the structure is a supramolecular isomer of compounds 3 and 4, and, although the structure may at first seem to be the same as compound 5, projections of the crystal structure indicate significant structural differences between the two molecules. The composition, however, is verified to be the same by determining that there are twelve SBUs per molecule, and the final molecular formula is therefore $[\text{L}_2\text{Cu}_2(\text{bdc})_2]_{12}$, which gives $Z = 2$, and is the same composition as compound 5

4.3.3. Space-filling models

Figure 4.4: Space filling models of compound 6, $[L_2Cu_2(bdc)_2]_{12}^*$



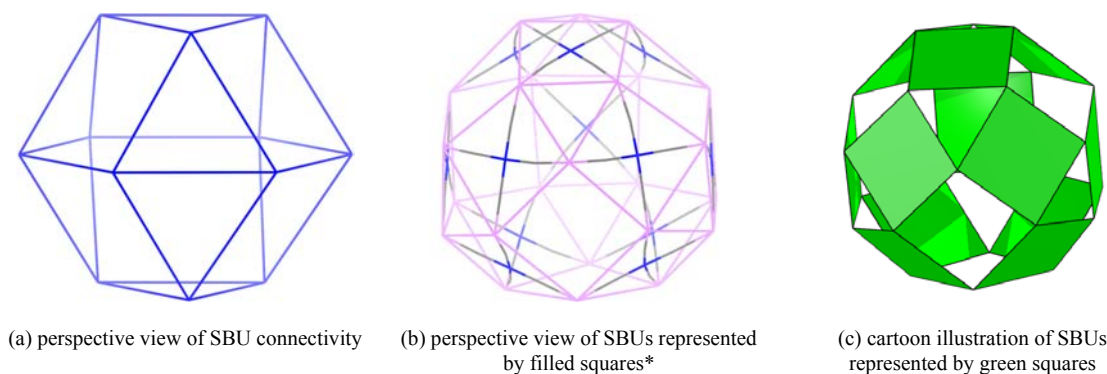
* Carbon (grey), oxygen (red), hydrogen (white); coordinated ligand is represented as a single oxygen with remaining atoms deleted for clarity; non-coordinated solvent/guest removed for clarity

4.3.4. Illustrative description

Unlike compound 5, schematics did not precede the observation of compound 6. Nevertheless, the structure is closely related to compound 5 and can therefore be rapidly analyzed in a similar manner. Figure 4.5 illustrates the schematic representations of compound 6 that correspond to the same type of schematics presented for compound 5 in Figure 4.3.

As was emphasized previously, it is not immediately obvious that there are differences between compounds 5 and 6. This underscores the importance of examining schematics in gaining a complete understanding of a crystal structure and its components.

Figure 4.5: Schematic illustration of compound 6, $[L_2Cu_2(bdc)_2]_{12}^*$



* SBU nodes are blue, isophthalate nodes are orchid; grey connections illustrate chemical connectivity, orchid connections the boundaries of the square SBUs

Figure 4.5a clearly illustrates the fundamental difference in the connectivity of the SBUs in compound 6. It was demonstrated that the net representing the connectivity of the SBUs in compound 5 was congruent with the edge-skeleton of a cuboctahedron. The net representing the connectivity of the SBUs in compound 6 is congruent with the edge-skeleton of a Triangular orthobicupola, a Johnson Solid (Appendix C provides a list and description of the 92 Johnson Solids).

The cartoon illustration of compound 6, which was derived from the coordinates of the net illustrated in Figure 4.5b, does not correspond to any known solid. In fact, the faceted solid illustrated in Figure 4.5c cannot be constructed by the assembly of uniform squares at their vertices; it can only be constructed by the assembly of kites and squares at their vertices.

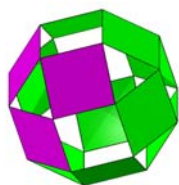
The geometric center of the spheres lies at the special position $(1/3, 1/6, 1/4)$. The most interior copper is 7.977 \AA from the center, which gives a maximum desolvated effective interior volume of 1159 \AA^3 . The most interior coordinated oxygen is 5.788 \AA from the center, giving a maximum hydrated interior volume of 326 \AA^3 . The molecular volume is just slightly less than compound 5 at 10008 \AA^3 .

4.4. Discussion

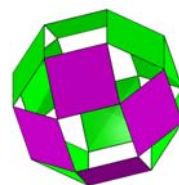
There are several structural features that require further consideration: the fundamental difference between the discrete spherical assemblies and the two-dimensional networks, and the fundamental differences between the two supramolecular isomers of the discrete assemblies. The latter is of particular interest, as the synthesis of compound 6 was not anticipated based on the initial hypothesis.

Compounds 3 and 4 have been described as being the result of the self-assembly of nanoscale SBUs (nSBUs). Compound 3 results from the assembly of square nSBUs (i.e. an aggregate of four SBUs), and compound 4 results from the assembly of triangular nSBUs (i.e. an aggregate of three SBUs). Figure 4.6 illustrates how compounds 5 and 6 can be described as being the result of the self-assembly of triangular *and* square nSBUs. Indeed, there are no regular or semi-regular tilings of the plane that can sustain the assembly of triangular and square aggregates of squares, suggesting that one of the keys to promoting the formation of the discrete assemblies is to promote the formation of triangular and square aggregates in solution.

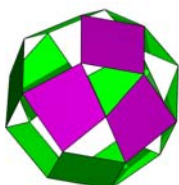
Figure 4.6: Cartoon illustrations of the nSBU components of compounds 5 and 6



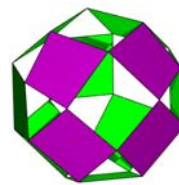
(a) triangular nSBU in compound 5



(b) square nSBU in compound 5



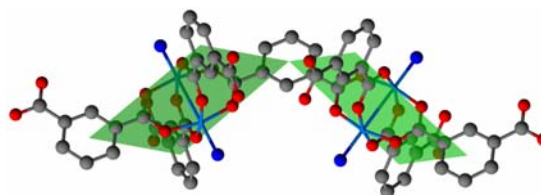
(c) triangular nSBU in compound 6



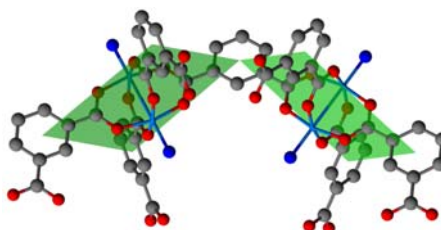
(d) square nSBU in compound 6

Another fundamental difference between the discrete supramolecular isomers and the two-dimensional supramolecular isomers is the ‘orientation’ of the carboxylates of the isophthalate ions. Figure 4.7a illustrates the connectivity of the molecular squares as observed in compounds 3 and 4. It should be obvious that there is no physical barrier preventing the isophthalate from rotating about the coordinated carboxylate to adopt alternate orientations. It must be noted that the electronically favored configuration for the carboxylate is to be co-planar with the phenyl ring due to combined delocalization of the carboxylate electrons with the aromatic phenyl electrons. This results in only two favored orientations, labeled as “up” and “down” (Figure 4.7). If the ‘uncoordinated’ carboxylate adopts the “up” orientation, it will promote the formation of the two-dimensional networks; if the ‘uncoordinated’ carboxylate adopts the “down” orientation, it will promote the formation of the discrete molecules.

Figure 4.7: Connectivity of the molecular squares (SBUs) in 5 and 6



(a) “up” orientation of isophthalate in compounds 3 and 4



(b) “down” orientation of isophthalate in compounds 5 and 6

To better understand the structural differences between the two discrete supramolecular isomers that can form when the isophthalates adopt the “down”

configuration, projections of the models down various axes of the two structures have been examined and compared. It is also possible to view the atomic representations of the molecules down the same axes; however, the value of the use of schematics is again underscored in the added insight that is gained by their use. Figure 4.8 illustrates the schematic projections of compound 5 viewed down selected axes. Figure 4.9 illustrates the schematic projections of compound 6 viewed down selected axes.

Figure 4.8: Orthographic projections of the schematic model of compound 5

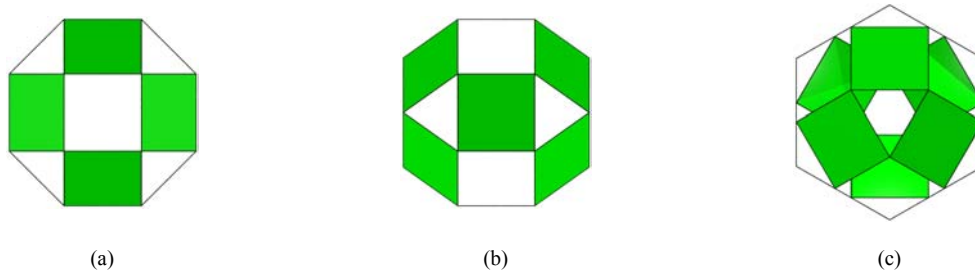
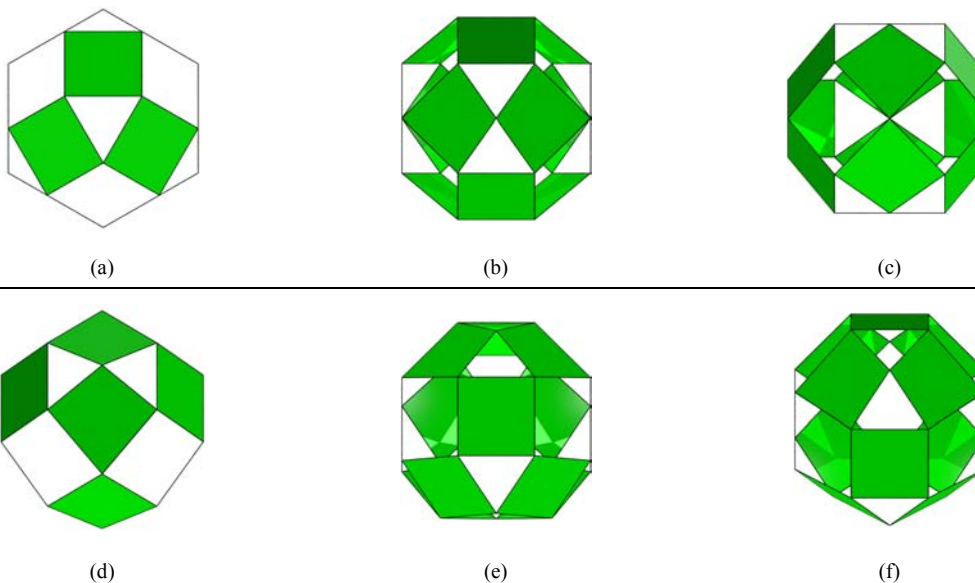


Figure 4.9: Orthographic projections of the schematic model of compound 6



An important similarity between the structures is that both models can be described as having a center ‘belt’ composed of six 4-gons around the equator (squares in compound 5, kites in compound 6) with triangular nSBU ‘caps’ at both ends. This can

most easily be observed in Figure 4.8c for compound 5, and in figures 4.9a-c for compound 6. The fundamental difference in the connectivity of the squares is revealed in a comparison of Figure 4.8c with Figure 4.9a: the triangular nSBU ‘caps’ are staggered in compound 5 and eclipsed in compound 6. It is due to the eclipsed configuration that the model of compound 6 cannot be constructed by squares alone. Indeed, the model illustrated in Figure 4.9 was constructed from six squares forming the triangular nSBU ‘caps’, and six kites forming the ‘belt’. The structural consequence to this is that there is a planar hexagonal ring circumscribing the equator of compound 6. This can be clearly seen in Figure 4.4.

Another important consideration in understanding the crystal structures of compounds 5 and 6 is the spatial distribution of the molecular spheres in the crystal. Based on the spherical nature of the molecules in compounds 5 and 6, it is unsurprising that they adopt packing arrangements consistent with modes of spherical close packing. The molecular spheres in compound 5 adopt a bcc (body centered cubic) arrangement; whereas the molecular spheres in compound 6 adopt an hcp (hexagonal close packed) arrangement. This is consistent with their respective space groups (i.e. $Im\bar{3}m$ and $P6_3/m$).

Furthermore, it is anticipated that such molecules will exhibit spatial supramolecular isomerism. Indeed, two other spatial supramolecular isomers of compound 5 have already been identified. A triclinic phase ($P\bar{1}$; $a = 26.202(9)$, $b = 27.756(10)$, $c = 28.408(10)$ Å; $\alpha = 92.583(5)$, $\beta = 96.393(5)$, $\gamma = 92.643(5)^\circ$; $V = 20483(12)$ Å³) and a monoclinic phase ($C2/c$; $a = 33.933(7)$, $b = 36.925(7)$, $c = 29.577(6)$ Å; $\beta = 93.4595(28)^\circ$; $V = 36991(13)$ Å³). Interestingly, the triclinic phase adopts a

packing arrangement that is closely related to bcc; whereas the monoclinic phase adopts an arrangement closely related to hcp.

4.5. Conclusions

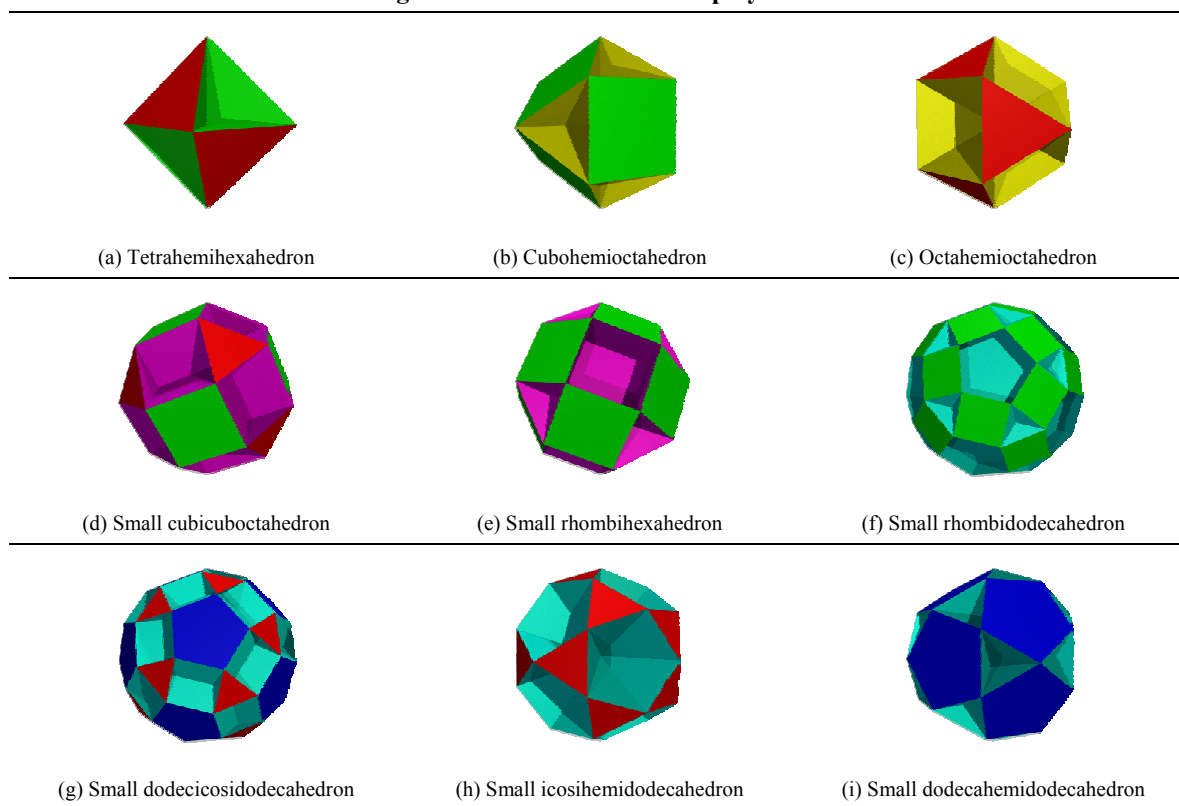
Compounds 5 and 6 are distinguished by the following features: they are neutral and soluble in organic solvents; they are chemically robust because of the stability of the square SBU (confirmed by high resolution mass spectrometry); they are likely to be chemically diverse because the dimetal tetracarboxylate SBU exists for so many metals, including magnetically active and catalytically active metals; they have both internal and external sites that are suitable for further chemical modification. Their interior cavities can be accessed via triangular or square windows, which are bowl shaped and contain organic guests. The thermal stabilities for both compounds are consistent with their structures and molecular components: crystals of compounds 5 and 6 appear stable indefinitely when in contact with mother liquor; weight losses of 36.9 and 38.3 %, respectively, corresponding to loss of guest molecules occur when heated (as measured by TG-MS). The samples do not remain as single crystals when heated. Loss of coordinated molecules occurs at higher temperatures.

Although other differences can be seen with respect to the orientations of the windows with respect to one another, the fundamental structural differences are exemplified by a comparison of the orientation of the triangular nSBU caps, and by the net describing the connectivity of the SBUs (i.e. cuboctahedron for compound 5; Triangular orthobicupola for compound 6).

Compound 5 illustrates the concept of exploiting knowledge of uniform polyhedra to design spherical molecular assemblies. Specifically, it illustrates the concept of

assembling molecular polygons at their vertices to generate molecular *faceted* polyhedra, which differ fundamentally from the spherical aggregates that have previously been reported. As was mentioned in the introduction, there has been primarily two strategies for generating molecular polyhedra: linking vertices of appropriate geometry with linear bifunctional spacer ligands, which necessarily generates open structures that conform to the edge-skeleton of Platonic or Archimedean solids; linking the edges of molecular polyhedra, which necessarily generates closed shell molecular polyhedra that conform to Platonic or Archimedean solids. The strategies described herein may be described as a hybrid strategy that necessarily generates molecular solids that allow access and egress, while also having facets that can sustain coordination and possibly chemical reactivity.

Figure 4.10: The nine faceted polyhedra



Compound 6 illustrates that it is important to also consider alternate arrangements of molecular polygons, as molecules do not necessarily have to adhere to the strict constraints imposed by solid geometry.

In summary, it has been demonstrated that regular molecular polygons can self-assemble at their vertices and use of appropriate templates facilitates isolation of nanoscale molecular architectures. They differ in terms of design and function from structures that are generated from Platonic and/or Archimedean building blocks. It is anticipated that the molecules in compounds 5 and 6 represent prototypal structures and that judicious selection of angular spacers in the presence of the appropriate molecular polygons should ultimately generate all nine faceted uniform polyhedra and their numerous structural isomers. Figure 4.10 illustrates the nine possible faceted polyhedra. Note that only three involve the assembly of squares, which limits the number of possible structures that can be expected to form from the assembly of SBUs.

Chapter 5

Additional Structures

5.1. Preamble

A thorough analysis of compound 2, followed by structural analysis of compounds 3 and 4 would indicate that there are likely no other planar two-dimensional topologies possible for $\{L_2Cu_2(bdc)_2\}_n$ coordination polymers. The identification of an unanticipated discrete supramolecular isomer, compound 6, has contradicted the hypothesis proposed previously that the set of supramolecular isomers that would be possible for this series of materials could be derived from the network architecture of compound 2. Furthermore, as a consequence of gaining an understanding of how the relative orientation of the carboxylates (i.e. “up” or “down”) can lead to various supramolecular isomers, a systematic search for additional supramolecular isomers was undertaken.

Thus far, the structures of four supramolecular isomers have been discussed: tetragonal two-dimensional network, trigonal two-dimensional network, and a zero-dimensional (i.e. discrete) molecular faceted polyhedra and a related discrete architectural supramolecular isomer. In the introduction, an example of two-dimensional network based on T-shaped nodes, the so-called bilayer architecture, was described, which was not considered as one of the possible two-dimensional architectures based on theoretical predictions. This was due to the finite thickness of the network, while theoretical

predictions were strictly confined to a plane. Furthermore, more complex three-dimensional networks were described for the same building blocks. The question that must now be addressed is whether similar architectures are possible for the assembly of dimetal tetracarboxylate SBUs.

Assuming the initial coordination of two SBUs occurs such that they can be considered as two molecular squares joined at their vertex, there are six additional carboxylates that can adopt one of two orientations (“up” or “down”). This corresponds to a total of sixty-four (2^6) possible combinations of orientations for the remaining carboxylates. Two of the possible combinations are illustrated in Figure 4.7: four “up”, two “down”; and six “down”. Another interpretation of the carboxylate orientations is to consider the orientations of the four uncoordinated carboxylates of a single SBU. In this instance there are sixteen possible orientations. The question as to whether all sixteen orientations will lead to different supramolecular isomers is highly topical and fundamentally important. The question can be broadened even further to consider the orientations of higher-order aggregates, which in turn leads to an infinite number of possible orientations. Therefore, the fundamental question that needs to be addressed is whether there are a finite or an infinite number of supramolecular isomers. The initial hypothesis was that there are a finite number possible for this system and that, furthermore, they could be derived from compound 2. The latter part of this hypothesis has been disproven; however, the identification of additional structures has provided new insight into the first part of the hypothesis.

5.2. Compound 7: $\{L_2Cu_2(btc)_2\}_n$

5.2.1. Experimental

In a typical reaction, crystals of compound 7 were obtained by layering an ethanolic solution of isophthalic acid (166 mg, 0.999 mmol) and quinoline (0.30 mL, 2.5 mmol), onto an ethanolic solution of copper nitrate hemipentahydrate (233 mg, 1.00 mmol) containing nitrobenzene (2 mL).

Selected crystallographic parameters are presented in Table 5.1. Complete crystallographic data for compound 7 can be found in Appendix A-7.

Crystal class	Trigonal
Space group (#)	$R\bar{3}c$
a = b =	30.337(2) Å
c =	18.380(2) Å
V =	14649(2) Å ³

5.2.2. Technical description

The structure results from μ_2 -coordination of each of the isophthalate carboxylates to two copper(II) ions. Each carboxylate is involved in the formation of a dicopper tetracarboxylate SBU. Each SBU has two coordinated quinoline molecules that were located and refined from the diffraction data. Additional electron density, attributed to disordered solvent or guest molecules present in the crystal lattice void space, was modeled as variable occupancy isotropic carbon atoms.

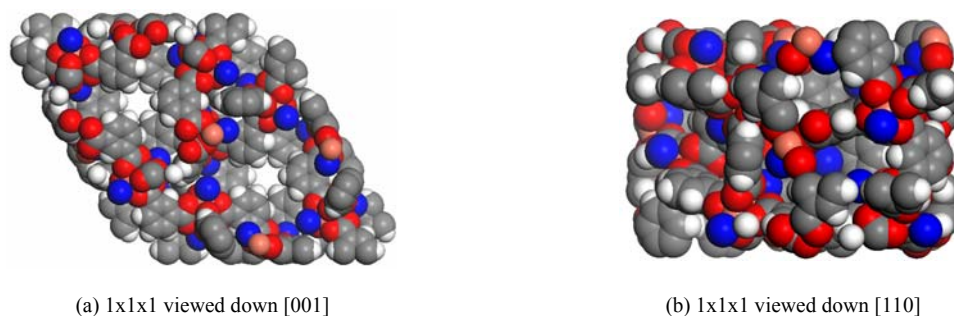
The crystal structure adopts a trigonal crystal class with $R\bar{3}c$ cell symmetry. There is one crystallographically independent copper ion that sits on a general position,

ca. 1.35 Å away from a center of inversion, which generates the core of the dimetal tetracarboxylate chromophore ($d_{\text{Cu}\dots\text{Cu}} = 2.6910(19)$ Å). There are four crystallographically independent oxygen atoms corresponding to equatorially coordinated isophthalates ($d_{\text{Cu}\dots\text{O1}} = 2.0063(54)$ Å; $d_{\text{Cu}\dots\text{O2}} = 1.9642(52)$ Å; $d_{\text{Cu}\dots\text{O3}} = 1.9733(51)$ Å; $d_{\text{Cu}\dots\text{O4}} = 1.9747(55)$ Å), and one nitrogen corresponding to the apically coordinated quinoline ($d_{\text{Cu}\dots\text{N1}} = 2.1958(68)$ Å). The other four oxygen atoms in the SBU are generated by the center of inversion. The structure is completed by ten independent carbon atoms corresponding to the isophthalates (four sit on a two-fold rotation axis), nine independent carbon atoms corresponding to the coordinated quinoline, thirteen calculated hydrogens and the appropriate space group symmetry operations.

The empirical formula, excluding disordered solvent/guest, is therefore $\text{CuC}_{17}\text{H}_{11}\text{NO}_4$, which gives $Z = 36$. To be consistent with previous analysis this is modified to illustrate the presence of the SBU: $\text{Cu}_2\text{C}_{34}\text{H}_{22}\text{N}_2\text{O}_8$ or, more generally, $\text{L}_2\text{Cu}_2(\text{bdc})_2$, where L = quinoline. This clearly illustrates that compound 7 is a supramolecular isomer of compounds 3 – 6. The structure is polymeric and the final molecular formula is therefore represented as $\{[\text{L}_2\text{Cu}_2(\text{bdc})_2]\}_n$, which gives $Z = 18$.

5.2.3. Space-filling models

Figure 5.1: Space filling models of compound 7, $\{[\text{L}_2\text{Cu}_2(\text{bdc})_2]\}_n$ *

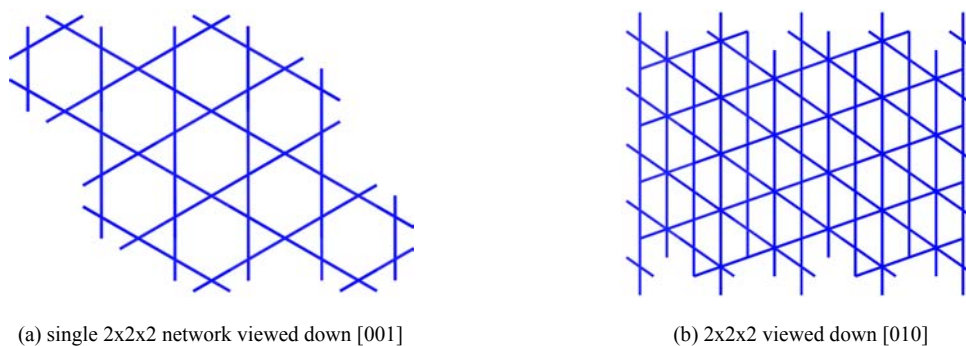


* Carbon (grey), nitrogen (blue), oxygen (red), hydrogen (white); coordinated quinoline is represented as a single nitrogen with remaining atoms deleted for clarity; non-coordinated solvent/guest removed for clarity

5.2.4. Illustrative description

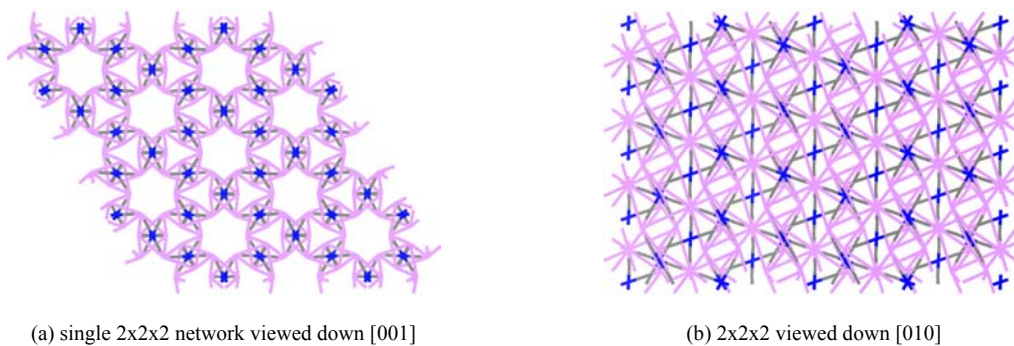
Compound 7 can be shown to be a single three-dimensional network, and has been shown to be a supramolecular isomer of compounds 3, 4, 5 and 6. It is therefore appropriate to examine the set of schematics illustrating the SBU connectivity network, and the molecular square connectivity representation. The prior is illustrated in Figure 5.2, and the latter in Figure 5.3.

Figure 5.2: Schematic illustration of the network observed in compound 7, $\{[L_2Cu_2(bdc)_2]\}_n^*$



* derived from crystal structure coordinates and unit cell

Figure 5.3: Schematic illustration of the connectivity of molecular squares observed in compound 7



* derived from crystal structure coordinates and unit cell

The most noticeable feature is that the projection of the network defining the SBU connectivity down [001] is a 3.6.3.6-net (the Kagomé net). Examination of the projection down [010] and [100] confirms that the structure does indeed exhibit three-dimensionality. Perhaps more remarkable than what is learned by examining the network

defining the SBU connectivity, is what is *not* learned by examining the schematic illustrating the connectivity of molecular squares. In the previous structures, substantial insight was gained from this set of schematics. Unfortunately, for compound 7, they do little to add to what is learned from the simpler connectivity network. Indeed, this schematic may do more to complicate our understanding of the structure than it does to simplify it.

The main structural feature in compound 7 is the hexagonal channels that run parallel to [001]. Although the channel in Figure 5.2a is 15.2 Å in diameter (measured between edges), the effective diameter is only 3.7 Å (measured from proton to proton; see Figure 5.1a). This assumes, of course, that the channel can be viewed as a straight “pipe”, or, alternatively, that the diameter can be approximated by the diameter of a ball that can be dropped straight through the channel. The channel has a much more complicated shape, with an effective minimum diameter of 3.7 Å, and an effective maximum dimension corresponding to a 12.5 x 9.2 Å ellipse. At its narrowest, the planes of three isophthalate rings are orthogonal to the channel direction with their 5-protons oriented toward the center; at its widest, there are opposing coordinated quinoline molecules whose mean planes are tangential to the channel wall.

5.3. Compound 8: $\{L_2Cu_2(btc)_2\}_n$

5.3.1. *Experimental*

In a typical reaction, green needle-like crystals of compound 8 were obtained after the addition of water (0.5 mL) to a DMF solution (14 mL) of copper nitrate hemipentahydrate (261 mg, 1.12 mmol), isophthalic acid (178 mg, 1.07 mmol) and pyridine (0.24 mL, 3.0 mmol).

Selected crystallographic parameters are presented in Table 5.2. Complete crystallographic data for compound 8 can be found in Appendix A-8.

Table 5.2: Selected crystallographic parameters for $\{[L_2Cu_2(btc)_2]\}_n$	
Crystal class	Monoclinic
Space group (#)	$P2_1/n$ (14; non-standard setting)
a =	10.6661(12) Å
b =	30.303(4) Å
c =	16.3650(19) Å
β =	95.877(2)°
V =	5261.5(10) Å ³

5.3.2. Technical description

The structure results from μ_2 -coordination of each of the isophthalate carboxylates to two copper(II) ions. Each carboxylate is involved in the formation of a dicopper tetracarboxylate SBU. There are three crystallographically independent SBUs, two have two coordinated pyridine molecules that were located and refined from the diffraction data, the other has two coordinated oxygen atoms that are ascribed as being water.

Additional electron density, attributed to disordered solvent or guest molecules present in the crystal lattice void space, was modeled as variable occupancy isotropic carbon atoms.

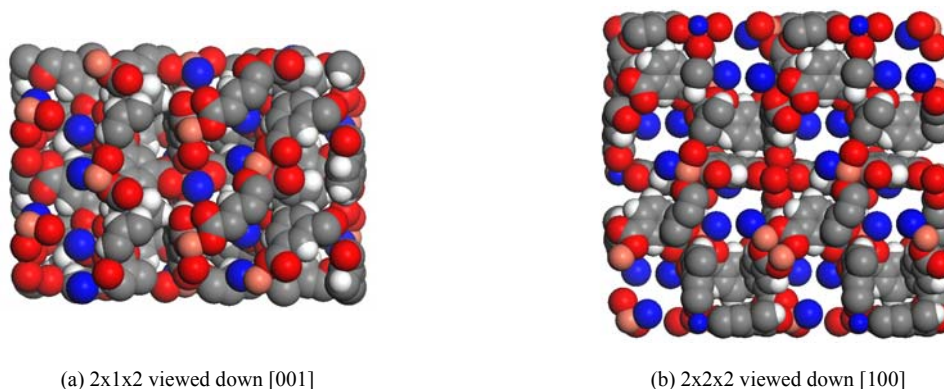
The crystal structure adopts a monoclinic crystal class with $P2_1/n$ cell symmetry. There are four crystallographically independent copper ions: two sit on general positions, forming the core of one dimetal tetracarboxylate chromophore ($d_{Cu2...Cu3} = 2.6553(9)$ Å); two sit next to a center of inversion forming the core of the other two chromophores ($d_{Cu1...Cu1} = 2.6476(13)$ Å; $d_{Cu4...Cu4} = 2.6640(13)$ Å). There are sixteen crystallographically independent oxygen atoms corresponding to equatorially coordinated isophthalates ($\bar{d}_{Cu...O} = 1.970$ Å, $\sigma = 0.009$), three nitrogen atoms corresponding to the

apically coordinated pyridine ($d_{\text{Cu}2\dots\text{N}} = 2.150(5) \text{ \AA}$; $d_{\text{Cu}3\dots\text{N}} = 2.145(5) \text{ \AA}$; $d_{\text{Cu}4\dots\text{N}} = 2.133(5) \text{ \AA}$), and one apically coordinated oxygen corresponding to coordinated water ($d_{\text{Cu}1\dots\text{O}} = 2.156(4) \text{ \AA}$). The structure is completed by thirty-two independent carbon atoms corresponding to the isophalates, fifteen independent carbon atoms corresponding to the coordinated pyridine, sixteen calculated hydrogens and the appropriate space group symmetry operations.

The empirical formula, excluding disordered solvent/guest, is therefore $\text{Cu}_4\text{C}_{47}\text{H}_{16}\text{N}_3\text{O}_{16}$, which gives $Z = 4$. To be consistent with previous analysis this is modified to illustrate the presence of the SBU: $\text{Cu}_2\text{C}_{23.5}\text{H}_8\text{N}_{1.5}\text{O}_8$ or, more generally, $\text{L}_2\text{Cu}_2(\text{bdc})_2$, where $\text{L} = \text{quinoline or water}$. More specifically, compound 8 can be represented as $\{[\text{L}_1\text{Cu}_2(\text{bdc})_2]_2[\text{L}_2\text{Cu}_2(\text{bdc})_2]_3\}_n$, where $\text{L}_1 = \text{water}$ and $\text{L}_2 = \text{pyridine}$. However, as has been the convention, it is assumed that the coordinated solvent/base can be removed without loss of network structure. Therefore compound 8 can be considered a supramolecular isomer of compounds 3 – 7. The structure is polymeric and the final molecular formula is therefore represented as $\{[\text{L}_2\text{Cu}_2(\text{bdc})_2]\}_n$, where $Z = 8$.

5.3.3. Space-filling models

Figure 5.4: Space filling models of compound 8, $\{[\text{L}_2\text{Cu}_2(\text{bdc})_2]\}_n^*$

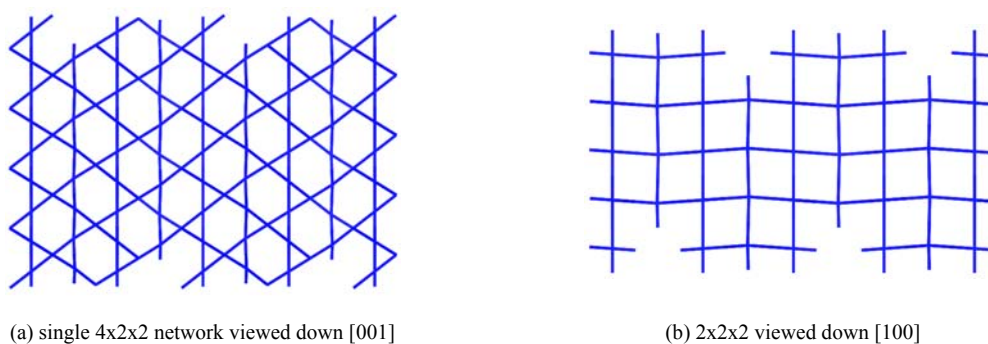


* Carbon (grey), nitrogen (blue), oxygen (red), hydrogen (white); coordinated ligands are represented as a single nitrogen with remaining atoms deleted for clarity; non-coordinated solvent/guest removed for clarity

5.3.4. Illustrative description

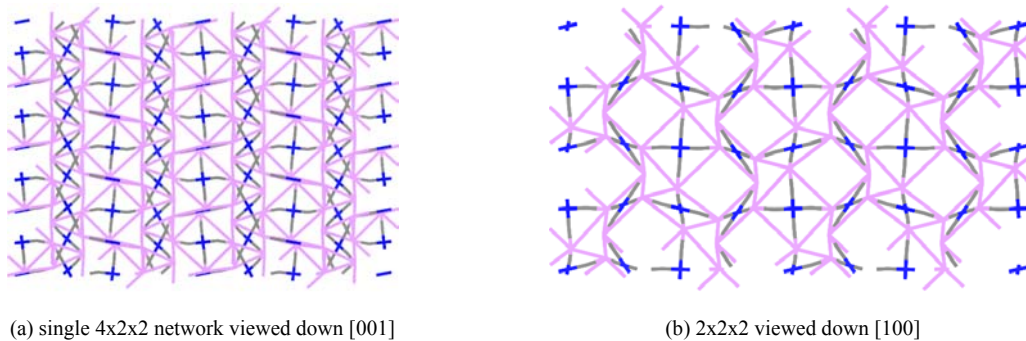
Compound 8 can be shown to be a single three-dimensional network, and has been shown to be a supramolecular isomer of compounds 3, 4, 5, 6 and 7. It is therefore appropriate to examine the set of schematics illustrating the SBU connectivity network, and the molecular square connectivity representation. The prior is illustrated in Figure 5.5, and the latter in Figure 5.6.

Figure 5.5: Schematic illustration of the network observed in compound 8, $\{[L_2Cu_2(bdc)_2]\}_n^*$



* derived from crystal structure coordinates and unit cell

Figure 5.6: Schematic illustration of the connectivity of molecular squares observed in compound 8



* derived from crystal structure coordinates and unit cell

At first glance, compound 8 may appear to be the same as compound 7. The projection down [001] is a 3.6.3.6-net, as in compound 7. The similarities, however, end there. The maximum diameter of the hexagonal channel in Figure 5.5a is 7.6 Å,

measured between opposing edges. Furthermore, the projections down the other main crystallographic axes are not coincident.

Unlike compound 7, there are no effective channels parallel to [001]. Figure 5.4b illustrates that there are, however, narrow channels parallel to [100]. The channels in compound 8 have a more regular shape and have an effective desolvated diameter of ca. 6 Å, and an effective hydrated (i.e. coordinated oxygen) diameter of ca. 2 Å. It should be stressed that, in Figure 5.4b, that the coordinated pyridine molecules are represented by a single nitrogen, and that a figure illustrating the complete pyridines would not indicate the presence of channels. Representing the pyridines in such a manner allows for the determination of the presence of channels through which coordinated solvent could, in principle, escape the crystal lattice without collapse of the polymeric network.

5.4. Discussion

Unfortunately, schematic representations of the connectivity of molecular squares for compounds 7 and 8 provide little insight into the fundamental structure of the materials, which mitigates against the comparison of the two structures. Although it can be definitively demonstrated that the compounds are different, a simple description of the structures to permit comparisons to its supramolecular isomers is difficult, at best. Therefore, it seems appropriate to more closely examine the networks illustrating the connectivity of the SBUs.

A comprehensive understanding of the networks can be gained through topological analysis, in the same way that the description of the networks for the two-dimensional supramolecular isomers was based on topology. The topology of a three-dimensional network is commonly described in terms of the number of unique nodes, the

number of smallest closed circuits that can be traced from each node, and the number of nodes on each circuit. For a 4-connected network, there are six possible circuits that can be traced, such that all circuits between two connections are defined: i.e. if the four connections are labeled i, ii, iii and iv; the six circuits would be traced between (start/finish) i/ii, i/iii, i/iv, ii/iii, ii/iv and iii/iv. It should be emphasized; however, the description of individual networks in the context of coordination polymers has focused more on descriptive nomenclature based on the structures of known materials and minerals (i.e. NbO, PtS, CdSO₄).

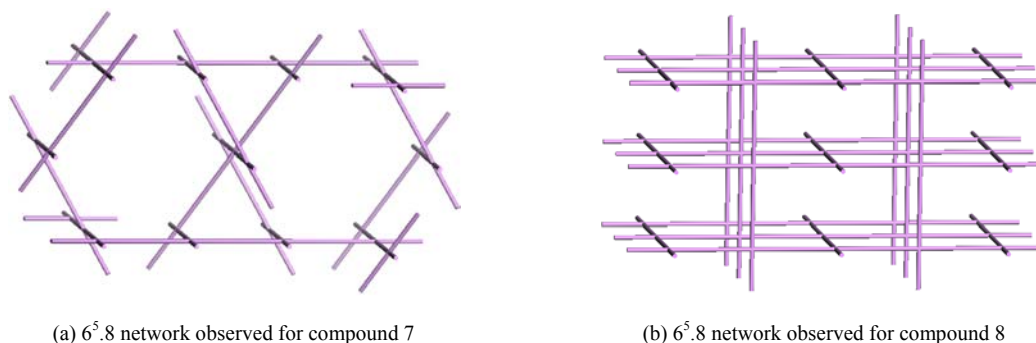
The networks for both compound 7 and compound 8 are 4-connected networks. The nodes are distorted square planar nodes; distorted due to the fact that angular ditopic spacers connect the square planar nodes. Incorporation of this into the network schematic does not provide additional structural information.

It can be shown that, in compound 7, there is only one unique nodal geometry and that, of the six shortest circuits that can be traced from these nodes, five have six nodes on the circuit and one has eight. Therefore, the circuit symbol is written as 6⁵.8. Interestingly, in compound 8, there is only one unique nodal geometry and that, of the six shortest circuits that can be traced from these nodes, there are five that have six nodes on the circuit and one that has eight. Therefore, the circuit symbol is also 6⁵.8.

A more rigorous analysis uses Schläfli notation, in which the number of shortest nodes that can be traced from each set of connections is indicated. For compound 7, it can be demonstrated that the Schläfli notation is 6₂.6₂.6₂.6₂.6₂.∞. The ∞ symbol (infinity), is used in the instance that the shortest circuit is short-circuited (i.e. one of the nodes on the circuit is connected to the central node at a different connection point). This

indicates that the eight-node circuit is short-circuited. It can also be demonstrated that the Schläfli notation for compound 8 is $6_2.6_2.6_2.6_2.6_2.\infty$. It remains clear, however, that the networks are different. This is underscored by Figure 5.7, which illustrates the two networks viewed down crystallographic axes chosen to best illustrate the overall network connectivity. Revealed in Figure 5.7 is that the network derived for compound 8 is topologically equivalent to the CdSO_4 network, which is, of course, also described by a $6_2.6_2.6_2.6_2.6_2.\infty$ Schläfli notation.

Figure 5.7: Perspective illustrations of the networks observed in compounds 7 and 8



This research is, to my knowledge, the first to identify of the network topology exhibited by compound 7, the hereinafter named USF-1 net. The ideal net has $R\bar{3}c$ symmetry, $a/c=\sqrt{(8/3)}$, with vertices at $18d$.²⁹⁵ The ideal CdSO_4 net has $P4_2/mmc$ symmetry, $c/a=2$ with vertices at $2a$.²⁹⁵ Although both networks are 4-connected, each vertex has six nearest neighbours. The connectivity of USF-1 is generated by connecting the vertices at $(1/2,0,0)$ and $(1/2,0,1/2)$, and $(1/2,0,0)$ and $(1/3,1/6,1/6)$. A 6-connected net can be generated by also connecting $(1/2,0,0)$ and $(5/6,1/6,1/6)$, the so-called USF-2 net, which has six equidistant edges. The connectivity of the CdSO_4 net is generated by connecting $(0,0,0)$ and $(0,0,1/2)$, and $(0,0,0)$ and $(1,0,0)$. The 6-connected cubic lattice can be generated by also connecting $(0,0,0)$ and $(0,1,0)$.

Although visual inspection of projections down various crystallographic vectors indicates that the networks are quite different, a more rigorous comparison was employed. The number of nearest neighbours (nn) was calculated for “shells” of adjacent vertices, such that each shell is a set of vertices equidistant from a particular vertex. These data are presented in Table 5.3.

Table 5.3: Number of vertices in nearest neighbor shells for 6⁵.8 networks

	nn ₁ *	nn ₂	nn ₃	nn ₄	nn ₅	nn ₆	nn ₇	nn ₈	nn ₉	nn ₁₀
USF-1	6	4	8	18	8	6	18	16	16	24
CdSO ₄	6	12	8	6	24	24	12	30	24	24

* nn₁ refers to the set of nearest neighbors, nn₂ the set of next nearest neighbors, etc...

These data show that there are 124 total vertices within the nn₁₀ shell for compound 7, and 170 vertices within the nn₁₀ shell for compound 8. These values can be used to describe a *topological density*, which is not the same as material density because the volume of the nn₁₀ shell for different nets is not the same. In this particular case, the material density (defined as vertices per unit volume) of USF-1 is 2.6% less than a CdSO₄ net with equal distances between nodes.

Cubic and hexagonal diamondoid networks are another example of 4-connected nets that are topologically different, yet have the same Schläfli notation (6₂.6₂.6₂.6₂.6₂.6₂). In this case, the nets have the same material density, but the hexagonal diamond net has ca. 48% less vertices in its nn₁₀ shell. Another method for comparing topologically similar nets is to calculate the *coordination sequence*.²⁹⁶ Hexagonal diamondoid is topologically denser than cubic diamondoid using this method.

A three-dimensional network related to compounds 7 and 8 has been recently reported, the so-called MOF-112 net. This particular network results from an increase in the torsion angle between the carboxylates imposed by a 4-substituted bromine on the

bdc. The net has a different basic topology, established by the circuit symbol ($6^2.8^4$) and Schläfli notation ($6_2.6_2.8.8.8.8$). This net has P4/mmm symmetry, $a/c=2$, with vertices at $1a$ and $2f$.²⁹⁵ The connectivity can be generated by connecting $(0,0,0)$ and $(1/2,0,0)$, and $(0,1/2,0)$ and $(0,1/2,1)$. The authors have also used this torsional strain to synthesize materials that exhibit the CdSO_4 ⁹³ and NbO ²⁹⁷ topologies from 2-bromo-1,4-benzene dicarboxylates.

A closer look at the conformation of the isophthalates in compounds 7 and 8 reveals that they also exhibit a degree of torsional strain, presumably imposed by the network topology rather than steric effects from covalent substitution. The two independent isophthalates in compound 7 have torsion angles of 25.3° and 16.5° for both carboxylates, respectively. This leads to the isophthalate imposing an out-of-plane torsional strain of 50.6° and 33.0° between vertex-connected molecular squares. All SBUs in compound 7 can be described as having an “up”-“down”-“up”-“down” orientation for the uncoordinated carboxylates. Of the four independent carboxylates in compound 8, one has coplanar carboxylates ($< 7^\circ$), whereas the others have carboxylates that are rotated by 12.9° and 32.6° , 30.7° and 25.8° , and 21.9° and 8.8° . All of the SBUs in compound 8 can also be described as having an “up”-“down”-“up”-“down” orientation for the uncoordinated carboxylates.

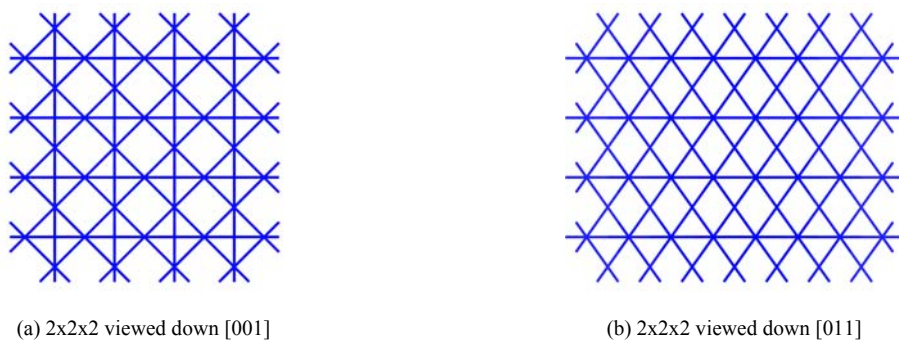
5.5. Conclusions

Topological analysis of compounds 7 and 8 by examining the schematic representations of their chemical connectivity has facilitated the description and comparison of two otherwise complex three-dimensional architectures. Furthermore, it has led to the identification of a previously unknown topology, USF-1. Compounds 7

and 8 underscore the difficulties faced in understanding the structure of, and relationship between, supramolecular isomers. The analysis of schematics illustrating the connectivity of molecular squares afforded no insight into the relationship between compounds 7 and 8, despite the prior value of such an analysis. It therefore seems appropriate to re-evaluate compounds 2 – 6 in the context of the net defining the connectivity of SBUs. Note that, at this point, the analysis is restricted to those structures that possess only the dimetal tetracarboxylate SBU.

It has already been illustrated that compounds 3 – 5 can be extracted from compound 2. The network defining the connectivity of the SBUs in compound 2 is illustrated in Figure 5.8. Note that this has not been previously illustrated.

Figure 5.8: Schematic illustration of the network observed in compound 2



Because each node (SBU) is connected to four btc moieties, which are each connected to two SBUs, this results in the formation of an eight connected net, which is congruent with the edge-skeleton of the close-packing arrangement of cuboctahedra and octahedra. The cuboctahedra has already been shown to describe the connectivity of the SBUs in compound 5 (the octahedral portion has incomplete SBUs at its vertices and is therefore not chemically possible). Although, nothing substantial is learned by examining this

network, it is worthwhile to examine the disposition of only the nodes of the network (Figure 5.9).

Figure 5.9: Schematic illustration of the nodes of the network observed in compound 2

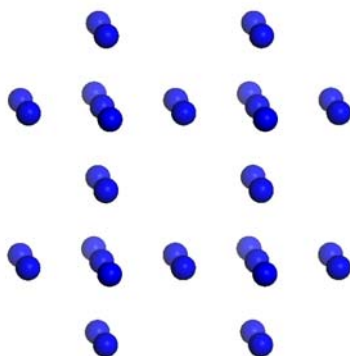
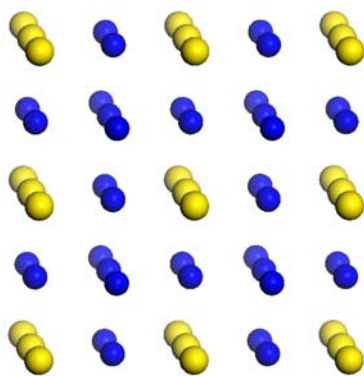


Figure 5.9 is viewed slightly off center to illustrate the position of all of the nodes. It may be obvious that these nodes represent a subset of the set of spheres that correspond to one of the spherical close packing lattices. Figure 5.10 illustrates this relationship by inserting the ‘missing’ spheres, viewed at the same angle as in Figure 5.9.

Figure 5.10: Schematic illustration of cubic close packing (ccp)



Therefore, the nodes representing the SBUs in compound 2 correspond to the ccp lattice, with a unit cell expanded by a factor of eight (2X each dimension) to allow $Fm\bar{3}m$ symmetry, where the spheres at $[0, 0, 0]$ and $[\frac{1}{2}, \frac{1}{2}, \frac{1}{2}]$ have been removed. It follows that the nodes corresponding to the SBUs in the trigonal and tetragonal two-dimension

networks (compounds 3 and 4), and the molecular faceted polyhedron (compound 5) can also be extracted from the ccp lattice, as it has already been demonstrated that they can be extracted from compound 2.

Figure 5.11: Schematic illustration of the nodes of the network observed in compound 7

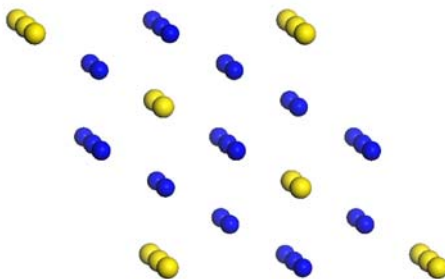
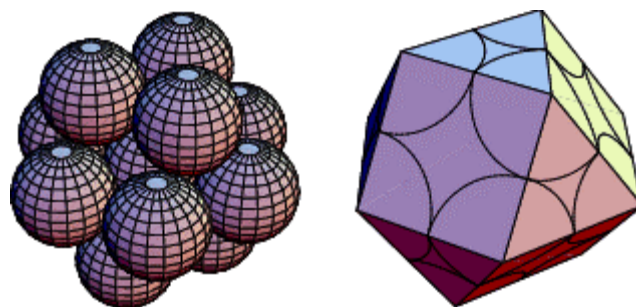


Figure 5.11 illustrates that the nodes representing SBUs of compound 7 (blue) can also be extracted from a spherical packing lattice. The ‘missing’ nodes have been inserted and highlighted in yellow. In this particular instance, however, the entire set of nodes corresponds to a hexagonal close packed (hcp) arrangement.

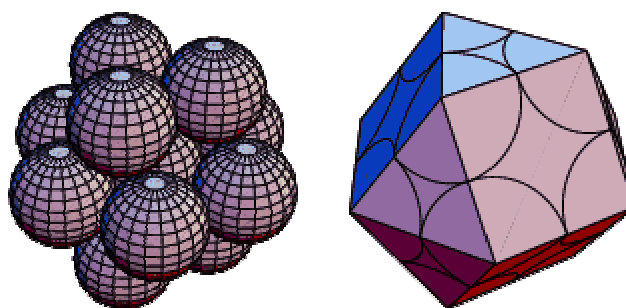
In hexagonal close packing, the layers of spheres are packed such that spheres in alternating layers superimpose one another. As in cubic close packing, each sphere is surrounded by 12 other spheres. Taking a collection of 13 such spheres gives the cluster illustrated in Figure 5.12a. Connecting the centers of the external 12 spheres gives the Johnson solid known as the Triangular orthobicupola, which corresponds to the connectivity of the SBUs in compound 6.

In cubic close packing, each sphere is also surrounded by 12 other spheres. Taking a collection of 13 such spheres gives the cluster illustrated in Figure 5.12b. Connecting the centers of the external 12 spheres gives a cuboctahedron, which, as was mentioned above, gives compound 5.

Figure 5.12: Schematic illustration of clusters of 13 spheres



(a) ccp (cubic close packing), also known as fcc (face centered cubic), and its relationship to the cuboctahedron

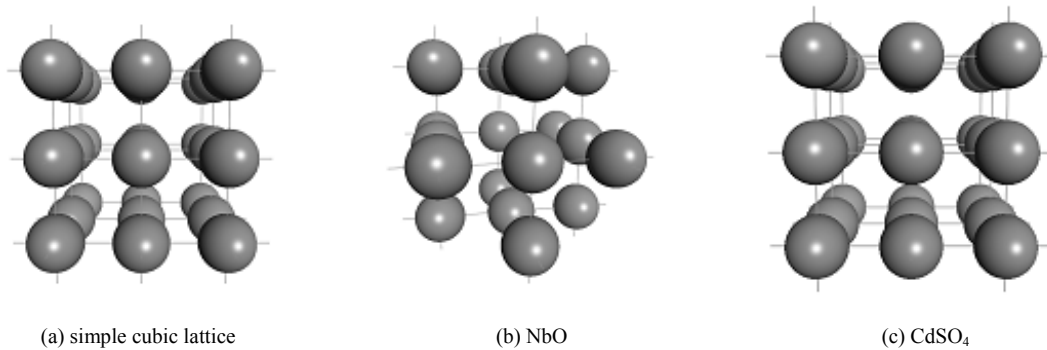


(b) hcp (hexagonal close packing) and its relationship to the Triangular orthobicupola

Lastly, we consider compound 8. It has already been illustrated that the network representing the connectivity of SBUs in compound 8 is topologically equivalent to the CdSO_4 network. Consider the transformation of the cubic close packed lattice (ccp) to a simple cubic lattice (spheres at the corners of a cube). First, take a primitive rhombohedral cell of the ccp lattice with unit cell lengths and $\alpha=60^\circ$. Next, it is simple to consider the transformation of α to 90° , which gives a rhombohedral cell with unit cell lengths and $\alpha=90^\circ$, i.e. a cubic unit cell. If we then consider the connectivity of these spheres, we have derived the octahedral topology, which is a 6-connected lattice. From this, we may now easily derive a subset of 4-connected networks by increasing the size of the unit cell and periodically removing spheres or connectivity lines so that each sphere has only four nearest neighbors. It should be obvious that the square grid, (4,4)-net is extracted by removing every other layer along a given axis, the NbO architecture by

removing every other sphere, and the CdSO_4 topology is derived by deleting alternating sphere connectivity (Figure 5.13).

Figure 5.13: Networks derived from simple cubic lattice



It has therefore been demonstrated that all of the supramolecular isomers discussed thus far (compounds 3 – 8), as well as compound 2, can be derived (i.e. extracted) from either the ccp or hcp lattice.

Chapter 6

Structure–Function: Magnetism

6.1. Preamble

The previous chapters have described in detail the structures of six supramolecular isomers of $\{L_2Cu_2(bdc)_2\}_n$ coordination polymers, and illustrated the geometric relationships between them. Additionally, the structure of a closely related material, $\{L_2Cu_2(btc)_{4/3}\}_n$, has been described. Fundamental structural similarities exist between all of these structures: they are electrically neutral, contain dicopper(II) tetracarboxylate chromophores (SBUs), and have resonance stabilized ligands that connect the SBUs. It is anticipated that the delocalization of π -electrons in the ligand will allow the SBUs to ‘communicate’ with each other, and will result in interesting and predictable cooperative magnetic behavior.

The magnetic phenomena of discrete dimetal tetracarboxylates (i.e. bis(bis- μ_2 -acetato- O,O' -metal(ii)) complexes) have been well characterized.²⁹⁸⁻³⁰⁰ They have been shown to exhibit room temperature paramagnetism, which decreases with temperature due to strong antiferromagnetic coupling ($-2J \approx 300 \text{ cm}^{-1}$) of the unpaired electrons on the two $Cu_2 d^9$ centers. The coupling constant, $-2J$, has been shown to be dependent on both the nature of the carboxylate bridges and the axial ligand, L.

The copper(II) dimers can be viewed as a single magnetic moment, resulting from the interaction between the two local doublet states. Therefore, the materials described

herein serve as an opportunity to study cooperative magnetic phenomena between these moments for a series of materials with essentially identical compositions. This can potentially provide fundamental insight into structure-function relationships. More specifically, the materials described herein offer the opportunity to study the relationship between topology and magnetic phenomena.

6.2. Magnetic susceptibility

The temperature-dependant magnetic susceptibility, $\chi(T)$, and field-dependant magnetization, $M(H)$, were measured using a commercial physical property measurement system (PPMS) from Quantum Design.

6.2.1. Three-dimensional structure

Compound 2, $\{L_2Cu_2(btc)_{4/3}\}_n$, described in chapter 2 was synthesized from zinc(II). It was also stated that an isostructural compound had been previously reported that had been synthesized from copper(II). In the context of magnetic phenomena, it is important to discuss the copper analogue, both because the zinc chromophore is diamagnetic and for the sake of uniformity. Williams has provided an analysis of the magnetic phenomena observed for this compound, and it has been reproduced here to facilitate easy comparison.

The general behavior observed in the two susceptibility plots (Figure 6.1a) for $\{L_2Cu_2(btc)_{4/3}\}_n$ ($L = H_2O$ and pyridine) is very similar but shows significant differences from the χ vs T plot of cupric acetate hydrate. The susceptibilities reach a minimum at around 70–80 K and then begin to increase at lower temperature. By contrast the minimum χ for copper acetate remains low until ca. 5 K. The low T magnetic behavior

for the two polymers was analyzed further in several ways. First a plot of $1/\chi$ vs. T was made for the low T region (Figure 6.1b). For $L = \text{pyridine}$ this is roughly linear between 20 and 65 K and fits the Curie–Weiss law $\chi = C / (T - \Theta)$, where C is the Curie constant and Θ is the intercept on the T axis when $\chi = 50$. From curve fitting, a value of $\Theta = 54.7$ K is found for $L = \text{pyridine}$, and supports a weak ferromagnetic interaction between SBUs. The field-dependant magnetic susceptibility is illustrated in Figure 6.2. The data exhibit little structure, and show no remnant magnetization.

Figure 6.1: Temperature-dependant magnetic susceptibility of $\{[L_2Cu_2(btc)_{4/3}]_n\}$

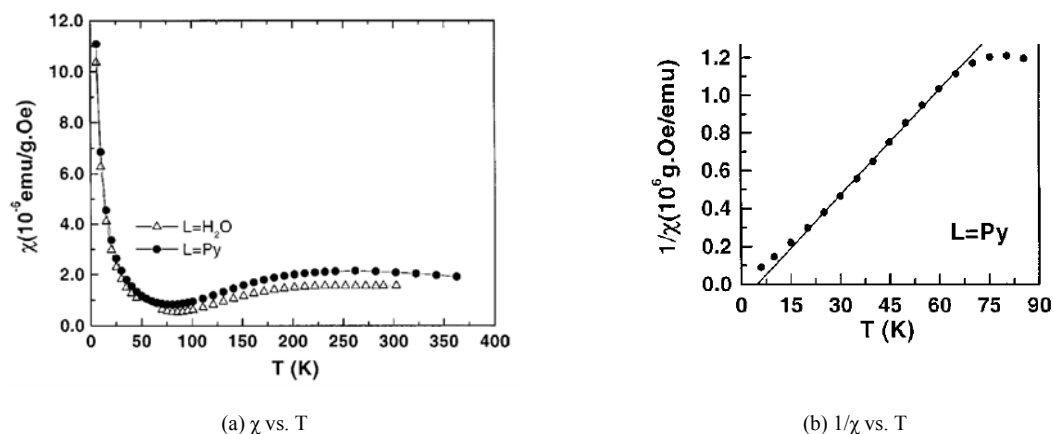
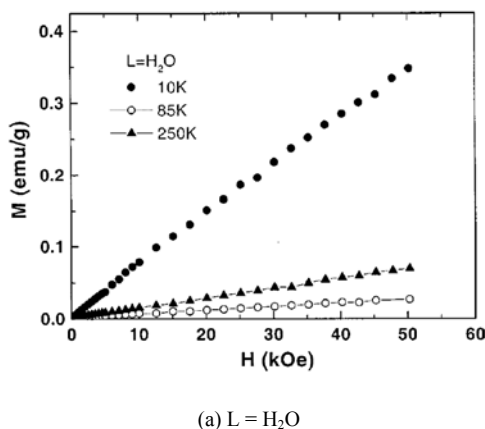


Figure 6.2: Field-dependant magnetic susceptibility of $\{[L_2Cu_2(btc)_{4/3}]_n\}$



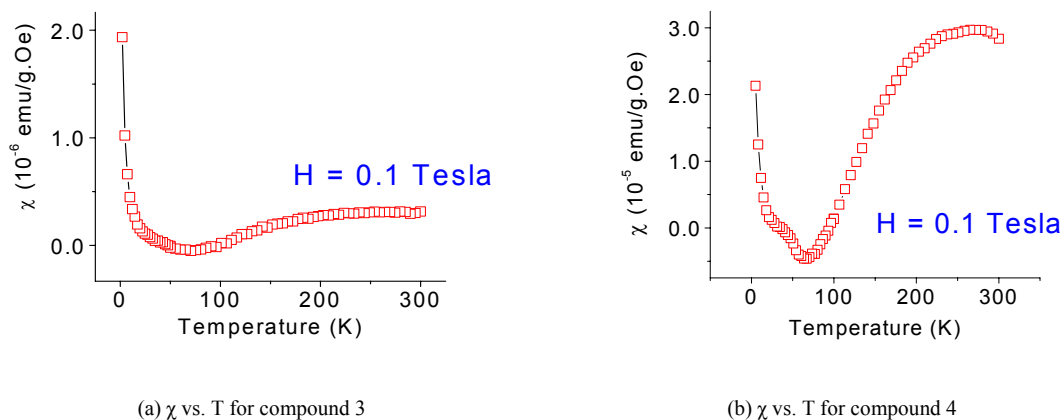
A magnetic interaction between SBUs is believed to be modulated by the aromatic bridges through which they are connected, since the through-space separation of

SBUs is not vastly different from the discrete molecular dimer systems. Studies of field cooled magnetization curves and use of variable fields to 5 T appear to support the hypothesis of dual interaction, that being intra- and inter-dimer coupling.

6.2.2. Two-dimensional structures

The temperature-dependant susceptibility data for compounds 3 and 4 are illustrated in Figure 6.3, which illustrates the zero-field cooled (ZFC) $\chi(T)$ data for these samples measured at 0.5 T (the field-cooled measurements did not differ significantly from these curves). The general behavior in both curves is similar with the susceptibility decreasing with temperature as the samples are cooled from room temperature. A minimum in $\chi(T)$ occurs around 70 K followed by an upturn as the temperature is decreased further. These results are also consistent with the three-dimensional framework. The susceptibility is plotted in units of cm^3/mol , consistent with the notation commonly used in molecular magnetism and all data are corrected for diamagnetic contributions using standard Pascal units.

Figure 6.3: Temperature-dependant magnetic susceptibility of $\{[\text{L}_2\text{Cu}_2(\text{bdc})_2]\}_n$ 2-D supramolecular isomers



Although the behavior is consistent with compound 2, in contrast the Curie-Weiss fits to the low-temperature susceptibility for the two-dimensional data were inconclusive and generally yielded negative Weiss temperatures (Θ). A more detailed understanding of the magnetic phenomena can be gained by modeling the behavior of the data using a modified Bleaney and Bowers (BB) equation,³⁰¹ which calculates the $\chi(T)$ for a dimeric copper(II) system in which the dominant magnetic interaction is considered to be the intra-dimer coupling (standard BB) with a minor contribution from inter-dimer coupling (modified BB). The BB equation is:

$$x_d(T) = \left[\frac{2Ng^2\beta^2}{\left(kT - \frac{2zJ'}{3 + e^{-J/kT}} \right) [3 + e^{-J/kT}]} \right] \quad (\text{Equation 6.1})$$

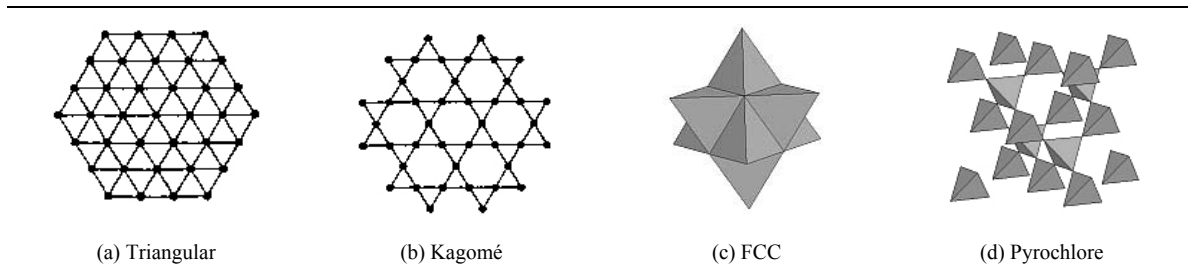
The parameters relevant to this discussion are J and J' , which correspond to the intra-dimer and inter-dimer coupling constants, respectively.

The solid lines superimposed on the data in Figure 6.3 are fits generated by use of equation 6.1, using J and J' as the main fit parameters. Quantitative values can therefore be determined for compound 3, the tetragonal 4⁴ supramolecular isomer: $J = -380 \text{ cm}^{-1}$ and $J' = -85 \text{ cm}^{-1}$; and for compound 4, the trigonal 3.6.3.6 supramolecular isomer: $J = -350 \text{ cm}^{-1}$ and $J' = -18 \text{ cm}^{-1}$. Not surprisingly, there is very little difference observed for the intra-dimer coupling, but a significant difference is observed for the inter-dimer coupling, which is attributed to the differences in the network topologies.

In chapter 3, it was noted that the 3.6.3.6 topology was also known as a Kagomé lattice. The Kagomé lattice has physical importance in the context of magnetism as it represents an example of a triangular lattice that is theoretically predicted to exhibit spin

frustration. Although there are many possible triangular networks, four such networks have attracted the most attention: the 2-D triangle, 2-D Kagomé, 3-D Face-centered cubic (FCC) and 3-D Pyrochlore lattices. In addition to the obvious classification based on the dimensionality of the network, these four systems can also be classified according to the connectivity of the triangles. In this regard, the triangle and FCC lattices result from edge shared triangles and the Kagomé and Pyrochlore lattices are based on vertex shared triangles (Figure 6.4). Examples of the latter include SCGO(x) materials, such as the Kagomé compound $\text{SrCr}_{9x}\text{Ga}_{3x}\text{O}_{19}$,³⁰² and the Pyrochlore compound CsNiMnF_6 ,³⁰³ both of which have been shown to have spin-liquid type behavior by neutron scattering.

Figure 6.4: Spin frustrated triangular lattices



Geometric frustration in magnetic materials has been theoretically predicted to lead to a variety of novel magnetic ground states.³⁰⁴ Such phenomena have recently been observed in a wide range of materials, where it is proposed that the frustration suppresses spin ordering for temperatures well within the energy scale of spin-spin interactions. Although for certain materials, such as $\text{Y}_2\text{Mo}_2\text{O}_7$,³⁰⁵ the magnetic behavior mimics the spin glass transitions in disordered magnets, it is important to differentiate between the two types of magnetic phenomena as there is virtually no disorder in geometrically frustrated systems. Figure 6.5 illustrates several possible geometric arrangements of spins and illustrates the origin of the frustration in the Kagomé lattice. Figure 6.6

illustrates two of the *ordered* ground states for the Kagomé lattice, which necessarily exhibit spin frustration.

Figure 6.5: Geometric arrangement of spins

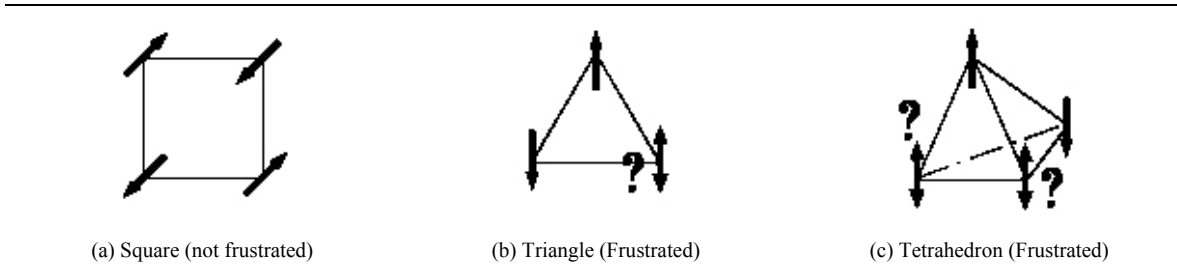


Figure 6.6: Examples of x-y spin ground states for the Kagomé lattice

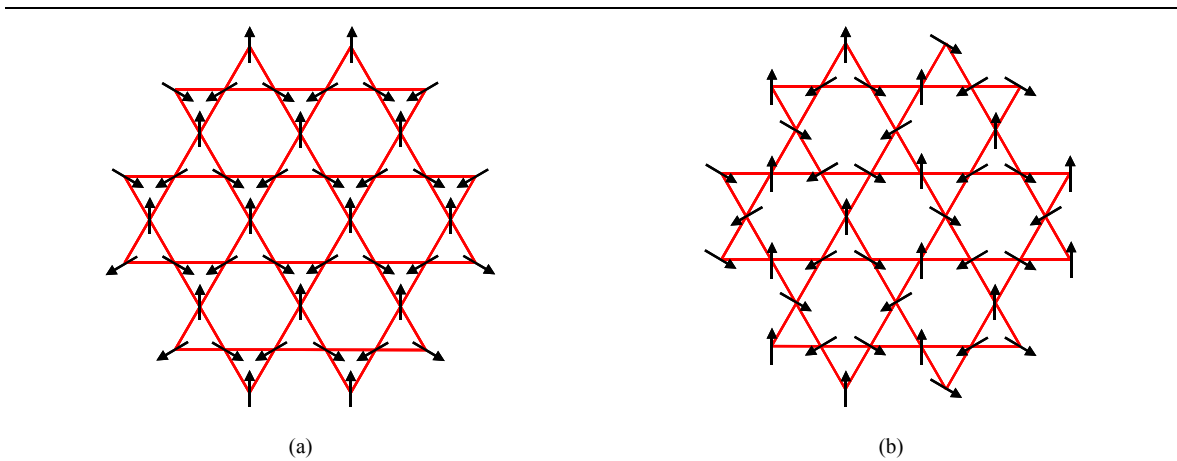
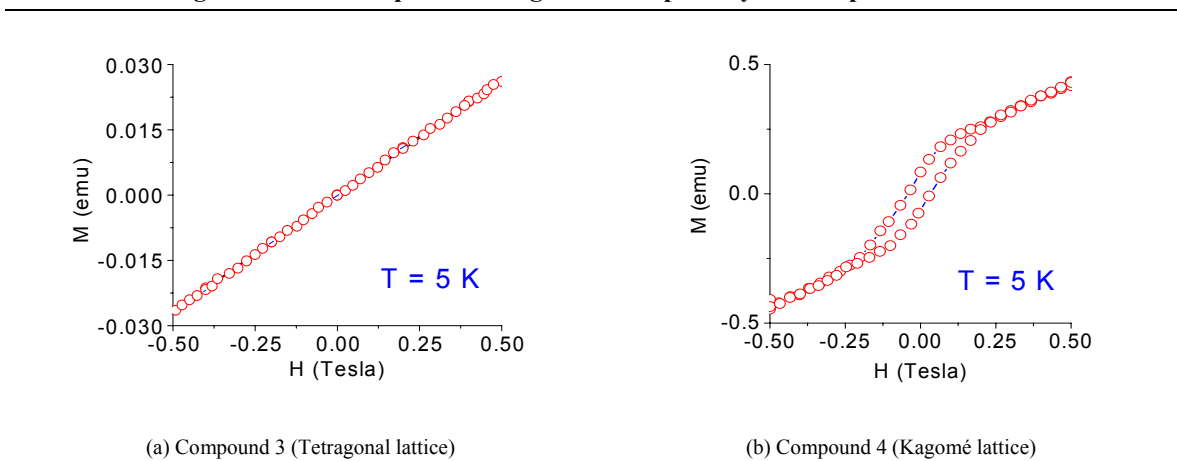


Figure 6.7: Field-dependant magnetic susceptibility for compounds 3 and 4



A clue as to the nature of the geometrically frustrated antiferromagnetic state for compound 4 is revealed in the $M(H)$ data Figure 6.7. A well-defined hysteresis loop is

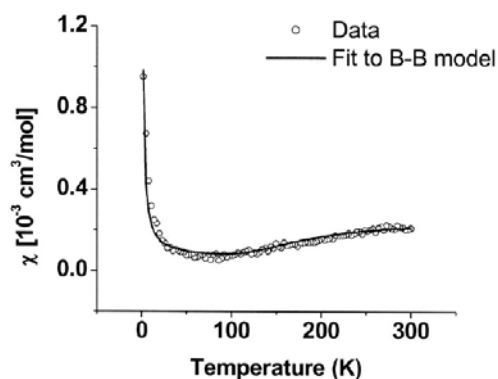
observed indicative of ferromagnetic behavior. We have also confirmed the presence of hysteresis at 300K.

Compound 3 exhibits a 4^4 two-dimensional square grid topology. From geometry considerations, spin frustration is ruled out and this is reflected in the magnetic measurements shown in Figure 6.6. To keep the comparison direct and simple, the $\chi(T)$ and $M(H)$ data have been plotted using an identical set of conditions. The magnetic data for compound 3 are very similar to the magnetic phenomena observed for compound 2. The salient feature for these systems is the lack of hysteresis with the $M(H)$ data exhibiting a straight line, representative of more traditional paramagnetic behavior.

6.2.3. Zero-dimensional (discrete) structures

Figure 6.8 illustrates the $\chi(T)$ data for compound 7. Fits to equation 6.1 yield much larger values with $J=-600 \text{ cm}^{-1}$ and $J'=-500 \text{ cm}^{-1}$. This is qualitatively consistent with the fact that coordination of the metal ions and the bridging ligands in this structure results in larger interaction strengths. Although there is no obvious structural feature to account for this, it is interesting to note that the spherical molecules are a rare example of an SBU in which the metals are not equivalent; i.e. there is an inner metal and an outer

Figure 6.8: Temperature-dependant magnetic susceptibility of $\{[L_2Cu_2(bdc)_2]\}_{12}$



(a) χ vs. T for compound 7

metal in each SBU. What effect, if any, this should have on the magnetic properties is currently being investigated. The influence of inter-particle interactions has also directly observed mediated through the ligands by comparing the magnetic properties of these spherical molecules with others in which the bdc has been covalently modified to achieve variability in the inter-dimer coupling and inter-particle distance. A comprehensive comparative study and analysis of the magnetic response in a broader class of these supramolecular isomers is currently underway, and will possibly form the basis of future publications and dissertations.

6.3. Conclusions

Our results dramatically underscore the potential afforded by supramolecular chemistry for the design of molecular nanostructure assemblies with desirable physical properties and emphasize how the composition of a material is not the only feature one must consider when designing a material that exhibits molecular magnetism. One of the most important features of the examples illustrated above is their modularity. It is fully anticipated that the magnetic properties of compound 4 can be ‘fine-tuned’ via chemical modification of the components: substituting the metal; changing the oxidation state of the metals (i.e. redox); changing the coordinated ligand; covalent modification of the bdc ligand; incorporation of different guest molecules. We expect an observable effect on the magnetic properties for all of these modifications and combinations thereof, as it has already been shown that simply varying the apical coordinated ligand has a measurable effect on the magnetism exhibited by the SBU used in our study.³⁰⁶

The nanoscale size of these molecular structures and their assembly in periodic arrangements raise exciting possibilities for obtaining stable magnetic nanostructures that can be spin cast onto substrates for electromagnetic applications. More studies of static and dynamic properties are needed to establish the underlying physics of magnetism and its correlation with the topological variations in compounds afforded by crystal engineering techniques.

Chapter 7

Conclusions & Future Directions

7.1. Summary

The introduction to this work was structured so that it presented the basic concepts necessary to understand the underlying principles and motivation behind crystal engineering. Throughout, the discussion has purposefully been narrowed to focus primarily on coordination polymers, while several examples of supramolecular organic materials have been highlighted to illustrate that the concepts of design remain the same regardless of the nature of the components. This arbitrary division of results is for convenience purposes only, with the intention of presenting a clear and concise series of structures, from which design strategies can be derived.

At the outset, this project set out to prove the hypothesis that a series of supramolecular isomers could be predicted based on the structure of compound 2, or more specifically, that the set of all supramolecular isomers could be extracted from compound 2. Although several examples of structures that fit this hypothesis were synthetically prepared, the identification of additional isomers has led to the reinterpretation of the structures. This, in turn, has led to the formulation of a new hypothesis that the set of supramolecular isomers that are possible when connecting tetracarboxylate SBUs by 120° linkers can be derived from the set of 4-connected nets that can be extracted from the 12-connected network that corresponds to the connectivity

of the centers of the spheres in spherical close packed lattices; specifically the hcp and ccp lattices.

Additionally, it has been illustrated that the magnetic properties of these materials is critically dependent on the topology of the networks. Specifically, it was demonstrated that by positioning the SBUs at the nodes of a Kagomé lattice, a material that exhibits remnant magnetization is afforded. This is particularly striking in consideration of the fact that six other materials, that have essentially the same composition, show no indication of remnant magnetization and, furthermore, that the origin of the magnetic moment comes from dicopper tetracarboxylates, which are not known as exceptionally strong molecular magnets.

7.2. “Intelligent” Design

What is meant by *intelligent* design? It is perhaps surprising that no mention has been made of this prior to this point, in consideration of the fact that it is the main title of this dissertation. There are many concepts implicit by the use of the term “intelligent”, and a complete understanding of the reasons behind its use can probably best be understood after all of the components of the work have been presented.

As was the case with the term “engineering”, let us examine the definition of the word “intelligent”, which is given by the Oxford English Dictionary as: “1. Having the faculty of understanding; possessing intelligence or intellect. 2. Having a high degree or full measure of understanding; quick to understand; knowing, sensible, sagacious. b. Of action, speech, etc.: Showing a high (or fair) degree of understanding. 3. That understands or knows (a particular thing, circumstance, or subject); cognizant of; acquainted with; versed in. 4. ‘Bearing intelligence, giving information, communicative’

(Schmidt Shaks. Lex.). *Obs.* 5. Of a device or machine: able to vary its behavior in response to varying situations and requirements and past experience; spec. (esp. of a computer terminal) having its own data-processing capability; incorporating a microprocessor.”

Clearly, the use of the term implies a certain level of understanding; however, the key to its use lies in the ability to vary one’s behavior in response to varying situations and requirements, and past experiences. A common criticism of people who proclaim to have “designed” materials is that the so-called design of the material came after the synthesis of the material. In many cases this is the truth, indeed the synthesis of some of the compounds described herein came as the result of serendipitous discovery. These discoveries, however, add to “past experiences”, which in turn, motivates intelligent design. Unfortunately, the design phase is perhaps the most difficult, and as such, some people find it more efficient to approach the problem in a combinatorial approach. This is not meant to diminish the valuable contribution that this research makes to the field, because it is the accumulation of this data that makes the design of materials possible.

I believe that there are three fundamental components to crystal engineering: design, synthesis and application. This is not to say that one who participates in only one of these phases should not be considered a practitioner of the discipline; on the contrary, I believe that individual focused efforts on all three phases will contribute significantly to the overall progress of the field. “Intelligent” design is intended to describe the design of new materials, whereby all three phases are considered concomitantly, and this can only be successfully practiced with the ability to vary one’s behavior in response to varying situations and requirements, and past experiences.

7.3. Predicted structures

Several directions for future research have become apparent as a consequence of the work described herein:

- Modification of compounds 1 – 8
- Synthesis of other faceted polyhedra
- Synthesis of the other three-dimensional faceted polyhedral network
- Synthesis of derivatives of compound 1
- Use of alternate chromophores for the design of topologically related materials
- Synthesis of other “frustrated” molecular magnetic materials
- Enumeration of networks that can be derived from hcp and ccp lattices

The possibilities for modifying compounds 1 – 8 have been discussed in some detail. Therefore, the focus of this section will be restricted to the other future research directions listed above.

7.3.1. *Faceted polyhedra*

Figure 4.10 illustrates the nine faceted polyhedra. The synthesis of the Small rhombihexahedron has been demonstrated to result from the linkage of molecular squares at their vertexes by 120° . The synthesis of the other examples should be possible by the determination of an appropriate molecular polygon with functionality that permits linkages at its vertexes, and use of a linker that subtends the appropriate angle. In the context of this work, the most obvious initial synthetic targets should be the three faceted polyhedra that result from the assembly of only squares (the Cubohemioctahedron and Small rhombidodecahedron, in addition to the Small rhombihexahedron), and the Small cubicuboctahedron, which has an edge-skeleton that is congruent to the Rhombicuboctahedron.

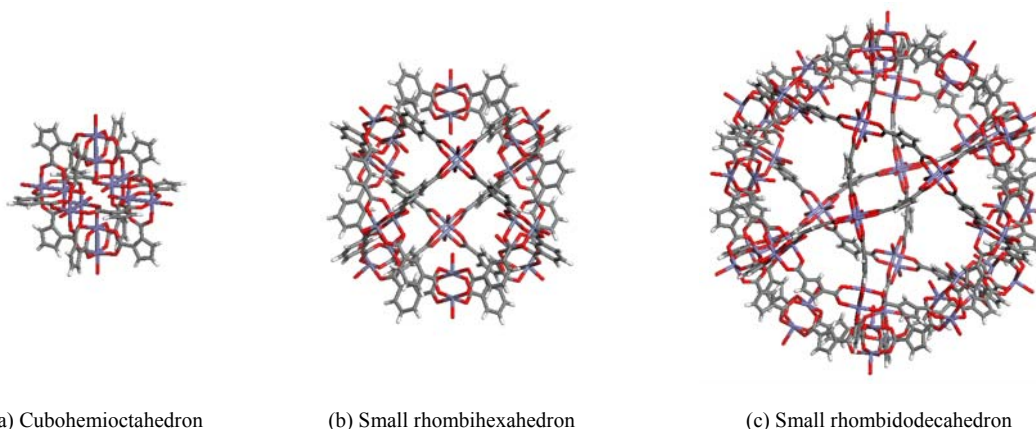
The Cubohemioctahedron results from the assembly of squares at their vertexes by a 90° linker. Exploitation of the dimetal tetracarboxylate SBU as a molecular square by use of a ligand like cubane-1,2-dicarboxylate may lead to such a structure. Synthesis might also be possible by using an organometallic dicarboxylate or even a supramolecular aggregate that has two exofunctional carboxylates predisposed at 90°. Perhaps another strategy is to exploit the knowledge that molecules have a degree of flexibility, and employ a ligand such as acenaphthene-1,2-dicarboxylate or *N*-methylpyrrole-3,4-dicarboxylate, each of which have two carboxylates that subtend an angle of 72°. It is reasonable to anticipate that the ligands will be able to sustain a distortion to achieve a 90° angle.

The Small rhombidodecahedron results from the assembly of squares at their vertexes by a 144° linker. This is more readily accessible by use of organic linkers, such as generic cyclopentadiene-1,3-dicarboxylates, which naturally predispose the carboxylates at 144°. Therefore, a ligand such as *N*-methylpyrrole-2,4-dicarboxylate or 2,5-thiophenedicarboxylate should lead to a molecular Small rhombidodecahedron. It should be noted that the *N*-methylpyrrole-2,4-dicarboxylate has the ability to afford chiral molecular sphere, if it orients precisely in the solid. Figure 7.1 illustrates models of a molecular Cubohemioctahedron and Small rhombidodecahedron, using a generic cyclopentadiene core, and compares them to the model of the molecular Small rhombihexahedron (compound 3). The models are shown at the same scale so that their relative size is apparent.

The synthesis of a Small cubicuboctahedron requires that molecular squares and triangles be linked at an angle of approximately 120°. It has already been shown that

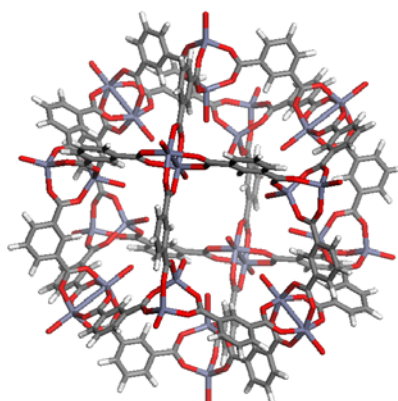
triangles and squares can be linked at 120° in compound 1. Indeed, a model of a molecular Small cubicuboctahedron can be extracted from the crystal structure of

Figure 7.1: Predicted structures of some molecular faceted polyhedra



compound 1. It should, in principle, be able to synthesized from bdc and zinc(II), in the same way that the Small rhombihexahedron was synthesized. A significant difference between the two molecules is that the Small cubicuboctahedron will necessarily be a +8 cation. This will significantly alter the bulk physical properties, such as solubility, and may make characterization a challenge. A model of the predicted structure is illustrated in Figure 7.2.

Figure 7.2: Predicted structure of the Small cubicuboctahedron



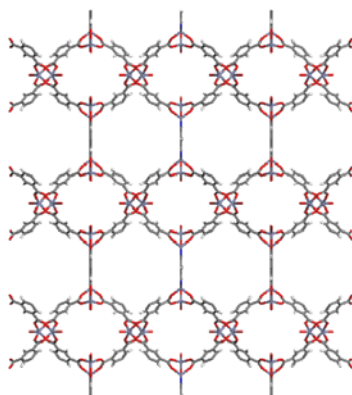
7.3.2. *Three-dimensional structure*

Chapter 2 described the synthesis of two three-dimensional networks based on the geometry of space-filling polyhedra. Figure 2.8 illustrates the schematics of these packing arrangements, along with another: octahedra and cuboctahedra. The faceted version of this packing involves the packing of Cubohemioctahedra, which, as mentioned above, results from the assembly of squares at 90° angles. The geometry of the three-dimensional network imposes an additional constraint if the synthesis is based on dimetal tetracarboxylates: the carboxylates must be orthogonal to the plane of a square planar node. In the previous structures, the carboxylates had to be coplanar with the trigonal node. Cubane-1,2,4,7-tetracarboxylate exemplifies such a ligand; although this ligand is not known, 1,2,4,7-tetrakis(Carboxymethyl)cubane has been characterized. Another interpretation of this structure can be realized if both the ligand and the SBU are considered nodes. In this instance, the network would be considered to possess the CdSO₄ topology.

7.3.3. *Derivatives of compound 1*

The main focus of this dissertation has been the derivation of networks based on compound 2. Are there networks that can be extracted from compound 1? Of course the answer is known, as a faceted polyhedron that can be extracted from compound 1 is illustrated in Figure 7.2. Furthermore, an analysis of various crystallographic planes reveals that there is a possible two-dimensional network that can be extracted by removing the (022) plane ± 4.5 Å. This network is comprised of vertex linked triangles and squares and is necessarily ionic. This is illustrated in Figure 7.3.

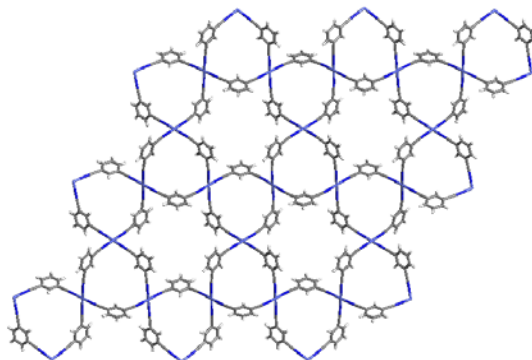
Figure 7.3: Predicted structure of a two-dimensional coordination polymer



7.3.4. Other chromophores

As has been stressed throughout, the design principles described herein are not confined to dimetal carboxylate chromophores. For example, in the context of magnetic topologies, it may be beneficial to position single metal centers at the nodes of a Kagomé lattice. Based on the design principles described herein, this can be accomplished by exploitation of a square planar metal, or an octahedral metal with apically coordinated ligands. The use of an angular ligand should afford the tetragonal 4^4 lattice and the Kagomé lattice under varying conditions. Figure 7.4 illustrates the predicted structure for a Kagomé lattice that is composed of cobalt(II) and 1,3-dicyanobenzene.

Figure 7.4: Predicted structure of a monometal Kagomé lattice



7.3.5. Geometrically frustrated molecular magnetic materials

Figure 6.4 illustrates four examples of frustrated lattices that have been studied theoretically in terms of predicted magnetic phenomena. The synthesis of the first supramolecular Kagomé lattice has been described herein. Synthesis of supramolecular examples of the other lattices remains a goal. In the context of vertex-connected lattices, it is important to note that the Kagomé topology is 4-connected, and the pyrochlore topology is 6-connected. The angles are not 90° in either case, however, judicious choice of an *angular* ditopic ligand may result in the formation of the Kagomé lattice from a square planar metal coordination sphere, and the pyrochlore lattice from an octahedral metal coordination sphere. The critical factor in the design of these networks is therefore identification of a ditopic ligand that permits communication between coordinated metals and possesses the appropriate angle (120° for the Kagomé lattice) for the generation of the desired lattice. The fact that square planar and octahedral geometries are common amongst transition metals, it offers great promise that additional examples of these topologies will be realized.

7.3.6. Enumeration of networks

Despite the progress made in the discipline, it seems obvious that many topologies remain unrealized in molecular network solids. Therefore, it is unsurprising that the enumeration of new networks has drawn recent interest.³⁰⁷ Of particular interest has been the enumeration of 4-connected networks,³⁰⁸⁻³¹⁰ i.e. networks in which each node or vertex is connected to four other nodes. These networks have drawn focus due to the 4-connected nature of tetrahedral chromophores found in hydrates, silicates, and zeolites, in addition to many other systems.

Enumeration strategies have thus far focused on a divergent strategy by exploiting techniques developed within the field of combinatorial tiling theory.^{311,312} I believe there are two important limitations to this approach: too many topologies are generated and not all topologies are possible for molecular solids. For example, a recent study reports 1,052 topological types of networks based on tetrahedral tilings only, and if one considers the fourteen possible two-dimensional tilings of pentagons only three can be realized by molecular solids.

The results described herein, suggest that an alternate approach may be the development of a convergent strategy based on the connectivity of sphere close packings. The initial hypothesis is that all network topologies possible for molecular solids can be extracted from the networks that are defined by the connectivity of the centers of the spheres in hexagonal close packed (hcp) or cubic close packed (ccp/fcc) lattices, and simple transformations thereof. By imposing limitations on the number of spheres allowed per unit cell, and examining the set of periodic networks that have less than 12-connected nodes (note that for hcp and ccp lattices there are 12 closest contacts per sphere), a finite number of topologies can be derived. In essence, this strategy combines Kitaigorodskii's postulate³¹³ that crystals result from molecules desire to close pack and the premise of crystal engineering that crystals result from a series of directional molecular recognition events.

7.4. The last word

Finally, I would like to end where I began. In the introduction, I posed the question: what is crystal engineering? One of the goals of this work is to emphasize the “engineering” in crystal engineering. It is fascinating to revisit many of the historical

contributions to the field, with a modern understanding of the present state-of-the-art.

Wells' Three-dimensional Nets and Polyhedra, published in 1977, was a seminal work in this context, and I believe offers insight that remains currently topical, and should continue to serve as motivation for current research.

Even more remarkable, I believe, were the Feynman lectures in 1959. Feynman understood the enormous value of being able to control the precise arrangements of atoms in a material, and provided the motivation for generations of future researchers.

Although it appeared in the introduction, I believe it is worth repeating here:

“What would the properties of materials be if we could really arrange the atoms the way we want them? They would be very interesting to investigate theoretically. I can't see exactly what would happen, but I can hardly doubt that when we have some control of the arrangement of things on a small scale we will get an enormously greater range of possible properties that substances can have, and of different things that we can do.”

What I hope to have demonstrated here is that the key to realizing this dream may lie in our ability to control the arrangement of molecules, as opposed to atoms. Indeed, the ability to control the arrangement and orientation of molecules necessarily implies a control of the constituent atoms. Our ability to address this challenge, albeit limited, invites us to look beyond the “if” we can arrange the atoms, to “where” do we want to put them.

References

1. Feynman, R. *Eng. Sci.* **1960**, 22-36.
2. Schmidt, G. M. J. *Pure Appl. Chem.* **1971**, 27, 647-678.
3. Pepinsky, R. *Phys. Rev.* **1955**, 100, 971.
4. Lehn, J. M. *Pure Appl. Chem.* **1978**, 50, 871-892.
5. Lehn, J. M. *Supramolecular Chemistry: Concepts and Perspectives*; VCH: Weinheim, 1995.
6. Dunitz, J. D. *Pure Appl. Chem.* **1991**, 63, 177-185.
7. Dunitz, J. D. *Perspectives in Supramolecular Chemistry, Vol. 2* Wiley: New York, 1996; Vol. 2.
8. Bernstein, J.; Davey, R. J.; Henck, J. O. *Angew. Chem., Int. Ed. Engl.* **1999**, 38, 3441-3461.
9. Dunitz, J. D.; Bernstein, J. *Acc. Chem. Res.* **1995**, 28, 193-200.
10. Batten, S. R.; Robson, R. *Angew. Chem., Int. Ed. Engl.* **1998**, 37, 1461-1494.
11. Fan, J.; Whiteford, J. A.; Olenyuk, B.; Levin, M. D.; Stang, P. J.; Fleischer, E. B. *J. Am. Chem. Soc.* **1999**, 121, 2741-2752.
12. Rodriguez-Hornedo, N.; Murphy, D. *J. Pharm. Sci.* **1999**, 88, 651-660.
13. Bernstein, J. *Polymorphism in Molecular Crystals* ; Oxford University Press: New York, 2002.
14. Tanaka, K.; Toda, F. *Chem. Rev.* **2000**, 100, 1025-1074.
15. Toda, F. *Acc. Chem. Res.* **1995**, 28, 480-486.
16. Metzger, J. O. *Angew. Chem., Int. Ed. Engl.* **1998**, 37, 2975-2978.
17. Loupy, A. *Top. Curr. Chem.* **1999**, 206, 153-207.

18. MacGillivray, L. R.; Reid, J. L.; Ripmeester, J. A. *J. Am. Chem. Soc.* **2000**, *122*(32), 7817-7818.
19. Xiao, J.; Yang, M.; Lauher, J. W.; Fowler, F. W. *Angew. Chem., Int. Ed. Engl.* **2000**, *39*, 2132-2135.
20. Kane, J. J.; Liao, R. F.; Lauher, J. W.; Fowler, F. W. *J. Am. Chem. Soc.* **1995**, *117*, 12003-12004.
21. Hamilton, T. D.; Papaefstathiou, G. S.; Macgillivray, L. R. *J. Am. Chem. Soc.* **2002**, *124*, 11606-11607.
22. Desiraju, G. R.; Gavezzotti, A. *Chem. Commun.* **1989**, 621-623.
23. Desiraju, G. R. *Acc. Chem. Res.* **1991**, *24*, 290-296.
24. Desiraju, G. R. *Angew. Chem., Int. Ed. Engl.* **1995**, *34*, 2311-2327.
25. Etter, M. C. *J. Phys. Chem.* **1991**, *95*, 4601-4610.
26. Etter, M. C.; MacDonald, J. C.; Bernstein, J. *Acta Crystallogr.* **1990**, *B46*, 256-262.
27. Etter, M. C. *Acc. Chem. Res.* **1990**, *23*, 120-126.
28. Allen, F. H.; Kennard, O. *Chem. Des. Autom. News* **1993**, *8*(1), 31-37.
29. Cohen, M. D. *Angew. Chem., Int. Ed. Engl.* **1975**, *14*, 386-393.
30. Green, B. S.; Heller, L. *Science* **1974**, *185*, 525-527.
31. Addadi, L.; Moradian, J.; Shay, E.; Maroudas, N. G.; Weiner, S. *Proc. Natl. Acad. Sci. U. S. A.* **1987**, *84*, 2732-2736.
32. Addadi, L.; Weiner, S. *Proc. Natl. Acad. Sci. U. S. A.* **1985**, *82*, 4110-4114.
33. Addadi, L.; Berkovitchyellin, Z.; Weissbuch, I.; Vanmil, J.; Shimon, L. J. W.; Lahav, M.; Leiserowitz, L. *Angew. Chem., Int. Ed. Engl.* **1985**, *24*, 466-485.
34. Addadi, L.; Vanmil, J.; Gati, E.; Lahav, M. *Origins of Life and Evolution of the Biosphere* **1981**, *11*, 107-118.
35. Addadi, L.; Lahav, M. *J. Am. Chem. Soc.* **1979**, *101*, 2152-2156.
36. Mann, S.; Archibald, D. D.; Didymus, J. M.; Douglas, T.; Heywood, B. R.; Meldrum, F. C.; Reeves, N. J. *Science* **1993**, *261*, 1286-1292.
37. Mann, S.; Heywood, B. R.; Rajam, S.; Walker, J. B. A. *ACS Symp. Ser.* **1991**, *444*, 28-41.

38. Jones, W.; Ramdas, S.; Theocharis, C. R.; Thomas, J. M.; Thomas, N. W. *J. Phys. Chem.* **1981**, *85*, 2594-2597.
39. Thomas, J. M. *Philos. Trans. R. Soc. London, A* **1974**, *277*, 251-287.
40. Davey, R. J.; Black, S. N.; Bromley, L. A.; Cottier, D.; Dobbs, B.; Rout, J. E. *Nature* **1991**, *353*, 549-550.
41. Davey, R. J.; Mullin, J. W. *J. Cryst. Growth* **1974**, *26*, 45-51.
42. Maddox, J. *Nature* **1988**, *335*, 201.
43. Desiraju, G. R. *Crystal Engineering: the Design of Organic Solids*; Elsevier: Amsterdam, 1989.
44. Gavezzotti, A. *Crystallogr. Rev.* **1998**, *7*, 5-121.
45. Muller, A.; Krickemeyer, E.; Meyer, J.; Bogge, H.; Peters, F.; Plass, W.; Diemann, E.; Dillinger, S.; Nonnenbruch, F.; Randerath, M.; Menke, C. *Angew. Chem., Int. Ed. Engl.* **1995**, *34*, 2122-2124.
46. Gavezzotti, A. *Acc. Chem. Res.* **1994**, *27*, 309-314.
47. Hofmann, D. W. M.; Apostolakis, J. *J. Mol. Struct.* **2003**, *647*, 17-39.
48. Motherwell, W. D. S.; Ammon, H. L.; Dunitz, J. D.; Dzyabchenko, A.; Erk, P.; Gavezzotti, A.; Hofmann, D. W. M.; Leusen, F. J. J.; Lommerse, J. P. M.; Mooij, W. T. M.; Price, S. L.; Scheraga, H.; Schweizer, B.; Schmidt, M. U.; Van Eijck, B. P.; Verwer, P.; Williams, D. E. *Acta Crystallogr.* **2002**, *58*, 647-661.
49. Hennigar, T. L.; MacQuarrie, D. C.; Losier, P.; Rogers, R. D.; Zaworotko, M. J. *Angew. Chem., Int. Ed. Engl.* **1997**, *36*, 972-973.
50. Abourahma, H.; Moulton, B.; Kravtsov, V.; Zaworotko, M. J. *J. Am. Chem. Soc.* **2002**, *124*, 9990-9991.
51. Moulton, B.; Zaworotko, M. J. *Chem. Rev.* **2001**, *101*, 1629-1658.
52. Zaworotko, M. J. *Chem. Commun.* **2001**, 1-9.
53. Swift, J. A.; Pivovar, A. M.; Reynolds, A. M.; Ward, M. D. *J. Am. Chem. Soc.* **1998**, *120*, 5887-5894.
54. Nangia, A.; Desiraju, G. R. *Chem. Commun.* **1999**, 605-606.
55. Sarma, J. A. R. P.; Desiraju, G. R. *Polymorphism and Pseudopolymorphism in Organic Crystals: a Cambridge Structural Database Study* Kluwer: Dordrecht, 1999; pp 325-356.

56. Braga, D.; Grepioni, F. *Chem. Soc. Rev.* **2000**, *29*, 229-238.
57. Dunitz, J. D. *Acta Crystallogr.* **1995**, *B51*, 619-631.
58. Threlfall, T. L. *Analyst* **1995**, *120*, 2435-2460.
59. Masciocchi, N.; Ardizzoia, G. A.; Lamonica, G.; Moret, M.; Sironi, A. *Inorg. Chem.* **1997**, *36*, 449-454.
60. Zerkowski, J. A.; MacDonald, J. C.; Whitesides, G. M. *Chem. Mater.* **1997**, *9*, 1933-1941.
61. Chin, D. N.; Palmore, G. T. R.; Whitesides, G. M. *J. Am. Chem. Soc.* **1999**, *121*, 2115-2122.
62. McCrone, W. C. *Polymorphism in Physics and Chemistry of the Organic Solid-State* Interscience: New York, 1965; Vol. 2, p 726.
63. Yu, L.; Stephenson, G. A.; Mitchell, C. A.; Bunnell, C. A.; Snorek, S. V.; Bowyer, J. J.; Borchardt, T. B.; Stowell, J. G.; Byrn, S. R. *J. Am. Chem. Soc.* **2000**, *122*, 585-591.
64. Bernstein, J. *Organic Solid-State Chemistry* Elsevier: Amsterdam, 1987; p 471.
65. Bernstein, J.; Sarma, J. A. R. P.; Gavezzotti, A. *Chem. Phys. Lett.* **1990**, *174*, 361-368.
66. Ball, P. *Nature* **1996**, *381*, 648-650.
67. Blake, A. J.; Champness, N. R.; Hubberstey, P.; Li, W. S.; Withersby, M. A.; Schroder, M. *Coord. Chem. Rev.* **1999**, *183*, 117-138.
68. Lahav, M.; Leiserowitz, L. *Angew. Chem., Int. Ed. Engl.* **1999**, *38*, 2533-2536.
69. Wen, R. W.; Bernal, I.; Fnonczek, F. R. *J. Coord. Chem.* **1999**, *49*, 33-43.
70. Cunningham, I. D.; Coles, S. J.; Hursthouse, M. B. *Chem. Commun.* **2000**, 61-62.
71. Kostyanovsky, R. G.; Avdeenko, A. P.; Konovalova, S. A.; Kadorkina, G. K.; Prosyaniuk, A. V. *Mendeleev Commun.* **2000**, 16-18.
72. Koshima, H.; Hayashi, E.; Matsuura, T. *Supramol. Chem.* **1999**, *11*, 57-66.
73. Sakamoto, M. *Chem. Eur. J.* **1997**, *3*, 684-689.
74. Wells, A. F. *Structural Inorganic Chemistry, 5th Ed*; Oxford University Press: Oxford, 1984.
75. Wells, A. F. *Three-Dimensional Nets and Polyhedra*; Wiley: New York, 1977.

76. Robson, R.; Abrahams, B. F.; Batten, S. R.; Gable, R. W.; Hoskins, B. F.; Liu, J. P. *ACS Symp. Ser.* **1992**, *499*, 256-273.
77. Abrahams, B. F.; Hoskins, B. F.; Robson, R. *J. Am. Chem. Soc.* **1991**, *113*, 3606-3607.
78. Fujita, M.; Kwon, Y. J.; Washizu, S.; Ogura, K. *J. Am. Chem. Soc.* **1994**, *116*, 1151-1152.
79. Abrahams, B. F.; Hoskins, B. F.; Liu, J. P.; Robson, R. *J. Am. Chem. Soc.* **1991**, *113*, 3045-3051.
80. Batten, S. R.; Hoskins, B. F.; Robson, R. *Chem. Commun.* **1991**, 445-447.
81. Gable, R. W.; Hoskins, B. F.; Robson, R. *Chem. Commun.* **1990**, 762-763.
82. Hoskins, B. F.; Robson, R. *J. Am. Chem. Soc.* **1990**, *112*, 1546-1554.
83. Abrahams, B. F.; Hoskins, B. F.; Robson, R. *Chem. Commun.* **1990**, 60-61.
84. Noro, S.; Kitagawa, S.; Kondo, M.; Seki, K. *Angew. Chem., Int. Ed. Engl.* **2000**, *39*, 2082-2084.
85. Kondo, M.; Shimamura, M.; Noro, S.; Kimura, Y.; Uemura, K.; Kitagawa, S. *J. Solid State Chem.* **2000**, *152*, 113-119.
86. Kondo, M.; Shimamura, M.; Noro, S.; Minakoshi, S.; Asami, A.; Seki, K.; Kitagawa, S. *Chem. Mater.* **2000**, *12*, 1288-1299.
87. Kabir, M. K.; Miyazaki, N.; Kawata, S.; Adachi, K.; Kumagai, H.; Inoue, K.; Kitagawa, S.; Iijima, K.; Katada, M. *Coord. Chem. Rev.* **2000**, *198*, 157-169.
88. Eddaoudi, M.; Li, H. L.; Yaghi, O. M. *J. Am. Chem. Soc.* **2000**, *122*, 1391-1397.
89. Li, H.; Eddaoudi, M.; O'Keeffe, M.; Yaghi, O. M. *Nature* **1999**, *402*, 276-279.
90. Xu, Z. F.; Moore, J. S. *Acta Polym.* **1994**, *45*, 83-87.
91. Li, H. L.; Laine, A.; O'Keeffe, M.; Yaghi, O. M. *Science* **1999**, *283*, 1145-1147.
92. Yaghi, O. M.; Li, H. L.; Davis, C.; Richardson, D.; Groy, T. L. *Acc. Chem. Res.* **1998**, *31*, 474-484.
93. Eddaoudi, M.; Kim, J.; Vodak, D.; Sudik, A.; Wachter, J.; O'keeffe, M.; Yaghi, O. M. *Proc. Natl. Acad. Sci. U. S. A.* **2002**, *99*, 4900-4904.
94. Eddaoudi, M.; Kim, J.; Rosi, N.; Vodak, D.; Wachter, J.; O'keeffe, M.; Yaghi, O. M. *Science* **2002**, *295*, 469-472.

95. Ermer, O.; Lindenberg, L. *Helv. Chim. Acta* **1988**, *71*, 1084-1093.
96. Ermer, O. *J. Am. Chem. Soc.* **1988**, *110*, 3747-3754.
97. Ermer, O.; Eling, A. *Angew. Chem., Int. Ed. Engl.* **1988**, *27*, 829-833.
98. Frankenbach, G. M.; Etter, M. C. *Chem. Mater.* **1992**, *4*, 272-278.
99. Su, D.; Wang, X.; Simard, M.; Wuest, J. D. *Supramol. Chem.* **1995**, *6*, 171-178.
100. Zaworotko, M. J. *Chem. Soc. Rev.* **1994**, *23*, 283-288.
101. Withersby, M. A.; Blake, A. J.; Champness, N. R.; Cooke, P. A.; Hubberstey, P.; Li, W. S.; Schroder, M. *Inorg. Chem.* **1999**, *38*, 2259-2266.
102. Keefe, M. H.; Slone, R. V.; Hupp, J. T.; Czaplewski, K. F.; Snurr, R. Q.; Stern, C. L. *Langmuir* **2000**, *16*, 3964-3970.
103. Branden, C.; Tooze, J. *Introduction to Protein Structure*; Garland: New York, 1999.
104. Belanger, S.; Keefe, M. H.; Welch, J. L.; Hupp, J. T. *Coord. Chem. Rev.* **1999**, *192*, 29-45.
105. Belanger, S.; Hupp, J. T. *Angew. Chem., Int. Ed. Engl.* **1999**, *38*, 2222-2224.
106. Belanger, S.; Hupp, J. T.; Stern, C. L.; Slone, R. V.; Watson, D. F.; Carrell, T. G. *J. Am. Chem. Soc.* **1999**, *121*, 557-563.
107. Benkstein, K. D.; Hupp, J. T.; Stern, C. L. *J. Am. Chem. Soc.* **1998**, *120*, 12982-12983.
108. Slone, R. V.; Benkstein, K. D.; Belanger, S.; Hupp, J. T.; Guzei, I. A.; Rheingold, A. L. *Coord. Chem. Rev.* **1998**, *171*, 221-243.
109. Kim, S.; Smith, T. J.; Chapman, M. S.; Rossmann, M. G.; Pevear, D. C.; Dutko, F. J.; Felock, P. J.; Diana, G. D.; McKinlay, M. A. *J. Mol. Biol.* **1989**, *210*, 91-111.
110. Stang, P. J.; Olenyuk, B. *Acc. Chem. Res.* **1997**, *30*, 502-518.
111. Slone, R. V.; Hupp, J. T. *Inorg. Chem.* **1997**, *36*, 5422-5423.
112. Manna, J.; Kuehl, C. J.; Whiteford, J. A.; Stang, P. J.; Muddiman, D. C.; Hofstadler, S. A.; Smith, R. D. *J. Am. Chem. Soc.* **1997**, *119*, 11611-11619.
113. Cao, D. H.; Chen, K. C.; Fan, J.; Manna, J.; Olenyuk, B.; Whiteford, J. A.; Stang, P. J. *Pure Appl. Chem.* **1997**, *69*, 1979-1986.

114. Olenyuk, B.; Whiteford, J. A.; Stang, P. J. *J. Am. Chem. Soc.* **1996**, *118*, 8221-8230.
115. Fujita, M.; Ogura, G. *Bull. Chem. Soc. Jpn.* **1996**, *69*, 1471-1482.
116. Fujita, M.; Sasaki, O.; Mitsuhashi, T.; Fujita, T.; Yazaki, J.; Yamaguchi, K.; Ogura, K. *Chem. Commun.* **1996**, 1535-1536.
117. Stang, P. J.; Olenyuk, B. *Angew. Chem., Int. Ed. Engl.* **1996**, *35*, 732-736.
118. Whitesell, J. K.; Davis, R. E.; Wong, M. S.; Chang, N. L. *J. Am. Chem. Soc.* **1994**, *116*, 523-527.
119. Yoshizawa, M.; Kusukawa, T.; Fujita, M.; Yamaguchi, K. *J. Am. Chem. Soc.* **2000**, *122*, 6311-6312.
120. MacGillivray, L. R.; Atwood, J. L. *J. Solid State Chem.* **2000**, *152*, 199-210.
121. Muller, A.; Shah, S. Q. N.; Bogge, H.; Schmidtmann, M.; Kogerler, P.; Hauptfleisch, B.; Leiding, S.; Wittler, K. *Angew. Chem., Int. Ed. Engl.* **2000**, *39*, 1614-1616.
122. Leininger, S.; Olenyuk, B.; Stang, P. J. *Chem. Rev.* **2000**, *100*, 853-907.
123. Sakamoto, S.; Fujita, M.; Kim, K.; Yamaguchi, K. *Tetrahedron* **2000**, *56*, 955-964.
124. Caulder, D. L.; Raymond, K. N. *Acc. Chem. Res.* **1999**, *32*, 975-982.
125. Olenyuk, B.; Levin, M. D.; Whiteford, J. A.; Shield, J. E.; Stang, P. J. *J. Am. Chem. Soc.* **1999**, *121*, 10434-10435.
126. Orr, G. W.; Barbour, L. J.; Atwood, J. L. *Science* **1999**, *285*, 1049-1052.
127. MacGillivray, L. R.; Atwood, J. L. *Angew. Chem., Int. Ed. Engl.* **1999**, *38*, 1019-1034.
128. Takeda, N.; Umemoto, K.; Yamaguchi, K.; Fujita, M. *Nature* **1999**, *398*, 794-796.
129. Barbour, L. J.; Orr, G. W.; Atwood, J. L. *Nature* **1998**, *393*, 671-673.
130. Stang, P. J. *Chem. Eur. J.* **1998**, *4*, 19-27.
131. MacGillivray, L. R.; Atwood, J. L. *Nature* **1997**, *389*, 469-472.
132. Conn, M. M.; Rebek, J. *Chem. Rev.* **1997**, *97*, 1647-1668.
133. Hartshorn, C. M.; Steel, P. J. *Chem. Commun.* **1997**, 541-542.

134. Muller, A.; Reuter, H.; Dillinger, S. *Angew. Chem., Int. Ed. Engl.* **1995**, *34*, 2328-2361.
135. Fujita, M.; Oguro, D.; Miyazawa, M.; Oka, H.; Yamaguchi, K.; Ogura, K. *Nature* **1995**, *378*, 469-471.
136. Muller, A.; Hovemeier, K.; Krickemeyer, E.; Bogge, H. *Angew. Chem., Int. Ed. Engl.* **1995**, *34*, 779-781.
137. Zhang, Y. W.; Seeman, N. C. *J. Am. Chem. Soc.* **1994**, *116*, 1661-1669.
138. Abourahma, H.; Coleman, A. W.; Moulton, B.; Rather, B.; Shahgaldian, P.; Zaworotko, M. J. *Chem. Commun.* **2001**, 2380-2381.
139. Moulton, B.; Lu, J.; Mondal, A.; Zaworotko, M. J. *Chem. Commun.* **2001**, 863-864.
140. Meier, W. M.; Olson, D. H. *Atlas of Zeolite Structure Types*; Butterworth-Heinemann: Boston, 1992.
141. Acharya, R.; Fry, E.; Stuart, D.; Fox, G.; Rowlands, D.; Brown, F. *Nature* **1989**, *337*, 709-716.
142. Luo, M.; Vriend, G.; Kamer, G.; Minor, I.; Arnold, E.; Rossmann, M. G.; Boege, U.; Scraba, D. G.; Duke, G. M.; Palmenberg, A. C. *Science* **1987**, *235*, 182-191.
143. Hogle, J. M.; Chow, M.; Filman, D. J. *Science* **1985**, *229*, 1358-1365.
144. Proulxcurry, P. M.; Chasteen, N. D. *Coord. Chem. Rev.* **1995**, *144*, 347-368.
145. Wenninger, M. J. *Polyhedron Models*; Cambridge University Press: Cambridge, 1989.
146. Swiegers, G. F.; Malefetse, J. *Chem. Rev.* **2000**, *100*(9), 3483-3537.
147. Slone, R. V.; Yoon, D. I.; Calhoun, R. M.; Hupp, J. T. *J. Am. Chem. Soc.* **1995**, *117*, 11813-11814.
148. Cernak, J.; Abboud, K. A. *Acta Crystallogr.* **2000**, *C56*, 783-785.
149. Colacio, E.; Ghazi, M.; Kivekas, R.; Klinga, M.; Lloret, F.; Moreno, J. M. *Inorg. Chem.* **2000**, *39*, 2770-2776.
150. Guo, G. C.; Wang, Q. M.; Mak, T. C. W. *Inorg. Chem. Commun.* **2000**, *3*, 313-315.
151. Abrahams, B. F.; Lu, K. D.; Moubaraki, B.; Murray, K. S.; Robson, R. *Dalton Trans.* **2000**, 1793-1797.

152. Dong, Y. B.; Smith, M. D.; Zur Loye, H. C. *Inorg. Chem.* **2000**, *39*, 1943-1949.
153. Colacio, E.; Dominguez-Vera, J. M.; Ghazi, M.; Kivekas, R.; Moreno, J. M.; Pajunen, A. *Dalton Trans.* **2000**, 505-509.
154. Maekawa, M.; Sugimoto, K.; Kuroda-Sowa, T.; Suenaga, Y.; Munakata, M. *Dalton Trans.* **1999**, 4357-4362.
155. Colacio, E.; Dominguez-Vera, J. M.; Ghazi, M.; Kivekas, R.; Klinga, M.; Moreno, J. M. *Eur. J. Inorg. Chem.* **1999**, 441-445.
156. Mimura, M.; Matsuo, T.; Nakashima, T.; Matsumoto, N. *Inorg. Chem.* **1998**, *37*, 3553-3560.
157. Sun, Z. M.; Gantzel, P. K.; Hendrickson, D. N. *Polyhedron* **1998**, *17*, 1511-1516.
158. Stocker, F. B.; Troester, M. A.; Britton, D. *Inorg. Chem.* **1996**, *35*, 3145-3153.
159. Ellis, W. W.; Schmitz, M.; Arif, A. A.; Stang, P. J. *Inorg. Chem.* **2000**, *39*, 2547-2557.
160. Hong, M. C.; Su, W. P.; Cao, R.; Fujita, M.; Lu, J. X. *Chem. Eur. J.* **2000**, *6*, 427-431.
161. Ranford, J. D.; Vittal, J. J.; Wu, D. Q.; Yang, X. D. *Angew. Chem., Int. Ed. Engl.* **1999**, *38*, 3498-3501.
162. Jaunky, W.; Hosseini, M. W.; Planeix, J. M.; De Cian, A.; Kyritsakas, N.; Fischer, J. *Chem. Commun.* **1999**, 2313-2314.
163. Saalfrank, R. W.; Maid, H.; Hampel, F.; Peters, K. *Eur. J. Inorg. Chem.* **1999**, 1859-1867.
164. Mamula, O.; Von Zelewsky, A.; Bark, T.; Bernardinelli, G. *Angew. Chem., Int. Ed. Engl.* **1999**, *38*, 2945-2948.
165. Ezuhara, T.; Endo, K.; Aoyama, Y. *J. Am. Chem. Soc.* **1999**, *121*, 3279-3283.
166. Biradha, K.; Seward, C.; Zaworotko, M. J. *Angew. Chem., Int. Ed. Engl.* **1999**, *38*, 492-495.
167. Kaes, C.; Hosseini, M. W.; Rickard, C. E. F.; Skelton, B. W.; White, A. H. *Angew. Chem., Int. Ed. Engl.* **1998**, *37*, 920-922.
168. Whang, D.; Heo, J.; Kim, C. A.; Kim, K. *Chem. Commun.* **1997**, 2361-2362.
169. Psillakis, E.; Jeffery, J. C.; McCleverty, J. A.; Ward, M. D. *Dalton Trans.* **1997**, 1645-1651.

170. Withersby, M. A.; Blake, A. J.; Champness, N. R.; Hubberstey, P.; Li, W. S.; Schroder, M. *Angew. Chem., Int. Ed. Engl.* **1997**, *36*, 2327-2329.
171. Blake, A. J.; Champness, N. R.; Khlobystov, A. N.; Parsons, S.; Schroder, M. *Angew. Chem., Int. Ed. Engl.* **2000**, *39*, 2317-2320.
172. Hardie, R. J.; Godfrey, P. D.; Raston, C. L. *Chem. Eur. J.* **1999**, *5*, 1828-1833.
173. Katz, T. J. *Angew. Chem., Int. Ed. Engl.* **2000**, *39*, 1921-1923.
174. Corbin, P. S.; Zimmerman, S. C. *J. Am. Chem. Soc.* **2000**, *122*, 3779-3780.
175. Masciocchi, N.; Ardizzoia, G. A.; Lamonica, G.; Maspero, A.; Sironi, A. *Angew. Chem., Int. Ed. Engl.* **1998**, *37*, 3366-3369.
176. Bowyer, P. K.; Porter, K. A.; Rae, A. D.; Willis, A. C.; Wild, S. B. *Chem. Commun.* **1998**, 1153-1154.
177. Rowan, A. E.; Nolte, R. J. M. *Angew. Chem., Int. Ed. Engl.* **1998**, *37*, 63-68.
178. Wu, B.; Zhang, W. J.; Yu, S. Y.; Wu, X. T. *Dalton Trans.* **1997**, 1795-1796.
179. Pecaut, J.; Lefur, Y.; Masse, R. *Acta Crystallogr.* **1993**, *B49*, 535-541.
180. Etter, M. C.; Huang, K. S. *Chem. Mater.* **1992**, *4*, 824-827.
181. Panunto, T. W.; Urbanczyklickowska, Z.; Johnson, R.; Etter, M. C. *J. Am. Chem. Soc.* **1987**, *109*, 7786-7797.
182. Gorbitz, C. H.; Etter, M. C. *Perkin Trans. 2* **1992**, 131-135.
183. Leiserowitz, L. *Acta Crystallogr.* **1976**, *B32*, 775-802.
184. Melendez, R.; Robinson, F.; Zaworotko, M. J. *Supramol. Chem.* **1996**, *7*, 275-293.
185. Pepinsky, R.; Vedam, K. *Phys. Rev. A* **1960**, *117*, 1502-1503.
186. Pepinsky, R.; Vedam, K.; Hoshino, S.; Okaya, Y. *Phys. Rev. A* **1958**, *111*, 1508-1510.
187. Payan, F.; Haser, R. *Acta Crystallogr.* **1976**, *B32*, 1875-1879.
188. Swift, J. A.; Ward, M. D. *Chem. Mater.* **2000**, *12*, 1501-1504.
189. Gudbjartson, H.; Biradha, K.; Poirier, K. M.; Zaworotko, M. J. *J. Am. Chem. Soc.* **1999**, *121*, 2599-2600.

190. Fujita, M.; Kwon, Y. J.; Sasaki, O.; Yamaguchi, K.; Ogura, K. *J. Am. Chem. Soc.* **1995**, *117*, 7287-7288.
191. Min, K. S.; Suh, M. P. *J. Solid State Chem.* **2000**, *152*, 183-190.
192. Carlucci, L.; Ciani, G.; Proserpio, D. M. *Dalton Trans.* **1999**, 1799-1804.
193. Liu, C. M.; You, X. Z.; Chen, W. *J. Coord. Chem.* **1998**, *46*, 183-191.
194. Carlucci, L.; Ciani, G.; Proserpio, D. M. *Chem. Commun.* **1999**, 449-450.
195. Aakeroy, C. B.; Beatty, A. M. *Cryst. Eng.* **1998**, *1*, 39-49.
196. Fujita, M.; Sasaki, O.; Watanabe, K. Y.; Ogura, K.; Yamaguchi, K. *New J. Chem.* **1998**, *22*, 189-191.
197. Blake, A. J.; Champness, N. R.; Khlobystov, A.; Lemenovskii, D. A.; Li, W. S.; Schroder, M. *Chem. Commun.* **1997**, 2027-2028.
198. Losier, P.; Zaworotko, M. J. *Angew. Chem., Int. Ed. Engl.* **1996**, *35*, 2779-2782.
199. Nishikiori, S.; Iwamoto, T. *Inorg. Chem.* **1986**, *25*, 788-794.
200. Nishikiori, S.; Iwamoto, T. *J. Inclusion Phenom.* **1984**, *2*, 341-349.
201. Nishikiori, S.; Iwamoto, T. *Bull. Chem. Soc. Jpn.* **1983**, *56*, 3246-3252.
202. Miyoshi, T.; Iwamoto, T.; Sasaki, Y. *Inorg. Chim. Acta* **1972**, *6*, 59-64.
203. Batten, S. R.; Hoskins, B. F.; Robson, R. *New J. Chem.* **1998**, *22*, 173-175.
204. Abrahams, B. F.; Hardie, M. J.; Hoskins, B. F.; Robson, R.; Sutherland, E. E. *Chem. Commun.* **1994**, 1049-1050.
205. Groeneman, R. H.; MacGillivray, L. R.; Atwood, J. L. *Chem. Commun.* **1998**, 2735-2736.
206. Aoyagi, M.; Biradha, K.; Fujita, M. *Bull. Chem. Soc. Jpn.* **2000**, *73*, 1369-1373.
207. Subramanian, S.; Zaworotko, M. J. *Angew. Chem., Int. Ed. Engl.* **1995**, *34*, 2127-2129.
208. Gable, R. W.; Hoskins, B. F.; Robson, R. *Chem. Commun.* **1990**, 1677-1678.
209. Hagrman, D.; Hammond, R. P.; Haushalter, R.; Zubieta, J. *Chem. Mater.* **1998**, *10*, 2091-2100.
210. Lu, J.; Paliwala, T.; Lim, S. C.; Yu, C.; Niu, T. Y.; Jacobson, A. J. *Inorg. Chem.* **1997**, *36*, 923-929.

211. MacGillivray, L. R.; Groeneman, R. H.; Atwood, J. L. *J. Am. Chem. Soc.* **1998**, *120*, 2676-2677.
212. Park, S. H.; Kim, K. M.; Lee, S.; Jung, O. S. *Bull. Korean Chem. Soc.* **1998**, *19*, 79-82.
213. Moulton, B.; Zaworotko, M. J. *Rational Design of Polar Solids* Kluwer: Dordrecht, 1999; pp 311-330.
214. Kumar, R. K.; Goldberg, I. *Angew. Chem., Int. Ed. Engl.* **1998**, *37*, 3027-3030.
215. Biradha, K.; Fujita, M. *Chem. Commun.* **2001**, 15-16.
216. Dong, Y. B.; Smith, M. D.; Layland, R. C.; Zur Loye, H. C. *Chem. Mater.* **2000**, *12*, 1156-1161.
217. Sharma, C. V. K.; Rogers, R. D. *Cryst. Eng.* **1998**, *1*, 19-38.
218. Kondo, M.; Asami, A.; Fujimoto, K.; Noro, S.; Kitagawa, S.; Ishii, T.; Matsuzaka, H. *Int. J. Inorg. Mater.* **1999**, *1*, 73-75.
219. Dong, Y. B.; Smith, M. D.; Layland, R. C.; Zur Loye, H. C. *Dalton Trans.* **2000**, 775-780.
220. Carlucci, L.; Ciani, G.; Proserpio, D. M. *New J. Chem.* **1998**, *22*, 1319-1321.
221. Choi, H. J.; Suh, M. P. *J. Am. Chem. Soc.* **1998**, *120*, 10622-10628.
222. Masse, R.; Nicoud, J. F.; Bagieu-Beucher, M.; Bourgogne, C. *Chem. Phys.* **1999**, *245*, 365-375.
223. Withersby, M. A.; Blake, A. J.; Champness, N. R.; Cooke, P. A.; Hubberstey, P.; Schroder, M. *New J. Chem.* **1999**, *23*, 573-575.
224. Dong, Y. B.; Layland, R. C.; Pschirer, N. G.; Smith, M. D.; Bunz, U. H. F.; Zur Loye, H. C. *Chem. Mater.* **1999**, *11*, 1413-1415.
225. Power, K. N.; Hennigar, T. L.; Zaworotko, M. J. *New J. Chem.* **1998**, *22*, 177-181.
226. Rujiwatra, A.; Kepert, C. J.; Rosseinsky, M. J. *Chem. Commun.* **1999**, 2307-2308.
227. Kitagawa, S.; Kondo, M. *Bull. Chem. Soc. Jpn.* **1998**, *71*, 1739-1753.
228. Kepert, C. J.; Rosseinsky, M. J. *Chem. Commun.* **1999**, 375-376.
229. Atencio, R.; Biradha, K.; Hennigar, T. L.; Poirier, K. M.; Power, K. N.; Seward, C. M.; White, N. S.; Zaworotko, M. J. *Cryst. Eng.* **1998**, *1*, 203-212.

230. MacGillivray, L. R.; Subramanian, S.; Zaworotko, M. J. *Chem. Commun.* **1994**, 1325-1326.
231. Johnson, D. W.; Xu, J. D.; Saalfrank, R. W.; Raymond, K. N. *Angew. Chem., Int. Ed. Engl.* **1999**, *38*, 2882-2885.
232. Abrahams, B. F.; Egan, S. J.; Robson, R. *J. Am. Chem. Soc.* **1999**, *121*, 3535-3536.
233. Bruckner, C.; Powers, R. E.; Raymond, K. N. *Angew. Chem., Int. Ed. Engl.* **1998**, *37*, 1837-1839.
234. Olenyuk, B.; Whiteford, J. A.; Fechtenkotter, A.; Stang, P. J. *Nature* **1999**, *398*, 796-799.
235. Stang, P. J.; Olenyuk, B.; Muddiman, D. C.; Smith, R. D. *Organometallics* **1997**, *16*, 3094-3096.
236. Yu, S. Y.; Kusukawa, T.; Biradha, K.; Fujita, M. *J. Am. Chem. Soc.* **2000**, *122*, 2665-2666.
237. Fujita, M. *Chem. Soc. Rev.* **1998**, *27*, 417-425.
238. Otieno, T.; Rettig, S. J.; Thompson, R. C.; Trotter, J. *Inorg. Chem.* **1993**, *32*, 1607-1611.
239. Carlucci, L.; Ciani, G.; Proserpio, D. M.; Sironi, A. *Chem. Commun.* **1994**, 2755-2756.
240. Syozi, I. *Prog. Theor. Phys.* **1951**, *6*, 306-308.
241. Lopez, S.; Kahraman, M.; Harmata, M.; Keller, S. W. *Inorg. Chem.* **1997**, *36*, 6138-6140.
242. Hirsch, K. A.; Venkataraman, D.; Wilson, S. R.; Moore, J. S.; Lee, S. *Chem. Commun.* **1995**, 2199-2200.
243. Yaghi, O. M.; Li, G. M. *Angew. Chem., Int. Ed. Engl.* **1995**, *34*, 207-209.
244. Sinzger, K.; Hunig, S.; Jopp, M.; Bauer, D.; Bietsch, W.; Von Schutz, J. U.; Wolf, H. C.; Kremer, R. K.; Metzenthin, T.; Bau, R.; Khan, S. I.; Lindbaum, A.; Lengauer, C. L.; Tillmanns, E. *J. Am. Chem. Soc.* **1993**, *115*, 7696-7705.
245. Evans, O. R.; Xiong, R. G.; Wang, Z. Y.; Wong, G. K.; Lin, W. B. *Angew. Chem., Int. Ed. Engl.* **1999**, *38*, 536-538.
246. Keggin, J. F. *Nature* **1936**, *137*, 577.

247. Carlucci, L.; Ciani, G.; Proserpio, D. M.; Sironi, A. *Angew. Chem., Int. Ed. Engl.* **1995**, *34*, 1895-1898.
248. Robinson, F.; Zaworotko, M. J. *Chem. Commun.* **1995**, 2413-2414.
249. Yaghi, O. M.; Li, H. L. *J. Am. Chem. Soc.* **1996**, *118*, 295-296.
250. Holman, K. T.; Ward, M. D. *Angew. Chem., Int. Ed. Engl.* **2000**, *39*, 1653-1656.
251. Evans, C. C.; Sukarto, L.; Ward, M. D. *J. Am. Chem. Soc.* **1999**, *121*, 320-325.
252. Swift, J. A.; Reynolds, A. M.; Ward, M. D. *Chem. Mater.* **1998**, *10*, 4159-4168.
253. Biradha, K.; Domasevitch, K. V.; Moulton, B.; Seward, C.; Zaworotko, M. J. *Chem. Commun.* **1999**, 1327-1328.
254. Biradha, K.; Domasevitch, K. V.; Hogg, C.; Moulton, B.; Power, K. N.; Zaworotko, M. J. *Cryst. Eng.* **1999**, *2*(1), 37-45.
255. Biradha, K.; Mondal, A.; Moulton, B.; Zaworotko, M. J. *Dalton Trans.* **2000**, *21*, 3837-3844.
256. Soma, T.; Iwamoto, T. *Acta Crystallogr.* **1996**, *C52*, 1200-1203.
257. Atencio, R.; Domasevitch, K. V.; Zaworotko, M. J. *Cryst. Eng.* **2000**, *3*(1), 63-69.
258. Hollingsworth, M. D.; Werner-Zwanziger, U.; Brown, M. E.; Chaney, J. D.; Huffman, J. C.; Harris, K. D. M.; Smart, S. P. *J. Am. Chem. Soc.* **1999**, *121*, 9732-9733.
259. Hollingsworth, M. D.; Brown, M. E.; Hillier, A. C.; Santarsiero, B. D.; Chaney, J. D. *Science* **1996**, *273*, 1355-1359.
260. Brown, M. E.; Chaney, J. D.; Santarsiero, B. D.; Hollingsworth, M. D. *Chem. Mater.* **1996**, *8*, 1588-1591.
261. Hollingsworth, M. D. *Curr. Opin. Solid State Mater. Sci.* **1996**, *1*, 514-521.
262. Brown, M. E.; Hollingsworth, M. D. *Nature* **1995**, *376*, 323-327.
263. Hulliger, J.; Roth, S. W.; Quintel, A.; Bebie, H. J. *Solid State Chem.* **2000**, *152*, 49-56.
264. Langley, P. J.; Hulliger, J. *Chem. Soc. Rev.* **1999**, *28*, 279-291.
265. Hulliger, J.; Langley, P. J.; Roth, S. W. *Cryst. Eng.* **1998**, *1*, 177-189.
266. Roth, S. W.; Langley, P. J.; Quintel, A.; Wubbenhorst, M.; Rechsteiner, P.; Rogin, P.; Konig, O.; Hulliger, J. *Adv. Mater.* **1998**, *10*, 1543-1546.

267. Konig, O.; Burgi, H. B.; Armbruster, T.; Hulliger, J.; Weber, T. *J. Am. Chem. Soc.* **1997**, *119*, 10632-10640.
268. Hulliger, J.; Rogin, P.; Quintel, A.; Rechsteiner, P.; Konig, O.; Wubbenhorst, M. *Adv. Mater.* **1997**, *9*, 677-680.
269. Hoss, R.; Konig, O.; Kramerhoss, V.; Berger, U.; Rogin, P.; Hulliger, J. *Angew. Chem., Int. Ed. Engl.* **1996**, *35*, 1664-1666.
270. Hulliger, J.; Konig, O.; Hoss, R. *Adv. Mater.* **1995**, *7*, 719-721.
271. Sra, A. K.; Andruh, M.; Kahn, O.; Golhen, S.; Ouahab, L.; Yakhmi, J. V. *Angew. Chem., Int. Ed. Engl.* **1999**, *38*, 2606-2609.
272. Pan, L.; Huang, X. Y.; Li, J. *J. Solid State Chem.* **2000**, *152*, 236-246.
273. Yuen, T.; Lin, C. L.; Mihalisin, T. W.; Lawandy, M. A.; Li, J. *J. Appl. Phys.* **2000**, *87*, 6001-6003.
274. Li, J.; Chen, Z.; Wang, R. J.; Proserpio, D. M. *Coord. Chem. Rev.* **1999**, *192*, 707-735.
275. Chen, Z.; Wang, R. J.; Li, J. *Chem. Mater.* **2000**, *12*, 762-766.
276. Lawandy, M. A.; Huang, X. Y.; Wang, R. J.; Li, J.; Lu, J. Y.; Yuen, T.; Lin, C. L. *Inorg. Chem.* **1999**, *38*, 5410-5414.
277. Lu, J. Y.; Cabrera, B. R.; Wang, R. J.; Li, J. *Inorg. Chem.* **1999**, *38*, 4608-4611.
278. Hagrman, P. J.; Hagrman, D.; Zubieta, J. *Angew. Chem., Int. Ed. Engl.* **1999**, *38*, 2639-2684.
279. Hagrman, D.; Hagrman, P. J.; Zubieta, J. *Angew. Chem., Int. Ed. Engl.* **1999**, *38*, 3165-3168.
280. Zapf, P. J.; Haushalter, R. C.; Zubieta, J. *Chem. Commun.* **1997**, 321-322.
281. Newkome, G. R.; He, E. F.; Moorefield, C. N. *Chem. Rev.* **1999**, *99*, 1689-1746.
282. von Schnering, H. G. *Angew. Chem., Int. Ed. Engl.* **1981**, *20*, 33-51.
283. Lu, J.; Mondal, A.; Moulton, B.; Zaworotko, M. J. *Angew. Chem., Int. Ed. Engl.* **2001**, *40*(11), 2113-2116.
284. Chui, S. S. Y.; Lo, S. M. F.; Charmant, J. P. H.; Orpen, A. G.; Williams, I. D. *Science* **1999**, *283*, 1148-1150.
285. Breck, D. W. *Zeolite Molecular Sieves: Structure, Chemistry and Use*; Wiley Interscience: New York, 1974.

286. Coxeter, H. S. M.; Longuet-Higgins, M. S.; Miller, J. C. P. *Philos. Trans. R. Soc. London, A* **1954**, *246*, 401-450.
287. Holden, A. *Shapes, Space, and Symmetry*; Columbia University Press: New York, 1971.
288. Weisstein, E. W. *The CRC Concise Encyclopedia of Mathematics*; CRC Press: Boca Raton, 1999.
289. Wells, D. *The Penguin Dictionary of Curious and Interesting Geometry*; Penguin: London, 1991.
290. Andreini, A. *Mem. Soc. Ital. Sci.* **1907**, *14*, 75.
291. Bourne, S. A.; Lu, J.; Mondal, A.; Moulton, B.; Zaworotko, M. J. *Angew. Chem., Int. Ed. Engl.* **2001**, *40*(11), 2111-2113.
292. Moulton, B.; Lu, J.; Hajndl, R.; Hariharan, S.; Zaworotko, M. J. *Angew. Chem., Int. Ed. Engl.* **2002**, *41*(15), 2821-2824.
293. Atwood, J. L. *Nature Mater.* **2002**, *1*(2), 91-92.
294. Ramirez, A. P. *Annu. Rev. Mater. Sci.* **1994**, *24*, 453-480.
295. *International Tables for Crystallography - Volume A*; Second ed. Kluwer Academic: Boston, 1989.
296. O'Keeffe, M.; Hyde, B. G. *Crystal Structures I. Patterns and Symmetry*; Mineralogical Society of America: Washington, DD, 1996.
297. Eddaoudi, M.; Kim, J.; O'keeffe, M.; Yaghi, O. M. *J. Am. Chem. Soc.* **2002**, *124*, 376-377.
298. Kahn, O. *Molecular Magnetism*; VCH: Weinheim, Germany, 1993.
299. Jotham, R. W.; Marks, J. A.; Kettle, S. F. A. *Dalton Trans.* **1972**, 428-438.
300. Melnik, M. *Coord. Chem. Rev.* **1982**, *42*, 259-293.
301. Bleaney, B.; Bowers, K. D. *Proc. R. Soc. London, A* **1952**, *214*, 451-465.
302. Mondelli, C.; Mutka, H.; Payen, C.; Frick, B.; Andersen, K. H. *Physica B* **2000**, *284*, 1371-1372.
303. Harris, M. J.; Zinkin, M. P.; Tun, Z.; Wanklyn, B. M.; Swainson, I. P. *Phys. Rev. Lett.* **1994**, *73*, 189-192.
304. Moessner, R.; Chalker, J. T. *Phys. Rev. B* **1998**, *58*, 12049-12062.

305. Reimers, J. N.; Berlinsky, A. J.; Shi, A. C. *Phys. Rev. B* **1991**, *43*, 865-878.
306. Zhang, X. X.; Chui, S. S. Y.; Williams, I. D. *J. Appl. Phys.* **2000**, *87*, 6007-6009.
307. Friedrichs, O. D.; Dress, A. W. M.; Huson, D. H.; Klinowski, J.; Mackay, A. L. *Nature* **1999**, *400*, 644-647.
308. Han, S. X.; Smith, J. V. *Acta Crystallogr. A* **1999**, *55*, 342-359.
309. Han, S. X.; Smith, J. V. *Acta Crystallogr. A* **1999**, *55*, 360-382.
310. Han, S. X.; Smith, J. V. *Acta Crystallogr. A* **1999**, *55*, 332-341.
311. Delgado-Friedrichs, O. *Discrete & Computational Geometry* **2001**, *26*, 549-571.
312. Friedrichs, O. D.; Huson, D. H. *Discrete & Computational Geometry* **2000**, *24*, 279-292.
313. Kitaigorodskii, A. I. *Molecular Crystals and Molecules*; Academic Press: London, 1973.

Appendices

Appendix A-1. Crystal data and structure refinement for compound 1.

Empirical formula	C182 H36 N42 O72 Zn22
Formula weight	5400.67
Temperature	173(2) K
Wavelength	0.71073 Å
Crystal system	Cubic
Space group	Pm $\bar{3}$ m
Unit cell dimensions	a = 20.4702(11) Å $\alpha = 90^\circ$. b = 20.4702(11) Å $\beta = 90^\circ$. c = 20.4702(11) Å $\gamma = 90^\circ$.
Volume	8577.6(8) Å ³
Z	1
Density (calculated)	1.046 Mg/m ³
Absorption coefficient	1.565 mm ⁻¹
F(000)	2658
Crystal size	0.30 x 0.25 x 0.20 mm ³
Theta range for data collection	0.99 to 18.00°.
Index ranges	-17 ≤ h ≤ 15, -6 ≤ k ≤ 17, -17 ≤ l ≤ 17
Reflections collected	12984
Independent reflections	654 [R(int) = 0.0379]
Completeness to theta = 18.00°	99.7 %
Refinement method	Full-matrix least-squares on F ²
Data / restraints / parameters	654 / 0 / 85
Goodness-of-fit on F ²	1.769
Final R indices [I > 2σ(I)]	R1 = 0.1457, wR2 = 0.3763
R indices (all data)	R1 = 0.1593, wR2 = 0.3945
Largest diff. peak and hole	1.076 and -0.984 e.Å ⁻³

Appendix A-2. Crystal data and structure refinement for compound 2.

Empirical formula	C _{27.83} H ₄ O ₁₀ Zn ₂	
Formula weight	629.05	
Temperature	293(2) K	
Wavelength	0.71073 Å	
Crystal system	Cubic	
Space group	Fm $\bar{3}$ m	
Unit cell dimensions	a = 26.5367(13) Å	$\alpha = 90^\circ$.
	b = 26.5367(13) Å	$\beta = 90^\circ$.
	c = 26.5367(13) Å	$\gamma = 90^\circ$.
Volume	18687.0(16) Å ³	
Z	24	
Density (calculated)	1.342 Mg/m ³	
Absorption coefficient	1.588 mm ⁻¹	
F(000)	7464	
Crystal size	0.30 x 0.25 x 0.20 mm ³	
Theta range for data collection	1.33 to 26.01°.	
Index ranges	-32 ≤ h ≤ 32, -32 ≤ k ≤ 18, -28 ≤ l ≤ 32	
Reflections collected	24683	
Independent reflections	981 [R(int) = 0.0610]	
Completeness to theta = 26.01°	100.0 %	
Refinement method	Full-matrix least-squares on F ²	
Data / restraints / parameters	981 / 0 / 53	
Goodness-of-fit on F ²	1.047	
Final R indices [I > 2σ(I)]	R1 = 0.0647, wR2 = 0.1784	
R indices (all data)	R1 = 0.0778, wR2 = 0.1897	
Largest diff. peak and hole	0.733 and -0.723 e.Å ⁻³	

Appendix A-3. Crystal data and structure refinement for compound 3.

Empirical formula	C140 H72 Cu8 N8 O32
Formula weight	2886.38
Temperature	173(2) K
Wavelength	0.71073 Å
Crystal system	Tetragonal
Space group	P4/ncc
Unit cell dimensions	a = 18.7912(8) Å α = 90°. b = 18.7912(8) Å β = 90°. c = 16.8886(10) Å γ = 90°.
Volume	5963.5(5) Å ³
Z	2
Density (calculated)	1.607 Mg/m ³
Absorption coefficient	1.485 mm ⁻¹
F(000)	2912
Crystal size	0.20 x 0.20 x 0.05 mm ³
Theta range for data collection	1.53 to 28.27°.
Index ranges	-23 ≤ h ≤ 24, -20 ≤ k ≤ 25, -21 ≤ l ≤ 22
Reflections collected	33929
Independent reflections	3632 [R(int) = 0.0560]
Completeness to theta = 28.27°	97.9 %
Absorption correction	None
Refinement method	Full-matrix least-squares on F ²
Data / restraints / parameters	3632 / 0 / 231
Goodness-of-fit on F ²	0.866
Final R indices [I > 2σ(I)]	R1 = 0.0407, wR2 = 0.1063
R indices (all data)	R1 = 0.0680, wR2 = 0.1139
Largest diff. peak and hole	0.926 and -0.523 e.Å ⁻³

Appendix A-4. Crystal data and structure refinement for compound 4.

Empirical formula	C107.50 H54 Cu6 N6 O29	
Formula weight	2274.81	
Temperature	173(2) K	
Wavelength	0.71073 Å	
Crystal system	Trigonal	
Space group	P3c1	
Unit cell dimensions	a = 18.6200(17) Å	$\alpha = 90^\circ$.
	b = 18.6200(17) Å	$\beta = 90^\circ$.
	c = 19.804(3) Å	$\gamma = 120^\circ$.
Volume	5946.2(11) Å ³	
Z	2	
Density (calculated)	1.271 Mg/m ³	
Absorption coefficient	1.124 mm ⁻¹	
F(000)	2294	
Crystal size	0.15 x 0.15 x 0.05 mm ³	
Theta range for data collection	2.06 to 28.27°.	
Index ranges	-24 ≤ h ≤ 19, -16 ≤ k ≤ 24, -26 ≤ l ≤ 25	
Reflections collected	34893	
Independent reflections	9297 [R(int) = 0.0525]	
Completeness to theta = 28.27°	97.9 %	
Absorption correction	None	
Refinement method	Full-matrix least-squares on F ²	
Data / restraints / parameters	9297 / 1 / 518	
Goodness-of-fit on F ²	0.917	
Final R indices [I > 2σ(I)]	R1 = 0.0534, wR2 = 0.1491	
R indices (all data)	R1 = 0.1104, wR2 = 0.1665	
Absolute structure parameter	0.48(3)	
Largest diff. peak and hole	0.963 and -0.434 e.Å ⁻³	

Appendix A-5. Crystal data and structure refinement for compound 5.

Empirical formula	C _{245.84} H ₉₆ Cu ₂₄ O ₁₂₀
Formula weight	6494.21
Temperature	200(2) K
Wavelength	0.71073 Å
Crystal system	Cubic
Space group	Im $\bar{3}$ m
Unit cell dimensions	a = 27.6895(17) Å $\alpha = 90^\circ$. b = 27.6895(17) Å $\beta = 90^\circ$. c = 27.6895(17) Å $\gamma = 90^\circ$.
Volume	21230(2) Å ³
Z	2
Density (calculated)	1.016 Mg/m ³
Absorption coefficient	1.235 mm ⁻¹
F(000)	6454
Crystal size	0.15 x 0.15 x 0.10 mm ³
Theta range for data collection	2.75 to 23.25°.
Index ranges	-30 ≤ h ≤ 27, -26 ≤ k ≤ 30, -29 ≤ l ≤ 30
Reflections collected	36316
Independent reflections	1501 [R(int) = 0.0865]
Completeness to theta = 23.25°	99.6 %
Absorption correction	None
Refinement method	Full-matrix least-squares on F ²
Data / restraints / parameters	1501 / 0 / 100
Goodness-of-fit on F ²	1.138
Final R indices [I > 2σ(I)]	R1 = 0.0784, wR2 = 0.2725
R indices (all data)	R1 = 0.1069, wR2 = 0.2954
Largest diff. peak and hole	1.277 and -0.445 e.Å ⁻³

Appendix A-6. Crystal data and structure refinement for compound 6.

Empirical formula	C309.50 H96 Cu24 O120	
Formula weight	7258.82	
Temperature	173(2) K	
Wavelength	0.71073 Å	
Crystal system	Hexagonal	
Space group	P6 ₃ /m	
Unit cell dimensions	a = 28.6458(19) Å	α = 90°.
	b = 28.6458(19) Å	β = 90°.
	c = 28.165(3) Å	γ = 120°.
Volume	20015(3) Å ³	
Z	2	
Density (calculated)	1.204 Mg/m ³	
Absorption coefficient	1.317 mm ⁻¹	
F(000)	7218	
Crystal size	0.20 x 0.20 x 0.15 mm ³	
Theta range for data collection	3.80 to 22.56°.	
Index ranges	-21 ≤ h ≤ 30, -27 ≤ k ≤ 27, -22 ≤ l ≤ 30	
Reflections collected	39590	
Independent reflections	8931 [R(int) = 0.0664]	
Completeness to theta = 22.56°	99.1 %	
Absorption correction	None	
Refinement method	Full-matrix least-squares on F ²	
Data / restraints / parameters	8931 / 0 / 736	
Goodness-of-fit on F ²	1.032	
Final R indices [I > 2σ(I)]	R1 = 0.0879, wR2 = 0.2515	
R indices (all data)	R1 = 0.1511, wR2 = 0.2777	
Largest diff. peak and hole	0.739 and -0.896 e.Å ⁻³	

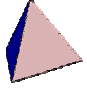


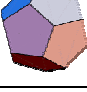








Appendix A-7. Crystal data and structure refinement for compound 7.

Empirical formula	C ₃₄ H ₂₂ Cu ₂ N ₂ O ₈	
Formula weight	713.62	
Temperature	200(2) K	
Wavelength	0.71073 Å	
Crystal system	Rhombohedral	
Space group	R $\bar{3}c$	
Unit cell dimensions	a = 30.337(2) Å	$\alpha = 90^\circ$.
	b = 30.337(2) Å	$\beta = 90^\circ$.
	c = 18.380(2) Å	$\gamma = 120^\circ$.
Volume	14649(2) Å ³	
Z	18	
Density (calculated)	1.456 Mg/m ³	
Absorption coefficient	1.359 mm ⁻¹	
F(000)	6516	
Crystal size	0.10 x 0.05 x 0.02 mm ³	
Theta range for data collection	1.34 to 23.26°.	
Index ranges	-33 ≤ h ≤ 33, -33 ≤ k ≤ 30, -20 ≤ l ≤ 11	
Reflections collected	18919	
Independent reflections	2352 [R(int) = 0.1775]	
Completeness to theta = 23.26°	99.7 %	
Absorption correction	None	
Refinement method	Full-matrix least-squares on F ²	
Data / restraints / parameters	2352 / 0 / 243	
Goodness-of-fit on F ²	0.841	
Final R indices [I > 2σ(I)]	R1 = 0.0497, wR2 = 0.1137	
R indices (all data)	R1 = 0.1205, wR2 = 0.1630	
Largest diff. peak and hole	0.994 and -0.396 e.Å ⁻³	







Appendix A-8. Crystal data and structure refinement for compound 8.

Empirical formula	C _{53.25} H ₃₁ Cu ₄ N ₃ O ₁₇
Formula weight	1238.97
Temperature	200(2) K
Wavelength	0.71073 Å
Crystal system	Monoclinic
Space group	P2 ₁ /n
Unit cell dimensions	a = 10.6661(12) Å α = 90°. b = 30.303(4) Å β = 95.877(2)°. c = 16.3650(19) Å γ = 90°.
Volume	5261.5(10) Å ³
Z	4
Density (calculated)	1.564 Mg/m ³
Absorption coefficient	1.670 mm ⁻¹
F(000)	2494
Crystal size	0.20 x 0.05 x 0.05 mm ³
Theta range for data collection	1.34 to 28.32°.
Index ranges	-13 ≤ h ≤ 13, -25 ≤ k ≤ 40, -18 ≤ l ≤ 20
Reflections collected	29732
Independent reflections	12275 [R(int) = 0.0782]
Completeness to theta = 28.32°	93.7 %
Absorption correction	None
Refinement method	Full-matrix least-squares on F ²
Data / restraints / parameters	12275 / 0 / 684
Goodness-of-fit on F ²	1.038
Final R indices [I > 2σ(I)]	R1 = 0.0650, wR2 = 0.1457
R indices (all data)	R1 = 0.1129, wR2 = 0.1722
Largest diff. peak and hole	1.139 and -0.812 e.Å ⁻³

Appendix B-1: Geometric values for the Platonic and Archimedean Solids

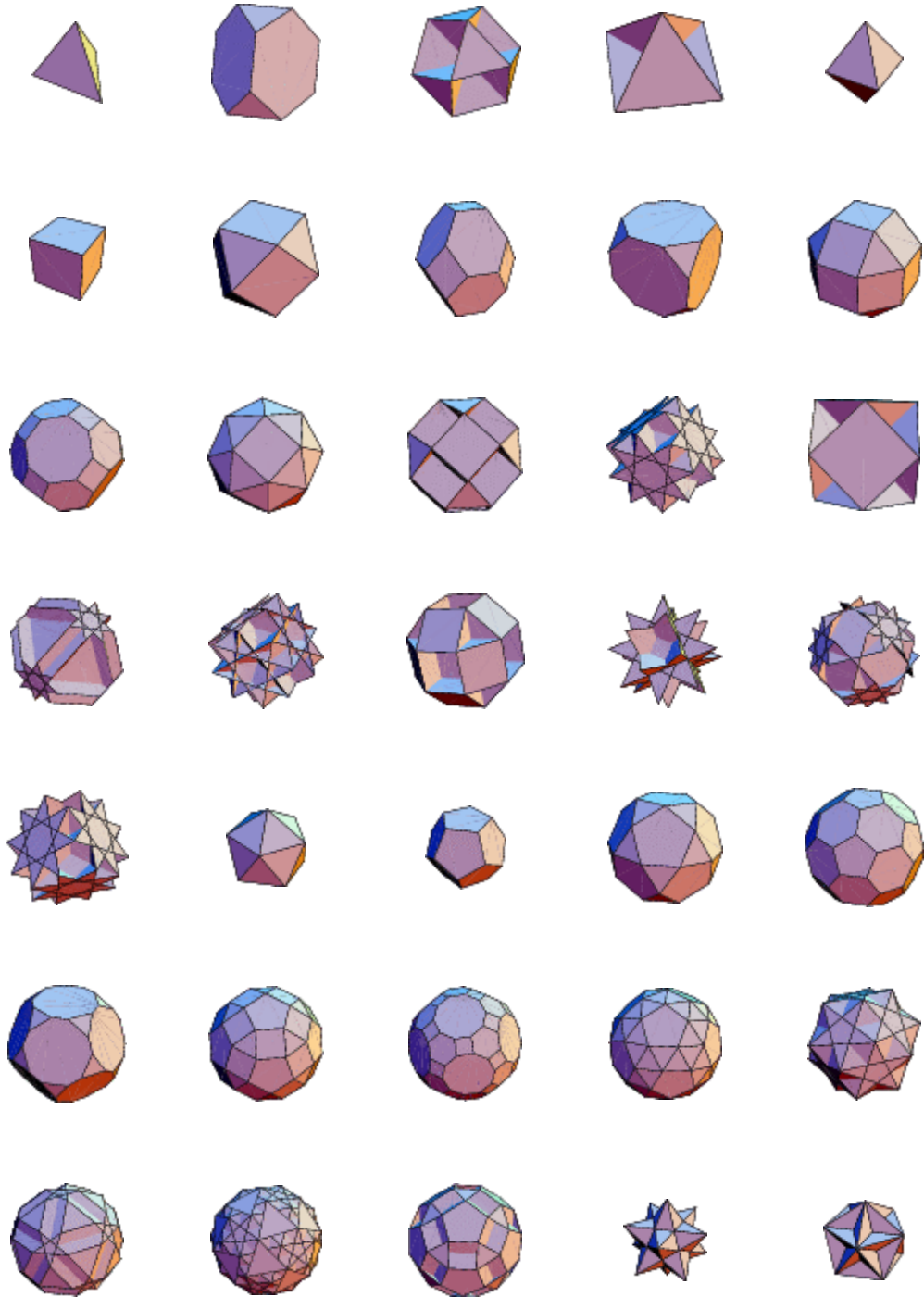
Figure	Name	Faces ¹	Vertices ²	Edges	Dihedral Angle ¹	CVC Angle ³
Platonic (Regular) Solids						
	Tetrahedron	4T	4(3)	6	70° 32'	
	Cube	6S	8(3)	12	90°	
	Octahedron	8T	6(4)	12	109° 28'	70° 32'
	Dodecahedron	12P	20(3)	30	116° 34'	
	Icosihedron	20T	12(5)	30	138° 11'	
Archimedean (semi-regular) solids						
	Truncated tetrahedron	8 (4H; 4T)	12(3)	18	70° 32' (H-H) 109° 28' (T-H)	
	Truncated cube	14 (8T; 6O)	24(3)	36	125° 16' (O-T) 90° (O-O)	
	Truncated octahedron	14 (6S; 8H)	24(3)	36	125° 16' (S-H) 109° 28' (H-H)	
	Truncated dodecahedron	32 (20T; 12D)	60(3)	90	116° 34' (D-D) 142° 37' (D-T)	
	Truncated Icosahedron	32 (12P; 20H)	60(3)	90	138° 11' (H-H) 142° 37' (H-P)	
	Cuboctahedron	14 (8T; 6S)	12(4)	24	125° 16'	109° 28' (T-T) 90° (S-S)
	Icosidodecahedron	32 (20T; 12P)	30(4)	60	142° 37'	138° 11' (T-T) 116° 34' (P-P)

Appendix B-1 (continued)

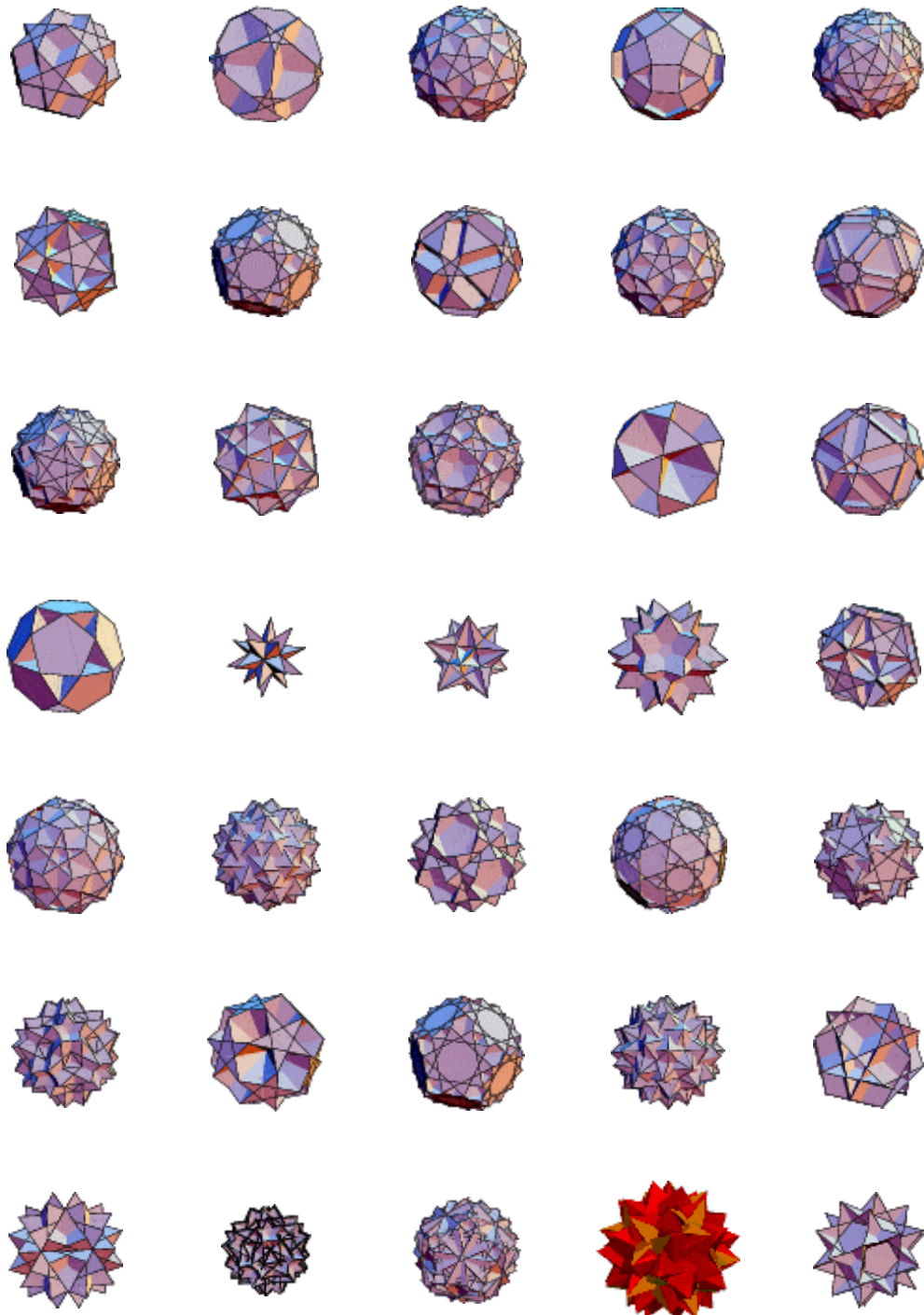
	Snub cuboctahedron	38 (32T; 6S)	24(5)	60	142° 59' (S-T) 153° 14'	
	Snub icosidodecahedron	92 (80T; 12P)	60(5)	150	152° 56' (P-H) 164° 11' (T-T)	
	Truncated cuboctahedron	26 (12S; 8H; 6O)	48(3)	72	135° (O-S) 125° 16' (O-H) 144° 44' (H-S)	
	Rhombicuboctahedron	26 (18T; 8S)	24(4)	48	135° (S-S) 144° 44' (T-S)	125° 16' (T-S) 117° 13' (S-S) 120° (S-S dihedral)
	Truncated icosidodecahedron	62 (30S; 20H; 12D)	120(3)	180	148° 17' (D-S) 142° 37' (D-H) 159° 6' (H-S)	
	Rhombicosidodecahedron	62 (20T; 30S; 12P)	60(4)	120	148° 17' (P-S) 159° 6' (T-S)	142° 37' (T-P) 135° 32' (S-S)

- 1 T = Triangle; S = Square; P = Pentagon; H = Hexagon; O = Octagon; D = Decagon
- 2 Number in parentheses is the number of edges that meet at each vertex
- 3 CVC is defined as the angle formed between the centroid of two polygons and the vertex that connects them

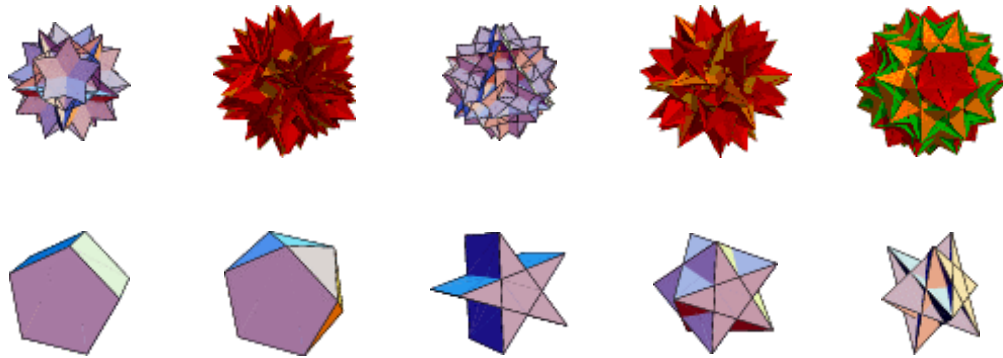
Appendix B-2: The 80 uniform polyhedra



Appendix B-2 (continued)

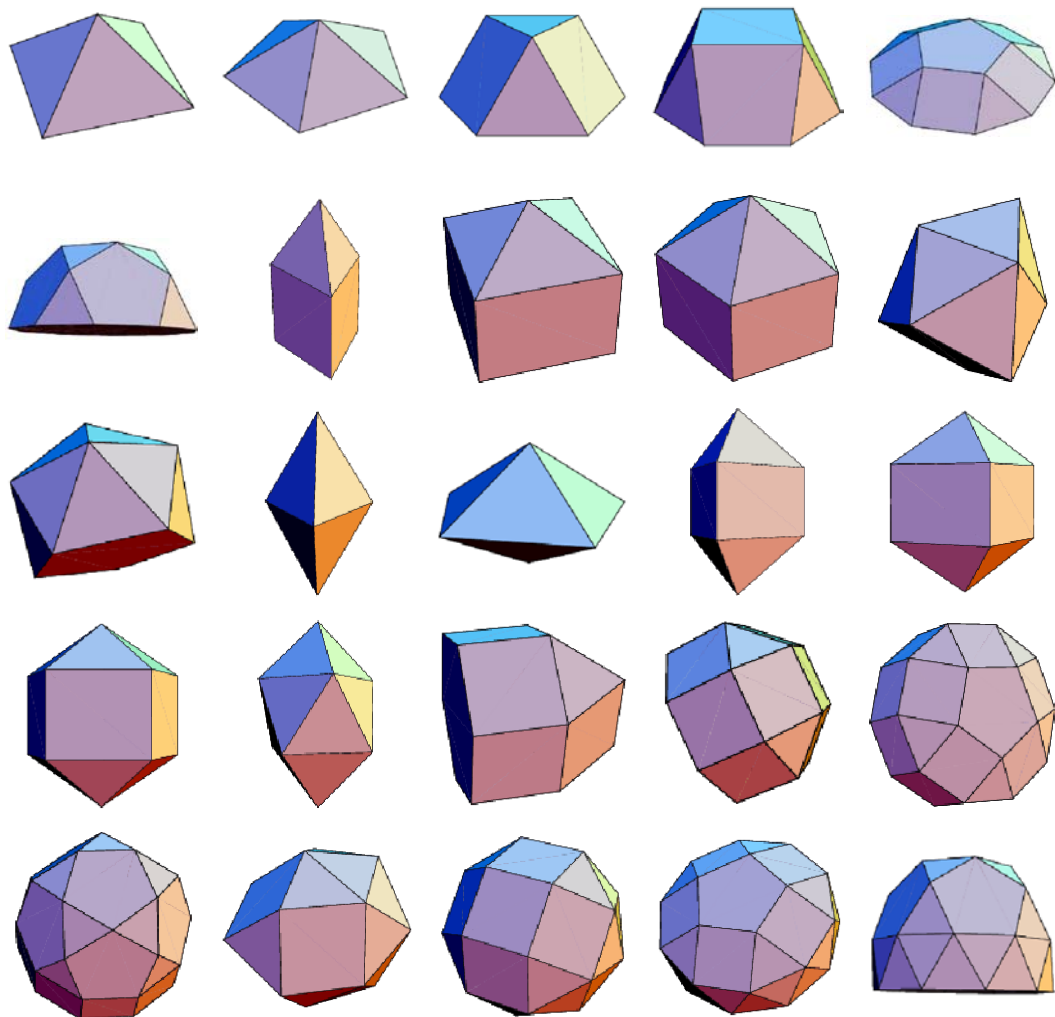


Appendix B-2 (continued)

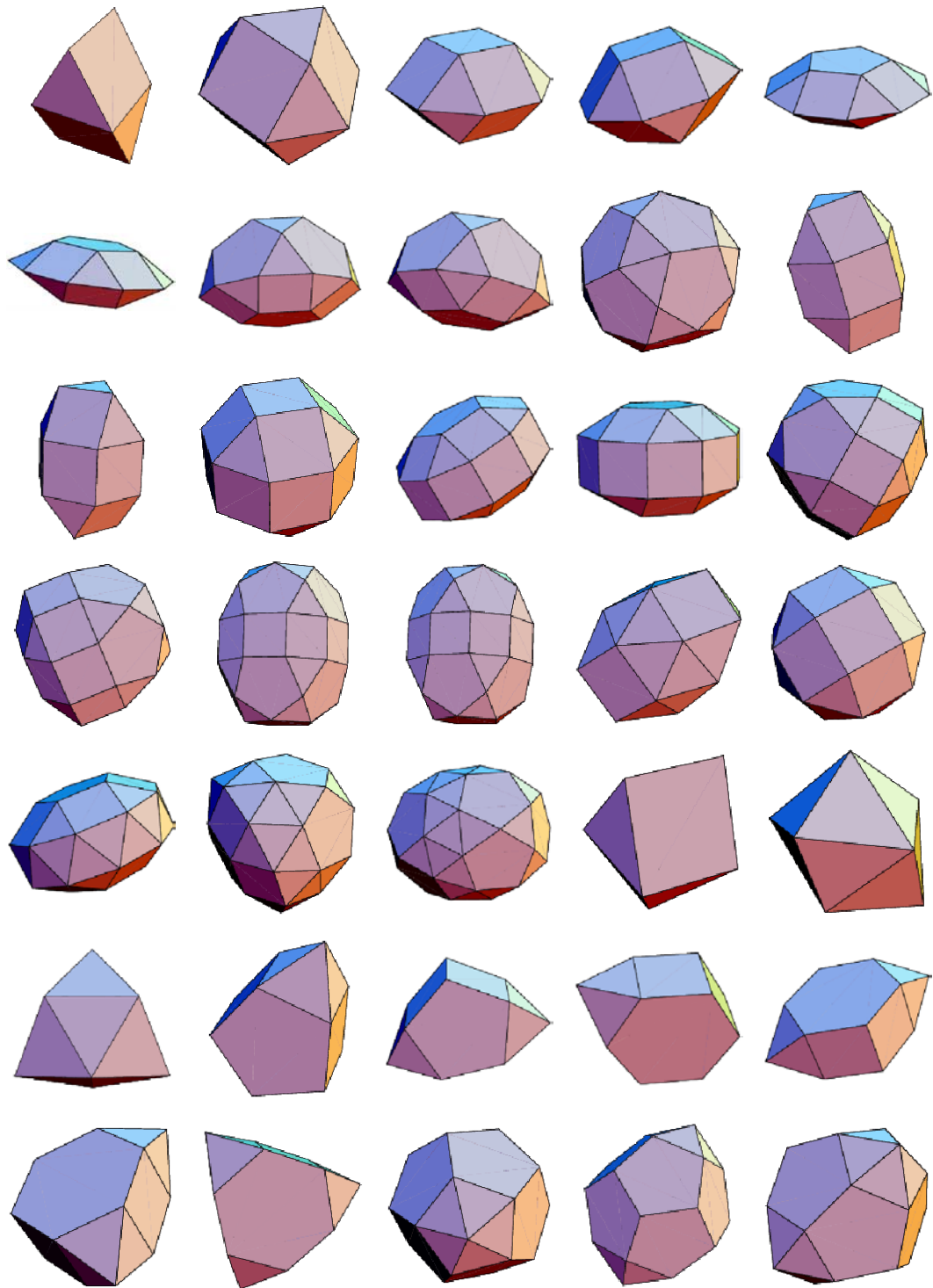


Appendix C: The 92 Johnson Solids

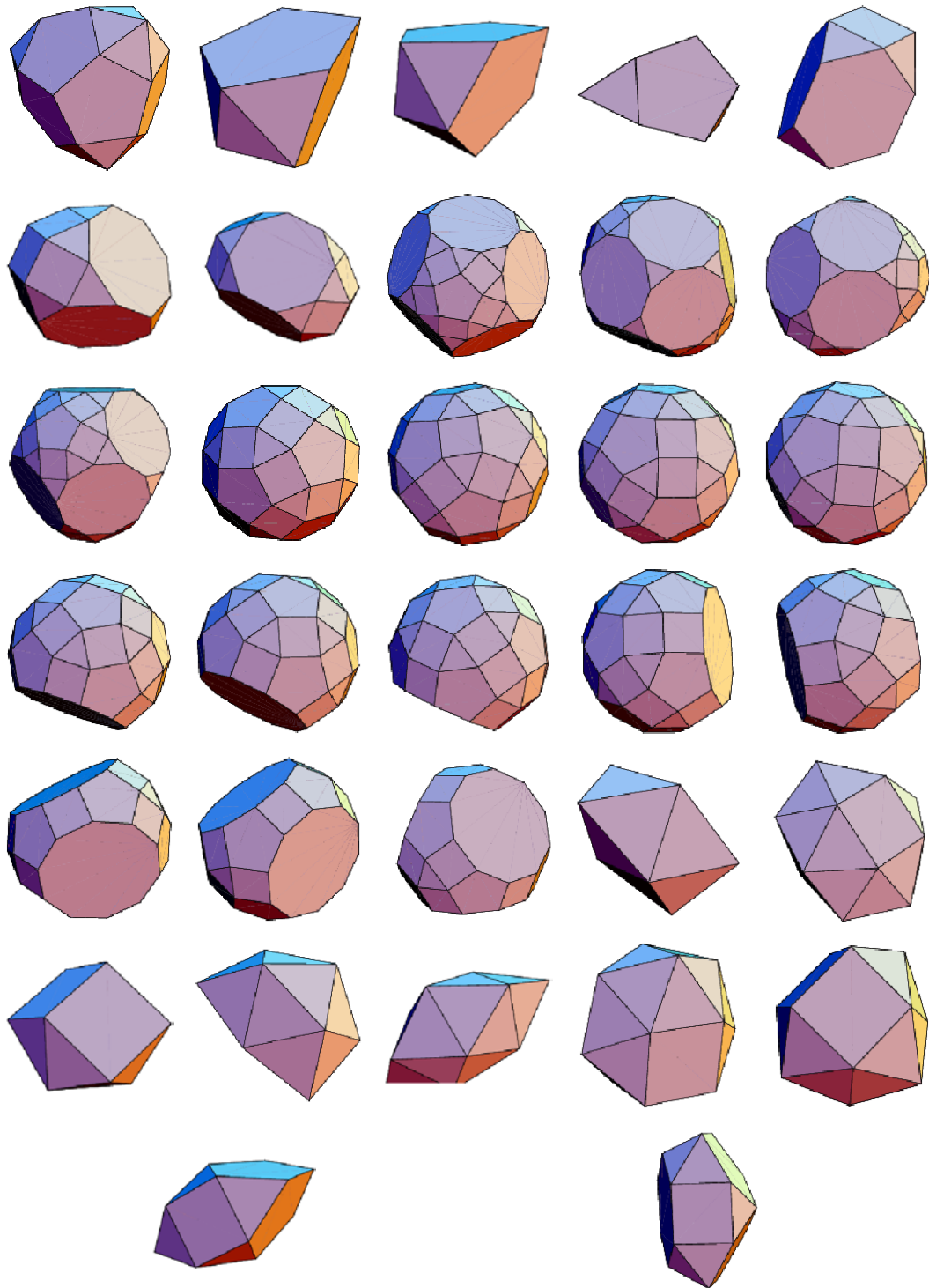
The Johnson solids are convex polyhedra having regular polygonal faces and equal edge lengths, excluding the Platonic and Archimedean solids. Note that in the latter, the polyhedra have congruent vertexes (all the same). The Johnson solids are the additional solids that can be constructed if this restriction is removed. The following table illustrates the 92 Johnson Solids (only possibilities):



Appendix C (continued)



Appendix C (continued)



About the Author

Brian Douglas Moulton earned his Bachelor's Degree in Chemistry from Dalhousie University in Halifax, Nova Scotia, Canada. He joined Diazans Limited in 1994, where he worked on the development of novel heterocyclic compounds for application in the pharmaceutical industry. In 1999, he accepted a position as a research associate at the University of Winnipeg (Canada) where he worked for one year on the development of new environmental sensors.

In 2000, Brian joined Prof. Michael Zaworotko's research group at the University of South Florida to pursue his Doctoral Degree in Chemistry. He was honored with several awards for his research and publications, including the 2001 Askounes-Ashford Award for outstanding PhD seeking graduate student in the Department of Chemistry. Brian has co-authored more than 25 peer-reviewed publications, is a co-inventor on two USPTO patent applications (pending) and has presented his research at numerous national and international scientific meetings.